Investigating the Role of ILDR2 in Hepatic Lipid Metabolism and Pancreas Islet Function

Elizabeth J. Millings

Submitted in partial fulfillment of the
requirements for the degree of
Doctor of Philosophy
under the Executive Committee
of the Graduate School of Arts and Sciences

COLUMBIA UNIVERSITY

2017

ABSTRACT

Investigating the Role of ILDR2 in Hepatic Lipid Metabolism and Pancreas Islet Function

Elizabeth J. Millings

Metabolic syndrome defines a cluster of related comorbidities including obesity, Type 2 diabetes, fatty liver disease, and cardiovascular diseases. Increasingly prevalent in Western countries, metabolic syndrome diseases are a major focus of efforts to understand the complex genetics that underlie disease risk and severity. Immunoglobulin domain-containing receptor 2 (ILDR2) is an endoplasmic reticulum transmembrane protein first identified as a candidate genetic modifier of diabetes susceptibility in the context of obesity. Obese, leptin-deficient mice with hypomorphic *Ildr2* expression had hypoinsulinemic hyperglycemia with reduced beta cell mass, suggesting that ILDR2 plays a role in maintain beta cell mass and function. Further studies proposed a role for ILDR2 in hepatic lipid metabolism as *Ildr2* shRNA-mediated knockdown (KD) caused hepatic steatosis in mice. The goal of this thesis work is to clarify the role of ILDR2 in diabetes and hepatic steatosis in an effort to elucidate the specific mechanism of ILDR2.

We developed a conditional *Ildr2* knockout (KO) allele, enabling tissue-specific ablation in mice. Liver-specific and hepatocyte-specific KO mice did not develop hepatic steatosis. However, liver-specific KO mice treated with adenoviral *Ildr2* shRNA accumulated hepatic triglycerides, suggesting off-target effects of the shRNA. Using RNA sequencing and sequence alignment, several gene candidates for shRNA off-targeting effect were identified. Future studies are proposed to elucidate role(s) of these genes in the previously described phenotype of *Ildr2* KD mice. I conclude that *Ildr2* ablation may contribute to the development of hepatic steatosis, but does not play a major role in hepatic lipid metabolism.

We also developed beta cell-specific (RIP2-cre) and pancreas-specific (*Pdx*-cre) *Ildr2* KO mice and characterized them for diabetic phenotypes. Pancreas-specific KO mice displayed impaired glucose tolerance, reduced insulin secretion and decreased calcium signaling in islets. These results confirm a role for ILDR2 in islet cell function. Experiments performed in RIP2-cre beta cell-specific KO mice were confounded by effects of the Cre construct, prohibiting definitive conclusions about the role of ILDR2 in the beta cell. Additionally, because *Ildr2* is expressed at low levels in beta cells, we propose that ILDR2 may function in islet macrophages.

Overall, this work defines the metabolic functions of ILDR2, clarifying its role in hepatic lipid metabolism, and confirming its role in islet cell function. In addition, I discuss preliminary evidence suggesting that ILDR2 may function in the brain to regulate body weight and metabolism.

Table of Contents

LIST OF FIGURES AND TABLES

ACKNOWLEDGEMENTS

I would first like to thank my advisor, Dr. Rudolph Leibel for his guidance and mentorship over the years. He has taught me how to think about science, how to do science, and especially, how to communicate science. It has been an honor to work with him. I am grateful to my thesis committee members and other faculty mentors for their insight, direction, and helpful advice throughout my thesis research. My colleagues and lab mates have provided exceptional support and collaboration, and contributed to an enjoyable work environment. I also want to acknowledge those who have researched the ILDR2 project over the years, specifically, Wendy Chung, Marija Dokmanovic-Chouinard, Elizabeth Watson, Maria Laura Cremona, and Kazuhisa Watanabe; their work laid the foundation for my efforts. I am additionally grateful to Maria Caterina de Rosa and Sarah Fleet who have worked alongside me to facilitate these discoveries. Finally, I thank my family for taking this journey with me and making it all worthwhile.

Chapter 1: Introduction

Chapter 1: Introduction

Diabetes mellitus

Diabetes mellitus is defined as a disease characterized by chronic hyperglycemia, due to insulin insufficiency [1]. Diabetes mellitus is classified into three disease types with different underlying causes but the same major symptom of hyperglycemia. Type 1 diabetes mellitus (T1D) - caused by autoimmune destruction of insulin-producing beta cells in the pancreas - and maturity onset diabetes of the young (MODY) - caused by loss-of-function mutations in specific genes responsible for glucose metabolism or insulin synthesis and secretion - account for 5-10% of all instances of diabetes mellitus. Greater than 90% of diabetes mellitus is classified as Type 2 (T2D) and is caused by failure of beta cells to produce sufficient insulin to meet the consequences of resistance of the body's metabolic organs to insulin action [2]. As the incipient disease progresses, increasing amounts of insulin are required to overcome this resistance and to maintain normal blood glucose levels. Eventually, beta cells become unable to meet the demand for insulin production and undergo apoptosis or dedifferentiation [3]. If left untreated, T2D results in chronic hyperglycemia and its complications of neuropathy, kidney disease and blindness. Often associated with obesity, T2D increases risk for developing other metabolic disorders such as fatty liver disease, hyperlipidemia, hypertension and cardiovascular disease [4]. Together classified as Metabolic Syndrome, these co-morbidities along with the complications of T2D have established it as a central metabolic disease and major health concern.

T2D is one of the most prevalent diseases worldwide, affecting 1 in 11 adults, and is predicted to become the 7th leading cause of death by the year 2030 (World Health Organization Diabetes Fact Sheet, June 2016, http://www.who.int/mediacentre/factsheets/fs312/en/). As such,

T2D is a significant public health burden across the globe. In the US alone, treatment for T2D and its complications costs ~$176 billion annually (Center for Disease Control 2014 National Diabetes Statistics report, https://www.cdc.gov/diabetes/data/statistics/2014statisticsreport.html). As the incidence of T2D continues to rise, there is an urgent need to better understand the causes of, and to develop treatments for, this disease.

There is a close and well-documented association of T2D with Western lifestyles, including diets high in refined sugars and fats but low in fiber, sedentary activities, and environmental pollutants [5]. However, while environmental factors may contribute to the risk for developing diabetes, they are not the sole determinants of disease. T2D also has a strong hereditary and genetic component. This is perhaps best illustrated by twin studies in which diabetes concordance between monozygotic and dizygotic twins was evaluated [6-8]. Monozygotic twins, who share the same genetics, were found to have ~76% concordance for T2D development [8] vs. 10% in dizygotic twins [7] who share the same intrauterine and familial environment, but have different genetics.

Large-scale genetic analyses of individuals and families segregating for T2D have contributed to the identification of several disease-associated genetic loci [9-12]. These studies have demonstrated repeatedly that genetic risk for T2D is primarily due to common variants with small effect size [9, 10]. However, despite the identification of numerous genetic loci [13-18] we are still able to attribute only 6-8% of the known T2D genetic risk [10, 12, 19], indicating that there are other genes contributing to T2D susceptibility that are yet to be identified.

Identifying T2D susceptibility genes

In 2008, Dokmanovic-Chouinard and colleagues published a study in which they intercrossed mouse strains with differing susceptibilities to diabetes in the context of obesity, with

the goal of identifying novel genetic predictors of T2D risk [20]. Obese C57/BL6J (B6) mice are resistant to developing diabetes [21] while DBA/2J (DBA) mice are diabetes -susceptible. Dokmanovic-Chouinard *et al*. intercrossed these mouse strains (also segregating for the *ob* gene) and identified a number of diabetes-susceptibility regions in the DBA genome, among which was a particularly strong (genetically and statistically) region on Chr. 1q23. Interestingly, this locus corresponds a region which in humans has been with associated T2D in several genome-wide association and linkage studies [22-24].

The Chr. 1 region was refined in B6.DBA *ob/ob* congenic animals to a 1.8Mb interval containing ~14 genes. Congenic mice segregating for DBA alleles in this variable interval exhibited hypoinsulinemic hyperglycemia and early reduction in beta cell proliferation leading to decreased beta cell mass in adults [20]. Expression of genes in the variable region was measured in congenic mice segregating for DBA vs. B6 alleles. The novel gene "*Lisch-like*" (re-named *Ildr2*) was found to display the most consistently decreased expression in DBA vs. B6 alleles in several tissues including liver, hypothalamus, islets and skeletal muscle [20]. These analyses strongly suggested that loss of *Ildr2* expression in DBA congenic mice was responsible for the diabetic phenotypes described above, and identified *Ildr2* as the likely causative gene in the Chr. 1 locus.

It should be noted that all congenic mice were studied in the context of either genetic ($Lep^{ob/ob}$) or diet-induced obesity. The absence of extreme obesity and/or leptin deficiency in later knockdown (KD) and knockout (KO) mouse models may explain some of the phenotypic differences between B6.DBA congenic mice and the various *Ildr2*-deficient models described below.

Immunoglobulin-like domain containing receptor (ILDR) family – structure and function

The first published reference to *Ildr2* describes the human homologue, *C1orf32*, identified in human retina in a screen for alternative transcriptional start sites in highly-expressed retinal genes [25]. The mouse *Ildr2* gene contains 10 exons which are alternatively spliced to produce 7 known isoforms [20, 26]. Isoform 1 is the full-length protein; isoforms 3 and 7 do not have a transmembrane domain, thus may function as cytosolic or secreted proteins. While *Ildr2* is ubiquitously expressed, specific isoforms predominate in different tissues. For example, isoform 2 is highly expressed in the brain, with low expression of isoform 4. Conversely, in the liver isoform 4 has much higher expression than isoform 2. Exons 1, 2, 3 and 10 are present in all known ILDR2 isoforms [26].

ILDR2 is a member of the immunoglobulin-like domain containing receptor (ILDR) family. Classified by structural similarity only, ILDR1/2/3 are Type 1 transmembrane receptor-like proteins with N-terminal immunoglobulin (IgG)-like domains, helical transmembrane domains, and C-terminal "tails" containing several putative signaling elements and binding sites [20].

ILDR3, also known as lipolysis-stimulated receptor (LSR), was the earliest identified ILDR family member. ILDR3 is a nominal lipoprotein remnant receptor activated by free fatty acids (FFAs) in the liver [27], and ILDR3-deficient mice exhibit hyperlipidemia consistent with decreased hepatic lipoprotein uptake [28, 29]. ILDR3 is also important for recruiting tricellulin for the formation of epithelial and endothelial tricellular tight junctions (tTJs) [30-32]. ILDR3 regulates cholesterol distribution in the brain [33] and may link cholesterol levels to amyloid stress in Alzheimer's disease [34]. ILDR3 also plays a role in blood-brain barrier (BBB) formation where it functions at tTJs to maintain BBB integrity [35].

ILDR1 has been implicated in autosomal recessive disorders of deafness in several families [36, 37], which has been linked to its function at epithelial tTJs [38]. *Ildr1*-deficient mice also exhibit specific hearing deficits due to loss of tTJ integrity in the inner ear [39-41]. ILDR1 may have a similar function in the kidney where tTJs help regulate water permeability [42]. ILDR1 also plays a role in sensing intestinal lipid to regulate cholecystokinin (CCK) secretion in the gut [43], which appears to be the only described role not linked to its location in tTJs.

Together, ILDR1/2/3 have recently been termed "angulins" due to their location at epithelial tTJs [38]. As described above, ILDR1 and ILDR3 appear to be critical for the integrity of tTJs in multiple tissues [32, 35, 41, 42]. However ILDR2 seems to have limited function in this capacity [38], which is consistent with previous findings placing ILDR2 at the endoplasmic reticulum (ER), rather than at the cellular membrane [26].

Location of ILDR2 in the endoplasmic reticulum membrane

ILDR1 and ILDR3 are expressed and localized to the plasma membrane. To determine the location of ILDR2 in the cell, fluorescently-labeled *Ildr2* was overexpressed in liver (Hepa1c1c7) and hypothalamic (GT1-7) cell lines along with markers for either the ER or the plasma membrane. Both C-terminal and N-terminal-tagged ILDR2 localized to the ER in both cell types [26], and did not change location in response to glucose, insulin, free fatty acids or low-density lipoprotein (LDL) in Hepa1c1c7 cells.

The location of ILDR2 in the ER membrane suggests a number of functional and mechanistic roles for this novel protein including regulation of various protein secretory pathways, such as lipid synthesis and secretion in the liver or insulin folding and secretion in beta cells, calcium homeostasis, or a role in ER stress and unfolded protein response (UPR) signaling

pathways. While ILDR2 may localize to the cell membrane in certain cell types or under specific conditions [38], further mechanistic studies suggest that its ER location is central to its function in metabolic diseases.

The ENU-mutagenized W87* *Ildr2*-deficient mouse

Since the identification of *Ildr2* as a candidate modifier of diabetes susceptibility, numerous attempts have been made to develop systemic and tissue-specific KD and KO models of *Ildr2*. One of the mouse models used to investigate the function of ILDR2 was an ENU-mutagenized mouse with a stop mutation at tryptophan-87 in the *Ildr2* gene sequence [20]. Located in exon 2, this mutation should cause severe truncation of *Ildr2* mRNA and degradation of any translated protein. Indeed, immunoblots of hypothalamic extracts from ENU-mutagenized (W87*) mice did not detect any ILDR2 protein [20]. W87* mice on a C3HebFeJ background were analyzed for diabetic phenotypes and showed decreases in beta cell replication similar to the B6.DBA congenic mice. However, there were only slight differences in insulin: glucose ratios and glucose tolerance between W87* and C3HebFeJ wild-type (WT) mice [20]. Additionally, 2D polyacrylamide gel (2D-PAGE) analysis of W87* hypothalamic and liver proteins revealed that several calcium binding and regulatory proteins were decreased in W87* mice, and suggested a role for ILDR2 in calcium homeostasis.

As described above, ILDR3 has been well-characterized as a lipoprotein receptor in the liver and *Ildr3*-deficient mice have defects in lipid homeostasis [29]. Hypothesizing that ILDR2 might be similarly involved in lipid metabolism, W87* mice were further characterized for additional metabolic phenotypes related to obesity and lipid metabolism. Low-fat chow fed W87* mice displayed increased adiposity vs. WT mice at 3 and 6 months, as well as increased fasted and

refed blood glucose levels. Serum cholesterol, low-density lipoprotein (LDL) and high-density lipoprotein (HDL) were also elevated in W87* mice. Hepatic triglyceride and cholesterol esters were slightly increased in W87* mice, but chylomicron clearance and hepatic VLDL secretion were unchanged in W87* vs. WT mice. These data suggested that lipid metabolism was dysregulated in W87* mice, but when hepatic *Ildr2* expression was measured, there was no difference in expression between W87* and WT mice. Further analyses revealed that some full-length *Ildr2* expression was retained in W87* mice, indicating that the stop mutation was not completely penetrant, and W87* mice were not true KOs.

The adenoviral-shRNA *Ildr2* KD mouse

Another *Ildr2*-deficient mouse was developed using an *Ildr2* short-hairpin RNA (shRNA). This shRNA was targeted again to exon 2 of the *Ildr2* gene sequence and cloned into an adenoviral construct [26]. Unlike the B6.DBA congenics or W87* mice, this KD model had a tissue-specific limitation in that adenovirus targets the liver almost exclusively. Aside from the liver phenotypes of W87* mice, which were shown to retain some *Ildr2* expression, there was no evidence that ILDR2 played any role in the liver. However, adenoviral-shRNA provided a way to investigate the mechanism of this novel gene in an *in vivo* setting.

Ildr2-shRNA adenovirus or a control *lacZ*-shRNA adenovirus were administered to 10-week-old B6 mice, which were then euthanized 3, 7, or 10 days post adenovirus infection. While major changes were not apparent after 3 days, by 7 days mice developed gross hepatic lipid accumulation which was even more striking at 10 days post adenovirus infection [26]. This hepatic steatosis was accompanied by hyperlipidemia, an HDL to VLDL shift in plasma lipoproteins, and widespread changes in hepatic lipid metabolic gene expression. Gene expression studies indicated

that at 3 days post-infection lipogenic genes were upregulated in livers of *Ildr2*-shRNA adenovirus-infected (ADKD) mice vs. controls, but by 10 days lipogenic genes were downregulated in ADKD mice [26]. These data suggested that lipogenesis is the primary pathway affected by *Ildr2* KD, and the steatosis observed at 10 days was the result of uncontrolled lipogenesis occurring at or around 3 days post-infection. Lipid synthesis genes might then have been downregulated at 10 days in response to excess lipid accumulation.

WT mice were also treated with adenoviruses over-expressing *Ildr2* or *Gfp* as a control. *Ildr2* overexpression (ADOX) had the opposite effect of KD, reducing hepatic lipid content in ADOX mice vs. controls [26]. Gene expression analysis revealed similar broad changes in lipid metabolic transcripts. However, in OX mice these genes were downregulated at 3 days post infection, and upregulated at 10 days after adenovirus administration. The converse changes in gene expression between these two time-points, as well as between ADKD vs. ADOX models suggests that lipogenic genes are tightly regulated to maintain a homeostatic balance and control hepatic lipid content.

Separate groups of C57BL/6J $Lep^{ob/ob}$ were included in both the KD and OX arms of these experiments. In both cases the phenotypes were consistent with results in WT mice. By 10 weeks of age $Lep^{ob/ob}$ mice had developed fatty liver, thus ADKD exacerbated their phenotype, while ADOX ameliorated the hepatic steatosis of $Lep^{ob/ob}$ mice [26].

Additional *Ildr2* overexpression experiments were performed in high-fat, high-fructose diet (HFHFD)-fed wild-type mice. Mice infected with ADOX for 10 days showed no difference in hepatic lipid content vs. control-infected mice. However, this may have been due to extensive fibrosis in the livers of HFHFD mice, which was absent in $Lep^{ob/ob}$ mice. *Ildr2* OX restored the albumin expression levels decreased by adenovirus infection and expression of specific UPR genes

- *Perk*, *eif2a*, and *Atf4* - were increased in ADOX mice, although activation (phosphorylation) of PERK and eIF2α was unchanged in ADOX mice vs. controls. In the aggregate, these *Ildr2* KD and OX experiments suggested that ILDR2 played a key role in the regulation of hepatic lipid metabolism.

Transcriptional regulation of *Ildr2* by USF1 and ER stress modulators

In addition to establishing *Ildr2*-deficient mouse models, efforts were also made to understand the molecular function of ILDR2 and to analyze how it modifies diabetes susceptibility. These studies were necessarily informed by the fatty liver phenotype of *Ildr2* ADKD mice and a desire to elucidate the mechanism of ILDR2 with respect to its putative role in hepatic lipid homeostasis.

In ADKD and ADOX mice, in addition to changes in lipid metabolic transcripts, several genes involved in the UPR were differentially regulated. Gene expression changes did not reflect a specific pattern of up- or down-regulation related to *Ildr2* KD or OX, but did suggest that these pathways were affected by *Ildr2* manipulation [26]. These results correlate with *in vitro* experiments in neuronal (GT1-7) and beta (BTC-6) cell lines as well as primary hepatocytes. *Ildr2* was knocked down for 48 hours via siRNA (GT1-7 and BTC-6) or adenoviral-shRNA (primary hepatocytes) and UPR genes were measured by quantitative PCR. Several genes were significantly up- or down-regulated as a result of *Ildr2* KD, but similar to the *in vivo* results, no clear pattern was observed to confirm activation or rescue of ER stress in the context of *Ildr2* KD.

To understand how *Ildr2* may be regulated by ER stress-related transcription factors, human and mouse Ildr2 promoter regions were analyzed for putative transcription factor binding sites. Two binding sites, an E-box motif and an ER stress response element (ERSE) were identified

in the human *ILDR2* promoter. Electro-mobility shift assays (EMSA) and luciferase assays confirmed that the transcription factor – upstream stimulatory factor 1 (USF1) – binds to the *Ildr2* promoter, activating its transcription. USF1 is a transcription factor that regulates several metabolic genes by binding E-box motifs in the promoter region of these genes [44-46]. *Ildr2* is upregulated by glucose treatment in HepG2 (human hepatoma) cell in a USF1-dependent manner. It has also been shown that *Ildr2* expression is increased in the livers of $Lep^{ob/ob}$ and HFD-fed mice compared to WT mice, but it is not known if this increase is USF1-dependent. In shRNA-mediated USF1 KD mice, *Ildr2* was decreased by 40% and hepatic triglyceride (TG) was increased 1.5-fold 3 days post-KD, but not as strikingly as seen in ADKD mice described earlier. These studies suggested that USF1 was probably not the single primary mechanism by which *Ildr2*'s action on lipid metabolism could be mediated.

DNA sequence comparisons between the human *ILDR2* promoter and the mouse *Bip* promoter revealed E-box and ERSE motifs in both. It was hypothesized that UPR transcription factors activating transcription factor 6 (ATF6) and X-box binding protein 1 (XBP1) which activate *Bip* might also bind the *Ildr2* promoter. This hypothesis was confirmed by EMSA and chromatin immunoprecipitation (ChIP) experiments, but measurement of *Ildr2* expression upon overexpression of ATF6 and XBP1 showed that these transcription factors suppress, rather than activate *Ildr2* expression. Further analysis of the transcription factor binding site revealed that the close alignment between the E-box and ERSE regions of the *Ildr2* promoter introduced physical constraints to USF1 and ATF6/XBP1 binding simultaneously. It is likely that competition between USF1 and ATF6/XBP1 determine which transcription factors bind and, consequentially, activate or inhibit *Ildr2*. This competitive binding could be a key aspect of how *Ildr2* expression is regulated.

Additional regulation of ILDR2 by UPR modulators was elucidated in co-immunoprecipitation experiments performed to identify novel binding interactions. Co-immunoprecipitation of ILDR2 and protein kinase R (PKR)-like ER kinase (*PERK*), an ER stress transducer, revealed ILDR2 cleavage products in PERK over-expressing cells. Since PERK has no known protease activity, the presence of these cleavage products suggests that ILDR2 is subject to protease degradation downstream of PERK, although whether the ILDR2 fragments are biologically active or, simply become substrates for proteosomal degradation, is unknown.

Co-immunoprecipitation of ILDR2 and inositol-requiring enzyme 1 (IRE1), the ER stress transducer of a second UPR pathway, resulted in complete degradation of *Ildr2* mRNA. Co-transfection with IRE1 mutants revealed that the endoribonuclease, but not the kinase, activity of IRE1 is required to degrade *Ildr2* transcript, suggesting that *Ildr2* may be a target of regulated IRE1-dependent decay (RIDD). RIDD describes a quality control mechanism in which IRE1 targets and degrades select mRNA transcripts [47]. RIDD appears to be activated separately from the UPR [48], and may be a parallel mechanism to decrease ER protein load. So *et al*. have shown that in states of excess lipid accumulation, RIDD may be activated to specifically degrade lipogenic transcripts and restore lipid homeostasis [49]. Additional studies indicated that *Ildr2* is down-regulated by chemical induction of ER stress both *in vivo* and *in vitro*, consistent with the results described above.

Taken together these studies highlight multiple pathways for modulating *Ildr2* expression at both the transcriptional and translational levels. Given its location in the ER membrane, ILDR2 may directly interact with ER stress transducers, but it appears to be regulated downstream of canonical ER stress molecules. If ER stress is a consequence of *Ildr2* manipulation, it would occur through feedback mechanisms as yet unknown.

ILDR2 specifically binds Apolipoprotein E

The ER localization of ILDR2 and the phenotype of *Ildr2* ADKD mice suggest that ILDR2 may be involved in lipid synthesis and secretion. Co-immunoprecipitation with various apolipoproteins showed that ILDR2 binds ApoE, but not ApoA, ApoB, or ApoC. ApoE specifically bound to a region in exon 7 of the ILDR2 amino acid sequence that has close similarity to the known binding site of ApoE in the amyloid beta protein [50]. Hypotheses can be made about the function of ILDR2-ApoE binding, e.g. ILDR2 may help to stabilize nascent lipoprotein particles in the ER. One part of the proposed mechanism that does not fit, however, is that exon 7 is in the C-terminal portion of ILDR2 which is predicted to be cytoplasmic, not lumenal. This orientation may suggest that ILDR2 interacts with ApoE in endosomes, helping to recycle ApoE through the endosomal pathway. Studies placing ILDR2 at the plasma membrane [38] may help explain the interaction of ILDR2 and ApoE, although the structurally-similar lipoprotein receptor, ILDR3, is thought to bind lipoproteins at its IgG-like domain.

ILDR2 interacts with ZNF70, a modulator of Notch signaling

In a tandem affinity purification screen to identify novel ILDR2 binding proteins ZNF70, a Kruppel C2H2-type zinc finger protein, was identified [51]. ZNF70 interacts with ZNF64 [52], a related zinc transcription factor and regulator of Notch signaling [53]. *Ildr2* shRNA KD in HEK293 cells resulted in nuclear translocation of ZNF70 and upregulation of *Hes1*, a canonical Notch target gene and transducer of Notch signaling [51]. This study suggests that ILDR2 may play a role in regulating Notch signaling pathways. Initially described as an essential developmental signaling mechanism [54], Notch has been implicated in metabolic and nutrient

signaling pathways as well [55, 56]. A link between ILDR2 and Notch signaling could account for ILDR2's putative roles in both hepatic lipid metabolism and diabetes development.

Summary and overview of chapters

Ildr2 was first identified as a candidate modifier of T2D in *Lep*$^{ob/ob}$ mice in which reduced *Ildr2* expression was associated with hypoinsulinemic hyperglycemia and other diabetic phenotypes [20]. The primary positioning of ILDR2 in the ER membrane [26] suggests that it might be involved in protein synthesis and secretion, calcium homeostasis or ER stress signaling, although ILDR2 has also been localized to the cell membrane and hypothesized to have a putative role in tight junction biology [38]. *Ildr2*-deficient mouse models have implicated *Ildr2* in lipid metabolism, evidenced by the striking hepatic steatosis observed in *Ildr2* KD mice, and the rescue of steatosis in *Lep*$^{ob/ob}$ mice by *Ildr2* overexpression [26].

Several mechanistic experiments have been performed to understand the molecular regulation of *Ildr2* and identify putative binding partners. These studies have shown that *Ildr2* is regulated by several UPR factors, binds ApoE, and is involved in modulating Notch signaling [51]. However a specific mechanism of ILDR2 that describes its function in modifying diabetes susceptibility or regulating lipid metabolism has yet to be elucidated.

The goal of my thesis work is to verify the functional role of ILDR2 in the liver and pancreas using tissue-specific *Ildr2* KO mouse models. Developed using the Cre-loxP system, these KO mice provide more specific, complete, and reliable *Ildr2* ablation than any of the *Ildr2*-deficient models previously used.

In **Chapter 2**, I describe several liver-specific and hepatocyte-specific Ildr2 KO mice, with either congenital (i.e. developmental) or acute *Ildr2* ablation. I find that liver-specific KO mice do

not recapitulate the fatty liver phenotypes of adenoviral shRNA-mediated *Ildr2* KD and do not exhibit any apparent metabolic abnormalities. I then show that the adenoviral *Ildr2* shRNA itself causes hepatic lipid accumulation regardless of *Ildr2* expression and suggest that off-target effects of the shRNA are responsible for the steatotic phenotype of ADKD mice. Following RNAseq of KD and KO liver samples, I propose gene candidates that may have been targeted by the *Ildr2* shRNA, and whose suppression could have contributed to the hepatic steatosis in ADKD mice. Experiments in this chapter confirm that ILDR2 does not play a major role in lipid metabolism.

In **Chapter 3**, I develop pancreas-specific and beta cell-specific *Ildr2* KO mice, with the goal of recapitulating the diabetic phenotype of the original *Ildr2*-hypomorphic, B6.DBA congenic mice and gaining a better understanding of the function of *Ildr2* in diabetes. I describe a phenotype of impaired glucose tolerance, reduced *in vivo* insulin secretion, and increased beta cell area in beta cell-specific (RIP2-cre) KO mice; while pancreas-specific (*Pdx*-cre) KO mice display impaired glucose tolerance, decreased *ex vivo* islet insulin secretion and calcium signaling, but normal islet morphology. I find that *Ildr2* expression is retained in the islets of beta cell-specific (RIP2-cre) KO mice, but is completely ablated in pancreas-specific (*Pdx*-cre) KOs, suggesting that expression in non-beta, islet cells is masking the beta cell KO of *Ildr2*. Expression studies indicating that *Ildr2* is expressed at low, though detectable, levels in beta cells corroborate this hypothesis. Since *Ildr2* appears to be expressed at similarly low levels in other islet endocrine cells, I hypothesize that islet macrophages could be the source of *Ildr2* expression in beta cell-specific KO mice, particularly as *Ildr2* is known to be expressed in liver and adipose tissue macrophages. However, confounding effects of the RIP2-cre construct may affect the phenotype of beta cell-specific *Ildr2* KO mice. I discuss how interpret these data in comparison with pancreas-specific KO mice.

In **Chapter 4**, I discuss how my work contributes to the general body of knowledge about ILDR2 and propose further studies to move this work forward. I revisit the identification of *Ildr2* as a diabetes susceptibility gene in *Lep*$^{ob/ob}$ and suggest that leptin may play a role in the biology of *Ildr2*. The *Ildr2*-related phenotypes observed in leptin-deficient mice – reduced beta cell mass with *Ildr2* hypomorphism, and rescue of hepatic steatosis by *Ildr2* overexpression – have not been replicated in WT mice, even with diet-induced obesity. I also review preliminary data proposing that *Ildr2* may regulate body mass composition, which could also involve leptin biology. Overall my work has clarified which phenotypes and proposed functions are or are not attributable to *Ildr2* expression, and established several mouse models enabling studies of the precise roles of ILDR2 in various tissues and disease states.

References

1. American Diabetes Association, *Diagnosis and Classification of Diabetes Mellitus.* Diabetes Care, 2014. **37**(Supplement 1): p. S81-S90.

2. Kahn, S.E., M.E. Cooper, and S. Del Prato, *Pathophysiology and treatment of Type 2 diabetes: Perspectives on the past, present and future.* Lancet, 2014. **383**(9922): p. 1068-1083.

3. Talchai, C., et al., *Pancreatic β Cell Dedifferentiation as a Mechanism of Diabetic β Cell Failure.* Cell, 2012. **150**(6): p. 1223-1234.

4. Liese, A.D., E.J. Mayer-Davis, and S.M. Haffner, *Development of the Multiple Metabolic Syndrome: An Epidemiologic Perspective.* Epidemiologic Reviews, 1998. **20**(2): p. 157-172.

5. Ershow, A.G., *Environmental Influences on Development of Type 2 Diabetes and Obesity: Challenges in Personalizing Prevention and Management.* Journal of Diabetes Science and Technology, 2009. **3**(4): p. 727-734.

6. Lo, S.S.S., et al., *Studies of diabetic twins.* Diabetes/Metabolism Reviews, 1991. **7**(4): p. 223-238.

7. Barnett, A.H., et al., *Diabetes in identical twins.* Diabetologia, 1981. **20**(2): p. 87-93.

8. Medici, F., et al., *Concordance rate for Type II diabetes mellitus in monozygotic twins: actuarial analysis.* Diabetologia, 1999. **42**(2): p. 146-150.

9. Scott, R.A., et al., *An Expanded Genome-Wide Association Study of Type 2 Diabetes in Europeans.* Diabetes, 2017.

10. Fuchsberger, C., et al., *The genetic architecture of type 2 diabetes.* Nature, 2016. **536**(7614): p. 41-47.

11. D. IAbetes Genetics Replication And Meta-analysis (DIAGRAM), C., et al., *Genome-wide trans-ancestry meta-analysis provides insight into the genetic architecture of type 2 diabetes susceptibility.* Nat Genet, 2014. **46**(3): p. 234-244.

12. Morris, A.P., et al., *Large-scale association analysis provides insights into the genetic architecture and pathophysiology of type 2 diabetes.* Nat Genet, 2012. **44**(9): p. 981-990.

13. Zeggini, E., et al., *Meta-analysis of genome-wide association data and large-scale replication identifies additional susceptibility loci for type 2 diabetes.* Nat Genet, 2008. **40**(5): p. 638-645.

14. Voight, B.F., et al., *Twelve type 2 diabetes susceptibility loci identified through large-scale association analysis.* Nat Genet, 2010. **42**(7): p. 579-589.

15. Qi, L., et al., *Genetic variants at 2q24 are associated with susceptibility to type 2 diabetes.* Human Molecular Genetics, 2010. **19**(13): p. 2706-2715.

16. Kooner, J.S., et al., *Genome-wide association study in individuals of South Asian ancestry identifies six new type 2 diabetes susceptibility loci.* Nat Genet, 2011. **43**(10): p. 984-989.

17. Cho, Y.S., et al., *Meta-analysis of genome-wide association studies identifies eight new loci for type 2 diabetes in east Asians.* Nat Genet, 2012. **44**(1): p. 67-72.

18. Shu, X.O., et al., *Identification of New Genetic Risk Variants for Type 2 Diabetes.* PLOS Genetics, 2010. **6**(9): p. e1001127.

19. Rich, S.S., *Diabetes: Still a geneticist's nightmare.* Nature, 2016. **536**(7614): p. 37-38.

20. Dokmanovic-Chouinard, M., et al., *Positional cloning of "Lisch-Like", a candidate modifier of susceptibility to type 2 diabetes in mice.* PLoS Genet, 2008. **4**(7): p. e1000137.

21. Clee, S.M. and A.D. Attie, *The genetic landscape of type 2 diabetes in mice.* Endocrine reviews, 2007. **28**(1): p. 48-83.

22. Das, S.K. and S.C. Elbein, *The search for type 2 diabetes susceptibility loci: The chromosome 1q story.* Current Diabetes Reports, 2007. **7**(2): p. 154-164.

23. Mondal, A.K., et al., *Allelic expression imbalance screening of genes in chromosome 1q21–24 region to identify functional variants for Type 2 diabetes susceptibility.* Physiological Genomics, 2013. **45**(13): p. 509-520.

24. Wang, H., et al., *Phenotypic and Molecular Evaluation of a Chromosome 1q Region with Linkage and Association to Type 2 Diabetes in Humans.* The Journal of Clinical Endocrinology & Metabolism, 2009. **94**(4): p. 1401-1408.

25. Roni, V., R. Carpio, and B. Wissinger, *Mapping of transcription start sites of human retina expressed genes.* BMC Genomics, 2007. **8**(1): p. 42.

26. Watanabe, K., et al., *ILDR2: an endoplasmic reticulum resident molecule mediating hepatic lipid homeostasis.* PLoS One, 2013. **8**(6): p. e67234.

27. Yen, F.T., et al., *Molecular Cloning of a Lipolysis-stimulated Remnant Receptor Expressed in the Liver.* Journal of Biological Chemistry, 1999. **274**(19): p. 13390-13398.

28. Yen, F.T., et al., *Lipolysis Stimulated Lipoprotein Receptor: A novel molecular link between hyperlidemia, weight gain, and atherosclerosis in mice.* Journal of Biological Chemistry, 2008. **283**(37): p. 25650-25659.

29. Narvekar, P., et al., *Liver-Specific Loss of Lipolysis-Stimulated Lipoprotein Receptor Triggers Systemic Hyperlipidemia in Mice.* Diabetes, 2009. **58**(5): p. 1040-1049.

30. Masuda, S., et al., *LSR defines cell corners for tricellular tight junction formation in epithelial cells.* Journal of Cell Science, 2011. **124**(4): p. 548-555.

31. Furuse, M., et al., *Lipolysis-stimulated lipoprotein receptor: a novel membrane protein of tricellular tight junctions.* Annals of the New York Academy of Sciences, 2012. **1257**(1): p. 54-58.

32. Iwamoto, N., T. Higashi, and M. Furuse, *Localization of Angulin-1/LSR and Tricellulin at Tricellular Contacts of Brain and Retinal Endothelial Cells in vivo.* Cell Structure and Function, 2014. **39**(1): p. 1-8.

33. Stenger, C., et al., *Brain region-specific immunolocalization of the lipolysis-stimulated lipoprotein receptor (LSR) and altered cholesterol distribution in aged LSR$^{+/-}$ mice.* Journal of Neurochemistry, 2012. **123**(4): p. 467-476.

34. Pinçon, A., et al., *Increased Susceptibility of Dyslipidemic LSR+/− Mice to Amyloid Stress is Associated with Changes in Cortical Cholesterol Levels.* Journal of Alzheimer's Disease, 2015. **45**(1): p. 195-204.

35. Sohet, F., et al., *LSR/angulin-1 is a tricellular tight junction protein involved in blood–brain barrier formation.* The Journal of Cell Biology, 2015. **208**(6): p. 703-711.

36. Borck, G., et al., *Loss-of-Function Mutations of ILDR1 Cause Autosomal-Recessive Hearing Impairment DFNB42.* The American Journal of Human Genetics, 2011. **88**(2): p. 127-137.

37. Mehrjoo, Z., et al., *Two novel mutations in ILDR1 gene cause autosomal recessive nonsyndromic hearing loss in consanguineous Iranian families.* Journal of Genetics, 2015. **94**(3): p. 483-487.

38. Higashi, T., et al., *Analysis of the 'angulin' proteins LSR, ILDR1 and ILDR2 – tricellulin recruitment, epithelial barrier function and implication in deafness pathogenesis.* Journal of Cell Science, 2013. **126**(4): p. 966-977.

39. Morozko, E.L., et al., *ILDR1 null mice, a model of human deafness DFNB42, show structural aberrations of tricellular tight junctions and degeneration of auditory hair cells.* Human Molecular Genetics, 2015. **24**(3): p. 609-624.

40. Sang, Q., et al., *ILDR1 deficiency causes degeneration of cochlear outer hair cells and disrupts the structure of the organ of Corti: a mouse model for human DFNB42.* Biology Open, 2015. **4**(4): p. 411-418.

41. Higashi, T., et al., *Deficiency of Angulin-2/ILDR1, a Tricellular Tight Junction-Associated Membrane Protein, Causes Deafness with Cochlear Hair Cell Degeneration in Mice.* PLOS ONE, 2015. **10**(3): p. e0120674.

42. Gong, Y., et al., *ILDR1 is important for paracellular water transport and urine concentration mechanism.* Proceedings of the National Academy of Sciences, 2017. **114**(20): p. 5271-5276.

43. Chandra, R., et al., *Immunoglobulin-like domain containing receptor 1 mediates fat-stimulated cholecystokinin secretion.* J Clin Invest, 2013. **123**(8): p. 3343-52.

44. Ribeiro, A., et al., *Cooperative Binding of Upstream Stimulatory Factor and Hepatic Nuclear Factor 4 Drives the Transcription of the Human Apolipoprotein A-II Gene.* Journal of Biological Chemistry, 1999. **274**(3): p. 1216-1225.

45. Wang, D. and H.S. Sul, *Upstream Stimulatory Factors Bind to Insulin Response Sequence of the Fatty Acid Synthase Promoter USF1 IS REGULATED.* Journal of Biological Chemistry, 1995. **270**(48): p. 28716-28722.

46. Wu, S., et al., *Upstream transcription factor 1 influences plasma lipid and metabolic traits in mice.* Human Molecular Genetics, 2010. **19**(4): p. 597-608.

47. Hollien, J., et al., *Regulated Ire1-dependent decay of messenger RNAs in mammalian cells.* The Journal of Cell Biology, 2009. **186**(3): p. 323-331.

48. Tam, Arvin B., Albert C. Koong, and M. Niwa, *Ire1 Has Distinct Catalytic Mechanisms for XBP1/HAC1 Splicing and RIDD.* Cell Reports, 2014. **9**(3): p. 850-858.

49. So, J.S., et al., *Silencing of lipid metabolism genes through IRE1alpha-mediated mRNA decay lowers plasma lipids in mice.* Cell Metab, 2012. **16**(4): p. 487-99.

50. Liu, Q., et al., *Mapping ApoE/Ab binding regions to guide inhibitor discovery.* Molecular BioSystems, 2011. **7**(5): p. 1693-1700.

51. Watanabe, K., et al., *ZNF70, a novel ILDR2-interacting protein, contributes to the regulation of HES1 gene expression.* Biochemical and Biophysical Research Communications, 2016. **477**(4): p. 712-716.

52. Ravasi, T., et al., *An Atlas of Combinatorial Transcriptional Regulation in Mouse and Man.* Cell, 2010. **140**(5): p. 744-752.

53. Sakamoto, K., et al., *Zfp64 participates in Notch signaling and regulates differentiation in mesenchymal cells.* Journal of Cell Science, 2008. **121**(10): p. 1613-1623.

54. Fortini, M.E., *Notch Signaling: The Core Pathway and Its Posttranslational Regulation.* Developmental Cell, 2009. **16**(5): p. 633-647.

55. Pajvani, U.B., et al., *Inhibition of Notch uncouples Akt activation from hepatic lipid accumulation by decreasing mTorc1 stability.* Nat Med, 2013. **19**(8): p. 1054-1060.

56. Szabat, M., et al., *Musashi expression in b-cells coordinates insulin expression, apoptosis and proliferation in response to endoplasmic reticulum stress in diabetes.* Cell Death and Dis, 2011. **2**: p. e232.

Chapter 2: The role of ILDR2 in hepatic lipid metabolism

Chapter 2: The role of ILDR2 in hepatic lipid metabolism

Introduction

Non-alcoholic fatty liver disease (NAFLD) is rapidly becoming the leading cause of liver failure and transplantation in the United States and is predicted to affect ~30% of adults in the US [1, 2]. Often considered the major liver manifestation of the metabolic syndrome, NAFLD is closely associated with obesity, diabetes and insulin resistance [3]. While the simple steatosis that defines NAFLD is relatively benign, it can progress to steatohepatitis (known as NASH) with inflammatory infiltration and fibrosis [4]. The physiological and metabolic factors that trigger progression from NAFLD to NASH remain poorly understood.

The *Ildr2* gene appeared to play a role in the development of NAFLD, possibly through mechanisms of endoplasmic reticulum (ER) stress. Initially characterized by positional genetics as a diabetes-susceptibility gene in mice [5], *Ildr2* knockdown via adenovirally-delivered shRNA (ADKD) resulted in gross hepatic steatosis and inflammation within 10 days of infection [6]. Gene expression analysis indicated initial upregulation of lipogenic transcripts (3 days post-adenovirus infection), followed by downregulation of these transcripts after development of steatosis, as well as differential expression of genes involved in the unfolded protein ("ER stress") response pathways [6].

In this previous study, we utilized an adenoviral delivery system to target short hairpin RNA (shRNA) to the liver in order to produce an acute liver-specific knockdown of *Ildr2*. In the absence (at the time) of any congenital *Ildr2* KO mouse models, the Adv-shRNA system allowed us to investigate the effects of acute knockdown of *Ildr2* transcripts in the liver. However this system is imperfect for several reasons: Adv infection is known to trigger inflammation [7-9]

which plays a role in the progression of NAFLD and development of NASH [10, 11]; Adv can also target other tissues and even though the majority is taken up by the liver [12-14], with potential consequences for gene expression in those tissues; and, finally, shRNA itself can have off-target effects and reduce expression of genes not intentionally targeted [15, 16].

Here we describe liver-specific *Ildr2* gene deletion models achieved using the Cre-loxP system. We discuss the development of liver-specific *Ildr2* knockout (KO) mice and further characterize them to understand the putative role of *Ildr2* in hepatic steatosis. The differing phenotypes observed in *Ildr2* Adv-shRNA KD vs. KO models highlight some of the pitfalls of using adenoviruses and shRNA for genetic manipulations; these are discussed below.

Results

Congenital, hepatocyte-specific *Ildr2* KO mice do not develop hepatic steatosis

To produce a conditional *Ildr2* knockout mouse model, we introduced loxP sites flanking exon 1 of the *Ildr2* gene (exon 1 is included in all seven known *Ildr2* transcript isoforms [5]) to create an *Ildr2* floxed mouse (*Ildr2*$^{fl/fl}$) (**Fig. 2.1A**). To explore the function of ILDR2 in the liver, we crossed *Ildr2*$^{fl/fl}$ mice with mice expressing Cre recombinase driven by the albumin promoter, obtaining hepatocyte-specific, congenital *Ildr2* knockout mice (see **Table 1** for nomenclature). *Ildr2* liver mRNA expression was reduced >99% in hepatocyte-specific *Ildr2* KO mice (*Ildr2*^{Alb} KO) compared to *Ildr2*$^{fl/fl}$ littermate controls (**Fig. 2.1B**). Although a subset of these mice retained *Ildr2* expression – indicating that the albumin-cre was not completely penetrant – these mice displayed no phenotypic differences vs. complete *Ildr2*^{Alb} KO mice.

When fed, ad libitum, low-fat (10% kcal as fat) chow diet, male, *Ildr2*^{Alb} KO mice did not differ in body weight and body composition from *Ildr2*$^{fl/fl}$ littermates (**Fig. 2.1C**). When fed *ad*

libitum a high-fat diet (HFD, 60% kcal as fat) from 6-23 weeks of age, they increased body weight and fat mass in tandem with their *Ildr2*$^{fl/fl}$ HFD-fed littermates (**Fig. 2.1D**).

23-week-old, chow-fed *Ildr2*^{Alb} KO mice did not exhibit hepatic steatosis by inspection, histology, or quantitative chemical analysis (**Fig. 2.1E-G**). They also had normal plasma triglyceride and total cholesterol concentrations (**Fig. 2.1H**). 23-week-old, HFD-fed mice showed hepatic lipid accumulation and elevated plasma lipids, but there was no significant difference between *Ildr2*^{Alb} KO mice and littermate controls fed the same HFD (**Fig. 2.1G,H**).

Acute, hepatocyte-specific *Ildr2* KO mice do not develop hepatic steatosis

The absence of steatosis in *Ildr2*^{Alb} KO mice led us to postulate that the congenital nature of the KO may have triggered gene compensation for the lack of ILDR2 during development. The mouse *albumin* gene is turned on at ~E10.5, about halfway through embryonic development [17], and Cre expression has been detected in fetal mouse hepatocytes from albumin-cre mice as early as E14.5, as immature cells begin to differentiate into hepatocytes [18]. Critical genes deleted at this stage in development may be functionally compensated by functionally similar [19-21]. Compensation for the loss of *Ildr2* in *Ildr2*^{Alb} KO mice could explain the absence of increased steatosis in the *Ildr2*^{Alb} KO mice.

To address this possibility, we designed a mouse model in which *Ildr2* can be acutely ablated in the adult animals, similar to the original Adv-shRNA KD mice (ADKD) mice. We utilized an adeno-associated virus (AAV) construct incorporating thyroid-binding globulin (TBG) promoter-driven Cre or GFP (control). This AAV8-TBG-Cre (developed by the Penn Vector Core) enables acute Cre expression specifically in hepatocytes, knocking out *Ildr2* (*Ildr2*^{AAV} KO). We injected AAV8-TBG-Cre intravenously into 13-week-old, chow-fed *Ildr2*$^{fl/fl}$ mice and examined

livers 10 days post-injection, in keeping with the timeline of development of steatosis in ADKD mice. Despite complete KO of *Ildr2* (**Fig. 2.2A**), livers of *Ildr2*^{AAV} KO mice were normal, showing no steatosis or any lipid metabolic abnormalities when compared to mice injected with the AAV8-TBG-GFP control construct (**Fig. 2.2B,C**). To determine the timing of AAV delivery and gene interruption, we measured hepatic mRNA expression of *Ildr2* isoforms 1 through 5 (only isoform 1 is shown) in mice at 2, 4, 6, 8, 10 and 12 days post injection and found that *Ildr2* transcript elimination occurred as early as 2 days post-injection (**Fig. 2.2D**). We also followed mice for 6 weeks after AAV infection, measuring plasma lipids at 20 days post-injection, then at 11-day intervals until sacrifice. *Ildr2*^{AAV} KO mice had normal plasma lipid levels and did not exhibit any hepatic lipid accumulation or metabolic abnormalities at 6 weeks post-injection with AAV (**Fig. 2.2E-G**).

Acute, Adv-mediated, liver-specific *Ildr2* KO mice do not develop hepatic steatosis

Next, we considered the possibility that loss of *Ildr2* in non-parenchymal liver cells may have contributed significantly to the steatosis observed in our original ADKD mice [6]. Both the AAV-TBG-Cre and the albumin-cre were designed to induce recombination and gene knockout specifically in hepatocytes. Hepatocytes comprise ~80% of liver tissue. However, the shRNA adenovirus used to produce ADKD mice would have targeted additional liver cell types, such as liver macrophages (Kupffer cells), stellate cells, and epithelial cells. While hepatic steatosis is defined as lipid accumulation in hepatocytes, non-parenchymal liver cells can accelerate the progression of steatosis to more advanced liver disease [22-25]. As resident liver macrophages, Kupffer cells initiate the immune response to metabolic injury, secreting pro-inflammatory chemokines and cytokines such as IL-1β and TNF, stimulating pro-apoptotic signaling pathways

in hepatocytes, and recruiting circulating immune cells to the liver [25-27]. Stellate cells play a key role in the induction of fibrosis in liver disease, and can transdifferentiate into myofibroblasts leading to increased production of collagen and extra-cellular matrix (ECM) factors [24, 27, 28].

To determine if *Ildr2* is expressed in non-parenchymal liver cells, or in hepatocytes only, primary hepatocytes and non-parenchymal cells were isolated from 12-week-old mice using liver collagenase digestion. Hepatocyte and non-hepatocyte cell fractions were separated by centrifugation [29]. Gene expression analysis of liver cell markers was used to confirm the cellular identity of each fraction. *Tbg*, a hepatocyte-specific marker, and *F4/80*, a macrophage-specific marker, were highly expressed in the hepatocyte and non-hepatocyte fractions, respectively (**Fig. 2.3A**). *Ildr2* was expressed in both cell fractions, although expression in the non-hepatocyte cell fraction was about one-third of *Ildr2* expression in the hepatocyte cell fraction (**Fig. 2.3A**). A caveat to this experiment is that because these cell fractions were sorted by centrifugation, there was some degree of cross-contamination as indicated by low level *Tbg* expression in the non-hepatocyte fraction, and *F4/80* expression in hepatocyte fraction (**Fig. 2.3A**). Microarray expression data from Xu, *et al*. also confirms that *Ildr2* is expressed in various populations of adipose tissue macrophages [30]. Taken together, these results suggest that *Ildr2* ablation in non-parenchymal liver cells could contribute to the steatotic phenotypes of the ADKD mice, and thus explain the lack of hepatic steatosis in the acute and chronic transgenic KO mice.

To address this question, we created another acute *Ildr2* KO model by employing an adenoviral-Cre construct rather than the AAV-TBG-Cre used previously. While the AAV-TBG-Cre construct is designed to impact only hepatocytes, adenoviral-Cre targets both parenchymal and non-parenchymal liver cells [31, 32]. 11-week-old, male, $Ildr2^{fl/fl}$ mice were intravenously injected with adenovirus-Cre or adenovirus-GFP as a control. Age-matched $Ildr2^{AAV}$ KO and

Ildr2^{AAV} GFP control mice were AAV-infected at the same time for parallel comparison. *Ildr2*^{Adv} KO mice were euthanized 10 days post-injection. No liver steatosis was seen despite complete *Ildr2* ablation in liver (**Fig. 2.3B,D,E**). *Ildr2*^{Adv} KO livers were heavier compared to *Ildr2*^{AAV} KO mice (**Fig. 2.3C**), and also showed histological evidence of inflammation. However as these phenotypes were also present in the *Ildr2*^{Adv} GFP control mice, we attributed them to the effects of adenovirus treatment (**Fig. 2.3F)** as has been documented previously [7-9].

Administration of adenoviral *Ildr2* shRNA causes TG accumulation in *Ildr2*^{Alb} KO mice

We have produced three distinct models of hepatic *Ildr2* KO: a congenital, hepatocyte-specific KO (*Ildr2*^{Alb} KO); an acute, hepatocyte-specific, KO (*Ildr2*^{AAV} KO); and an acute, liver-specific KO (*Ildr2*^{Adv} KO). None of these models showed the severe steatohepatitis observed in the adenoviral *Ildr2* shRNA (ADKD) model. Thus we were compelled to consider the possibility that some consequence of the shRNA antisense construct – unrelated primarily to the decrease in *Ildr2* expression – had caused the steatosis.

The original ADKD model was produced by treating mice with an adenovirally-delivered shRNA. Thus, either the adenovirus treatment or the shRNA itself may have triggered liver steatosis. We showed that adenoviral treatment alone does not cause hepatic steatosis, so we turned our attention to the shRNA. This shRNA was specifically designed to target exon 2 which is present in all isoforms of *Ildr2* mRNA; however, the construct may have had "off target" effects on other genes as discussed below [15, 16, 33].

To determine if other targets of the shRNA contributed to the KD liver phenotype, we infected *Ildr2*^{Alb} KO mice with the original KD adenoviral shRNA. Since these mice do not express *Ildr2* in the hepatocytes, any steatosis observed would be the result of shRNA targeting of other

genes affecting lipid metabolism. 10-week-old, male, *Ildr2*^{Alb} KO or *Ildr2*^{flfl} control mice were injected intravenously with the original adenovirus expressing *Ildr2* shRNA (ADKD), or with control adenovirus expressing lacZ shRNA (AD-lacZ). Mice were euthanized at 10 days post-adenovirus infection following a 24-hour fast. Gene expression analysis by qPCR confirmed that *Ildr2* was completely ablated in *Ildr2*^{Alb} KO mice, regardless of Adv treatment (**Fig. 2.4A**). In *Ildr2*^{flfl} mice, *Ildr2* shRNA (ADKD) reduced *Ildr2* mRNA by about 50% vs. AD-lacZ treated *Ildr2*^{flfl} mice (**Fig. 2.4A**). We did not observe gross liver steatosis, but chemical quantification of hepatic lipid content revealed that ADKD-treated mice had significantly increased hepatic TG compared to AD-lacZ treated mice, across both genotypes (3-fold in *Ildr2*^{flfl}, 1.5-fold in *Ildr2*^{Alb} KO) (**Fig. 2.4B**). Conversely, plasma TG was significantly decreased in *Ildr2* shRNA treated *Ildr2*^{Alb} KO and *Ildr2*^{flfl} mice vs. AD-lacZ treated mice for both genotypes (**Fig. 2.4C**).

These results confirm that the *Ildr2* shRNA is sufficient to cause hepatic steatosis despite the preexisting absence of *Ildr2*. *Ildr2* expression was reduced by 50% in *Ildr2* shRNA *Ildr2*^{flfl} mice, indicating that acute partial loss of *Ildr2* expression may contribute to the development of steatosis. However, the degree of steatosis and hypotriglyceridemia did not differ between *Ildr2* shRNA *Ildr2*^{flfl} and *Ildr2* shRNA *Ildr2*^{Alb} KO mice, suggesting that *Ildr2* expression is either irrelevant to the phenotype or has an equivalent effect at levels below a specific threshold, i.e. below 50%. In either case, the major trigger for hepatic steatosis is the *Ildr2* shRNA, not *Ildr2* ablation per se.

One explanation for these results is that the *Ildr2* shRNA targets another gene or genes involved in hepatic lipid metabolism, and that KD of this gene or genes is primarily responsible for the gross steatosis in the original *Ildr2* shRNA ADKD mice [6] and the less striking but still significantly increased TG accumulation observed here.

RNAseq analysis of *Ildr2* shRNA ADKD vs. *Ildr2*^{Adv} KO livers reveal candidate genes for shRNA off-target effects on hepatic steatosis

Our *Ildr2* shRNA was designed to target exon 2 of the *Ildr2* mRNA, which is present in all known *Ildr2* isoforms. The 19 base pair (bp) shRNA sequence, GTTCAAATCCTACTGCCAG, was tested for other gene targets by a BLAST search and no exact matches (other than *Ildr2*) were found. However it is possible that a partial match allowed for targeting and knockdown of a gene or genes essential for hepatic lipid homeostasis [16, 33].

We performed RNA sequencing to determine which additional gene(s) might have been knocked down by the *Ildr2* shRNA, and thus have contributed to development of steatosis in ADKD mice. Liver samples from ADKD and AD-lacZ mice (from our previously published ADKD study [6]) and *Ildr2*^{Adv} KO mice were analyzed (**Fig. 2.3**). ADKD and AD-lacZ samples were harvested 3 days post Adv infection to increase the likelihood of detection of primary effects of knocking down the gene versus secondary gene changes resulting from with hepatic steatosis per se.

RNAseq count expression data were analyzed with *DEseq*, a differential expression analysis program based on the negative binomial distribution [34]. Pairwise comparisons were made between *Ildr2* shRNA (ADKD), AD-lacZ; *Ildr2* shRNA ADKD and *Ildr2*^{Adv} KO; and AD-lacZ and *Ildr2*^{Adv} KO, using the Benjamini-Hochberg test for multiple comparisons. **Figure 2.5A-C** are "minus over average" (MA) scatter plots of differential gene expression profiles for each of the 3 comparisons. MA plots display the entire gene set, comparing fold change between samples (y-axis) to mean expression value (x-axis) with differentially expressed genes highlighted in red (**Figure 2.5A-C**). We screened for candidate genes that were: 1) significantly decreased in ADKD vs. AD-lacZ, 2), significantly decreased in ADKD vs. *Ildr2*^{Adv} KO, and, 3) unchanged between

AD-lacZ and *Ildr2*^{Adv} KO livers indicating a specific effect of the KD *Ildr2* shRNA shRNA (**Fig. 2.5D**). Using these parameters, we obtained a list of 102 candidate genes (**Table 2.2**).

This list was further refined by searching for genes that have been implicated in NAFLD genome-wide association studies (*Ppp1ca*) [35], genes associated with any other liver disease, (*Dguok, Ass1*) [36, 37], and obesity-related genes (*Slc39a1*) [38]. Since the shRNA was targeted to *Ildr2*'s exon 2 which encodes for an IgG domain, we identified genes that are part of the IgG-like family (*Neo1, Ptp4a1, Scn8a, Unc13b*); additionally, we found a gene located near *Ildr2* on chromosome 1 (*Pogk*) [5].

Initial BLAST searches of the shRNA sequence yielded no complete match apart from *Ildr2*. However, searching for truncated portions of the 19-bp sequence yielded a partial match in *Dgka*. *Dgka* is one of the 102 candidate genes identified by RNAseq analysis (**Table 2.2**) and has 63% homology to our *Ildr2* shRNA sequence. The first 12 bp of the shRNA sequence, GTTCAAATCCTA, are a sequence match to exon 4 of the *Dgka* mRNA. *Dgka* expression is downregulated by 50-60% in ADKD livers compared to AD-lacZ and *Ildr2*^{Adv} KO samples, suggesting that it could be targeted by the *Ildr2* shRNA. *Dgka* encodes diacylglycerol kinase alpha (DGKα), which functions to convert diacylglycerides (DAGs) to phosphatidic acid [39]. DAG species are increased in cell lines derived from *Dgka*-null mice [40] similar to increases in DAG species observed in steatotic human liver samples [41]. These data suggest that loss of *Dgka* expression could result in the steatosis observed in our ADKD mice. *In vitro* and *in vivo* studies are currently underway to characterize the function of *Dgka* and other genes to determine their functional relevance to understanding our *Ildr2* KD and KO mouse models.

Discussion and Conclusions

In this study we describe several mouse models developed in an effort to replicate the hepatic steatosis phenotype of adenoviral *Ildr2* shRNA KD mice. Using the Cre-loxP system, we created congenital and acute, hepatocyte-only and liver-specific *Ildr2* KO mice. However none of these KO models recapitulated the phenotype of hepatic steatosis observed in the adenoviral *Ildr2* shRNA KD mice [6].

RNAi-mediated knockdowns have been effectively used in many experimental settings, and are particularly useful in *in vitro* studies, and in instances in which a genetic knockout would be prohibitively expensive or difficult to make, or where the knockout is embryonically lethal. KD and KO models are generally quite similar, e.g., *Pparα* siRNA KD mice phenocopy the null transgenics [42] and connexin43 KO and KD mouse astrocytes have very similar transcriptional profiles [43].

However, discrepancies between RNAi-mediated KD and KO mouse models are not uncommon. siRNAs and shRNAs can have off-target effects due to sequence similarity to unintended gene targets [15, 16, 33]. As observed in this study, RNAi-mediated knockdowns can exhibit a more severe phenotype than the KO or null mutant due to disruption of the gene in a more mature developmental stage, when functional compensation is difficult [19, 44]. This situation has been documented, for example, for the genes *thymosin β4* and *Sprn*/*Prnp* in mice, and *ABP1* in *Arabdopsis thaliana* [45-47].

Our studies in which *Ildr2* shRNA KD adenovirus was administered to *Ildr2*^{Alb} KO mice revealed that lipid accumulation occurred with the adenovirus treatment, regardless of *Ildr2* genotype of the recipient mouse (**Fig. 2.4**). These experiments indicate that the hepatic lipid phenotype is due primarily to treatment with the adenovirus shRNA, rather than to loss of *Ildr2*

expression per se. They suggest that this shRNA targeted genes in addition to *Ildr2*. We identified *Dgka*, among other gene candidates, as a potential target of adenoviral *Ildr2* shRNA in ADKD mice. Given its homology to the shRNA sequence, its reduced expression in ADKD mice, and its functional role in lipid metabolism [40, 41, 48], we propose that shRNA targeting of *Dgka* could account for the difference in lipid accumulation between ADKD and KO mice.

Adenovirus is an efficient vector for introduction of gene products into cells both *in vitro* and *in vivo*. The most commonly used human adenovirus serotype 5 displays nearly exclusive liver tropism and thus is very useful for directing gene products to the liver. However, use of adenoviruses in these contexts can be problematic for several reasons. One obvious reason is that they are infectious agents and stimulate an inflammatory response in the infected cells [7-9]. This response can mask or confound the effect(s) of whatever biological molecules are being delivered to the cells. Another issue with adenovirus is that its tissue tropism, while fairly specific, is not exclusive, and it can affect tissues other than the target tissue [12]. Additionally, the various methods of measuring adenoviral titer make it difficult to control the amount of active virus that is administered in an experiment, which can lead to significant variation between experiments. The sensitivity of viral activity to temperature changes, i.e. freeze-thaw cycles, also contributes to experimental variability [49, 50].

The experiments described here highlight some of the difficulties in working with adenoviruses. In addition to possible aberrant RNAi gene targeting, the striking phenotype of the original ADKD mice may also have been due to adenovirus-induced inflammation and /or targeting of extra-hepatic tissues. While we confirmed that *Ildr2* expression was maintained in other tissues from ADKD mice [6], we cannot rule out that the Adv may have infected other organs. Another concern is that the amount of active *Ildr2* shRNA adenovirus used to infect *Ildr2*^{Alb}

KO mice may have decreased from its activity level at the time of ADKD infection. Although the same titer was used in both experiments ($3x10^{11}$ optical particle units (OPU)/mouse), this titer only measures adenovirus concentration, not viral activity. A reduction in adenoviral activity could also explain the difference in lipid accumulation and severity of steatosis between ADKD mice and *Ildr2*^{Alb} KO mice infected with Adv-*Ildr2* shRNA. Use of the appropriate controls enabled us to deconvolute the effects of *Ildr2* expression on hepatic steatosis in our various mouse models, however the confounds of using adenovirus as a primary delivery system remain a significant question.

We have conclusively shown that loss of *Ildr2* whether specifically in hepatocytes or in all liver cells is not sufficient to cause hepatic steatosis. We propose that interruption of other gene(s) played a major role in the steatotic phenotype of the original ADKD. RNA-seq identified 102 genes that are significantly reduced in ADKD mice vs. *Ildr2*^{Adv} KOs or AD-lacZ controls (**Table 2.2**). Of these candidates, one gene (*Dgka*) is a potential shRNA target with 67% sequence homology, thus the most likely candidate. Our future work will focus on studying the effects of *Dgka* KD, in addition to other candidates which could affect lipid metabolism in a manner similar to the ADKD. Hepatic lipid accumulation due to Adv-*Ildr2* shRNA treatment has only been observed in mice with at least a 50% reduction in *Ildr2* expression. Thus it is possible that KD of a candidate gene(s) interacts with *Ildr2* hypomorphism to induce steatosis.

Conclusions

In these experiments, we sought to build upon our previous work [6] which implicated ILDR2 in mechanisms of lipid metabolism and hepatic steatosis by gene KD via adenoviral shRNA. Development of more precise genetic models, including several liver-specific *Ildr2* KO mice, clarified that ILDR2 has a minimal function, if any, in hepatic lipid metabolism, and enabled us to

implicate other genes with potential roles in maintaining hepatic lipid homeostasis. This work has also highlighted some of the pitfalls in the use of both RNAi and viral delivery tools.

These studies indicate that contrary to the inferences reached based on acute shRNA-mediated KD, ILDR2 does not play a major role in hepatic lipid metabolism. *Ildr2* was initially identified as modifier of diabetes susceptibility [5] and ongoing work in our lab has confirmed its role in beta cell function and glucose homeostasis (**Chapter 3**). *Ildr2* is also highly expressed in the hypothalamus, leading us to postulate that it may also play a role in regulating body weight. Additionally, ILDR2, along with ILDR1 and ILDR3, are members of the angulin family which maintain membrane integrity at tricellular epithelial tight junctions [51, 52]. Our development of conditional KO mice to clarify the role of ILDR2 in the liver, can now facilitate the study of ILDR2 in various tissues and conditions, enabling a more complete understanding of this novel gene in mammalian biology.

Methods

Animal studies

We constructed a plasmid with loxP sites flanking exon 1 of the *Ildr2* gene. This plasmid was injected into BL6/129 hybrid ES cells which were then implanted into pseudopregnant dams. Mice segregating for the *Ildr2* floxed allele were backcrossed 9 times with C57BL6/J mice to produce mice with the floxed allele on a BL6 background. Mice possessing two floxed alleles ($Ildr2^{fl/fl}$) were bred with albumin-Cre mice (B6.Cg-Tg(Alb-cre)21Mgn/J, Jackson Labs stock #003574) until all offspring segregated for 2 floxed alleles and one or no copies of Cre.

All animal experiments were approved by Columbia Institutional and Animal Care Use Committee (Protocol# AAAH0707 and AAAR0416). Mice were housed in a 12-hr light/12hr-dark

vivarium, with ad libitum access to 5058 Purina PicoLab Mouse Diet 20 (9% fat) and water. High-fat diet (HFD) fed mice received chow with 60% kcal from fat (Research Diets #D12492i). Where noted, blood was collected by submandibular bleeding. Fat and lean mass were measured with an EchoMRI Analyzer (Bruker Optics), calibrated using mouse carcasses [53].

Adenovirus production and administration

Adenovirus expressing *Ildr2* shRNA was designed, produced and amplified as previously described [6]. Adenovirus expressing *lacZ* shRNA was designed and produced as previously described [6], but amplification and purification procedures were performed by Welgen, Inc (Worcester, MA). Mice were administered $3x10^{11}$ OPU/mouse via tail vein injection. AAV-TBG-Cre, AAV-TBG-eGFP, adenoviral-Cre, and adenoviral-GFP were obtained from the University of Pennsylvania Vector Core (Philadelphia, PA). Mice were administered $1.3x10^{11}$ genome copies/mouse via tail vein injection.

Lipid measurements in tissue and plasma

Capillary blood from submandibular bleeds was collected in heparinized tubes and centrifuged at 200 x *g* for 20 minutes at 4°C to separate plasma. Lipid extraction from liver was adapted from the Folch method [54]. Approximately 100 mg tissue were homogenized in 3 mL phosphate-buffered saline (PBS). 12 mL 2:1 chloroform: methanol ($CHCl_3$: MeOH) were added and mixture was vortexed twice for 15 seconds each. After centrifuging at 3000 rpm for 10 minutes, the organic lower layer was transferred to a 20-mL glass scintillation vial. An additional 10 mL 2:1 $CHCl_3$: MeOH were added to upper layer and vortexing and centrifugation were repeated. Organic lower layer was added to first extraction in scintillation vial. Solvent was dried down under nitrogen (N_2) gas followed by lipid resuspension in 1 mL 15% Triton X-100 in $CHCl_3$. Solvent was dried down again under N_2 gas and remaining lipid was resuspended in 1mL H_2O.

Triglyceride and total cholesterol in plasma and liver extracts were measured with the Infinity Triglycerides (Thermo Scientific) and Cholesterol E (Wako Diagnostics) kits, respectively.

Glycogen measurement

For glycogen extraction 100 mg tissue were homogenize in 1 mL H_2O on ice, boiled for 10 minutes, then centrifuged at 13,000 x *g* for 10 minutes to pellet insoluble material. Supernatant was transferred to a new tube and used for glycogen measurement. Glycogen was measured using a glycogen assay kit from Sigma-Aldrich (#MAK016)

Primary hepatocyte and non-parenchymal cell isolation

Primary hepatocytes were isolated as previously described [6]. The supernatant from primary hepatocyte centrifugation was collected and spun down at 500 x *g*, for 10 minutes at 4°C according to a protocol for isolating Kupffer cells by Xu, et al. [29]. The pelleted cells from this centrifugation were considered the non-parenchymal cell fraction.

Hematoxylin and eosin histology

Liver sections were fixed in aqueous zinc-buffered formalin (Anatech, Ltd.), sectioned and visualized by hematoxylin (Fisher) and eosin (Crystalgen) staining. Images were obtained using an Olympus IX73 inverted microscope (Olympus America).

RNA extraction, reverse transcription and quantitative PCR

Tissue and cell samples were homogenized in TRIzol® Reagent (Invitrogen) and extracted using the TRIzol® reagent protocol or the PureLink™ RNA Mini kit (Invitrogen). Reverse transcription was performed using the Transcriptor First Strand cDNA Synthesis kit (Roche). qPCR was performed using a Roche LightCycler® 480 instrument. qPCR primers are listed below. Tissue-specific standard curves for each gene (primer pair) were used to convert threshold crossing point (Cp) values to relative concentrations, which were then normalized to *36b4*, *Actb*, and/or

Gapdh expression. In instances in which standard curves were not used, Cp values are shown, with lower Cp values indication greater mRNA expression.

List of qPCR primers

Mouse gene name	**Forward primer (5' to 3')**	**Reverse primer (5' to 3')**
36b4	ACCTCCTTCTTCCAGGCTTTGG	CGAAGGAGAAGGGGGAGATGTT
Actb	CGGGCTGTATTCCCCTCCAT	GGGCCTCGTCACCCACATAG
Gapdh	CTGGAGAAACCTGCCAAGTATGATG	GAGACAACCTGGTCCTCAGTGTAGC
Ildr2 – isoform 1	GATTATGCCAGAGTGGGTGTTTGTC	CCCTGCTTCATACAAGGCCTGAG
Ildr2 – isoform 4	AACAGGGCTCGACGGTTAC	AACACCCACTCCAACACCAG
Tbg	GCAGAAAGGATGGGTTGAATTG	AAGTCAGCACTTTCAGCAAAGG
F480	CTTTGGCTATGGGCTTCCAGTC	GCAAGGAGGACAGAGTTTATCGTG

RNAseq

RNA was extracted from liver samples as detailed above and sample integrity was assessed with an Agilent 2100 Bioanalyzer with all samples having RIN numbers greater than 8.0, mRNA was isolated using a poly-A pulldown [55] and reverse transcription to generate cDNA. The cDNA was sequenced using single-ended sequencing on a HiSeq2000 according to manufacturer's recommendations (Illumina; San Diego, CA). The pass filter (PF) reads were mapped to mouse reference genome mm9 using TopHat (version 2.0.4). TopHat infers novel exon-exon junctions *ab initio*, and combines them with junctions from known mRNA sequences (refgenes) as the reference annotation [56]. For each read, we allowed up to 3 mismatches and 10 multiple

hits during the mapping. Analysis was performed using *DEseq* software with Benjamini-Hochberg test for multiple comparisons [34]. Differentially expressed genes were determined by adjusted p-values <0.05.

Figures and Tables

Figure 2.1: Albumin-cre, *Ildr2* KO mice do not develop hepatic steatosis

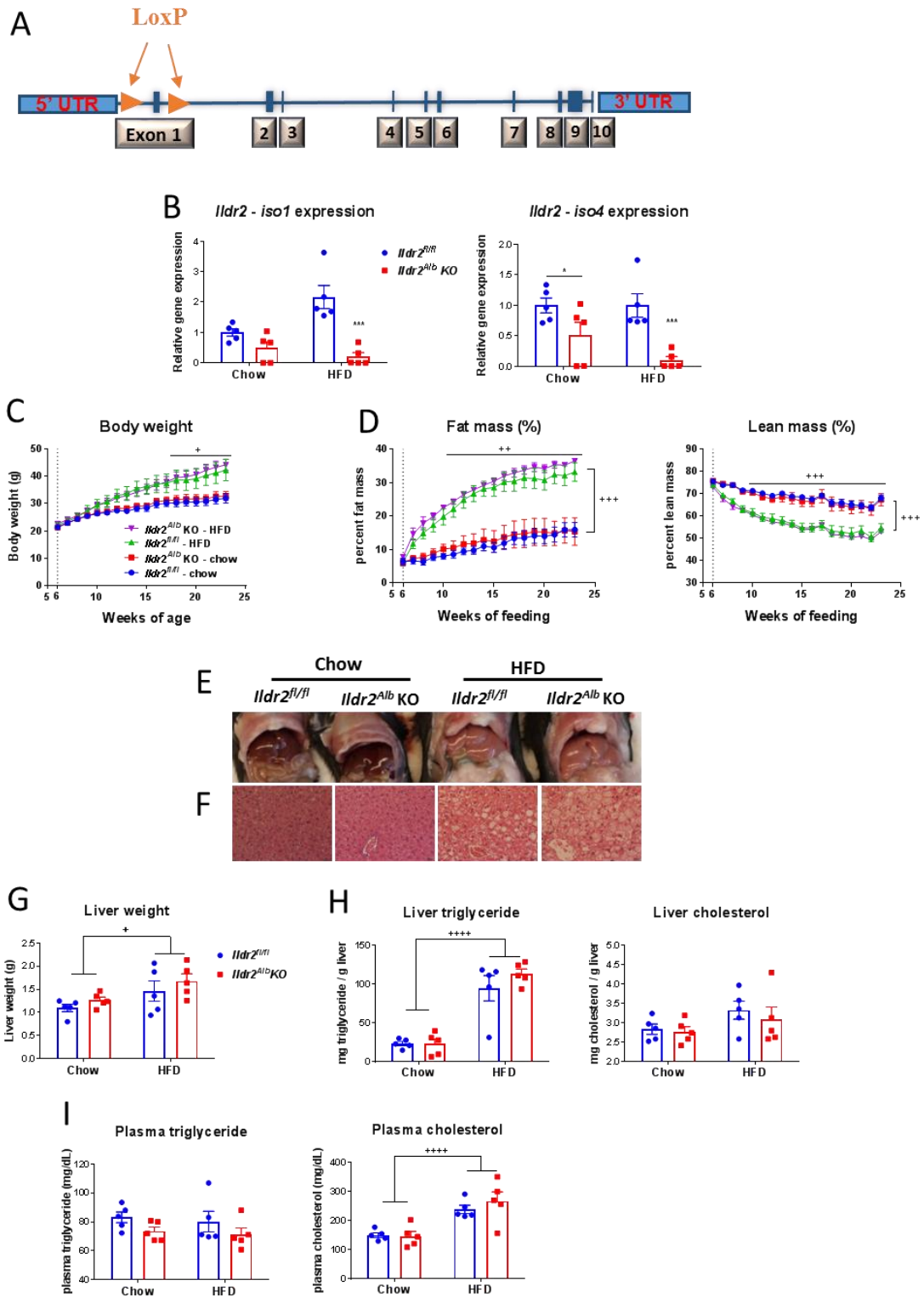

Figure 2.1: Albumin-cre, *Ildr2* KO mice do not develop hepatic steatosis.

(A) Schematic of the floxed *Ildr2* allele. (B) Expression of *Ildr2*, isoforms 1 and 4 in livers of 23-week old $Ildr2^{Alb}$ KO mice and littermate $Ildr2^{fl/fl}$ controls, fed chow or HFD for 17 weeks. Expression was measured by qPCR and normalized to *36b4*, *actb* and *Gapdh* expression. (C) Body weight curves of HFD and chow-fed, $Ildr2^{Alb}$ KO mice. (D) Percent fat mass and lean mass of HFD and chow-fed, $Ildr2^{Alb}$ KO mice measured weekly by NMR. (E) Photographs of livers excised from HFD and chow-fed, $Ildr2^{Alb}$ KO mice at 23 weeks of age and hematoxylin and eosin staining of representative liver sections at 50X magnification. (F) Liver weight at 23 weeks of age. (G) Liver triglyceride and total cholesterol content (measured in duplicate). (H) Plasma triglyceride and total cholesterol concentration at 23 weeks of age after a 4hr. fast. n=4-5 mice per group. Data are represented as mean ± standard error (SEM) * $p<0.05$, ** $p<0.01$, *** $p<0.001$ for $Ildr2^{Alb}$ KO vs. $Ildr2^{fl/fl}$ control. + $p<0.05$, ++ $p<0.01$, +++ $p<0.001$ for chow vs. HFD (Two-tailed t-test or two-way analysis of variance (ANOVA))

Figure 2.2: AAV *Ildr2* KO mice do not develop hepatic steatosis

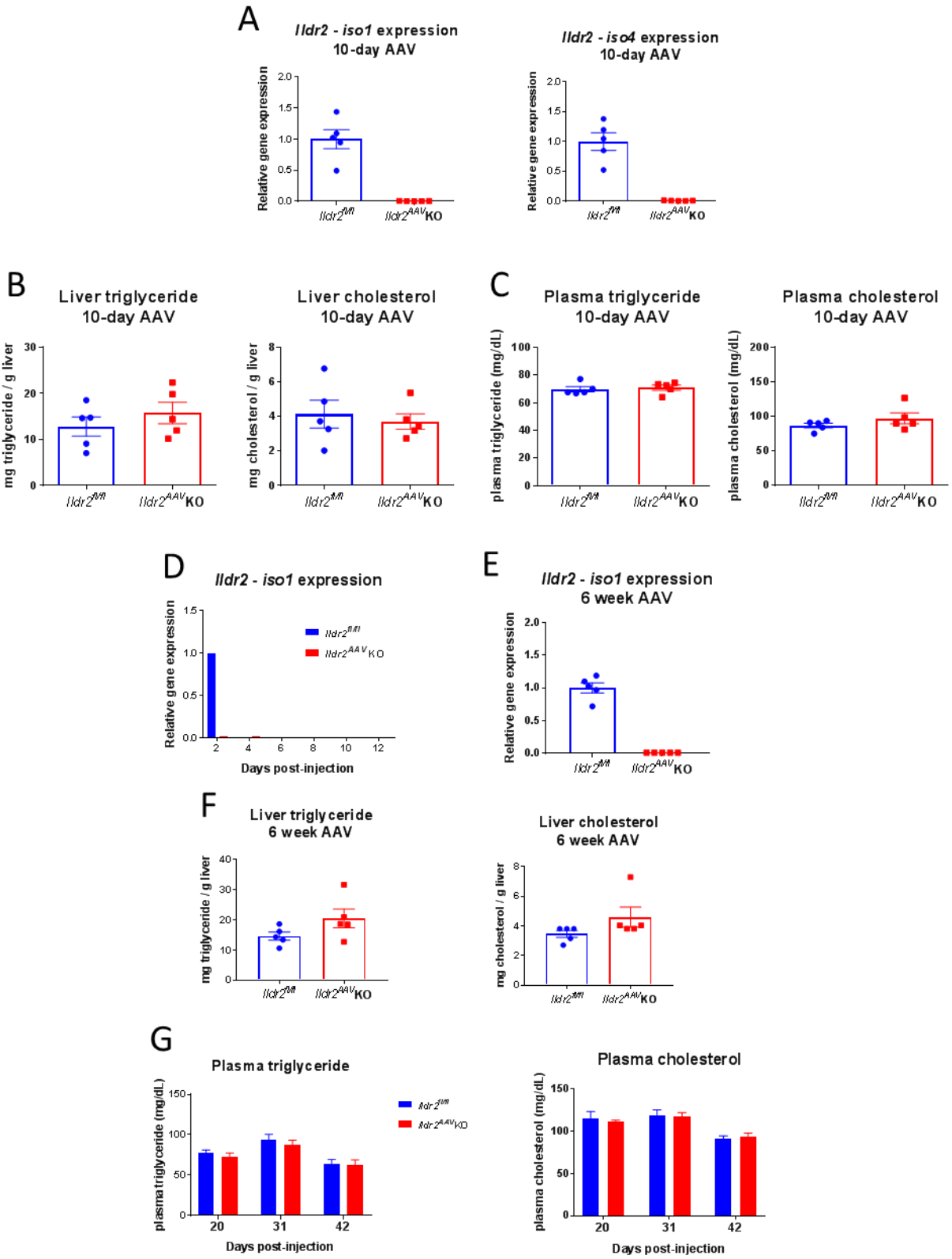

Figure 2.2: AAV *Ildr2* KO mice do not develop hepatic steatosis.

(A) qPCR expression of *Ildr2,* isoforms 1 and 4 in livers of 13-week old mice, 10 days after i.v. injection with AAV-TBG-Cre (*Ildr2*^{AAV} KO) or AAV-TBG-GFP (*Ildr2*$^{fl/fl}$ controls). (B) Liver triglyceride and total cholesterol content at 10 days. (C) Plasma triglyceride and total cholesterol concentration at 10 days. (D) qPCR expression of *Ildr2* (isoform 1 unless otherwise noted) in livers of 13-week old mice 2-12 days after i.v. injection with AAV-TBG-Cre (*Ildr2*^{AAV} KO). AAV-TBG-GFP was only administered for the 2-day timepoint (*Ildr2*$^{fl/fl}$ controls). (E) qPCR expression of *Ildr2* in livers of 18-week old mice, 6 weeks after AAV injection (F) Liver triglyceride and total cholesterol measurements. (G) Plasma triglyceride and total cholesterol concentration at 20, 31 and 42 days after AAV injection. Blood was collected after a 4hr fast. n=4-5 mice per group.

Figure 2.3: Adenoviral *Ildr2* KO mice do not develop hepatic steatosis

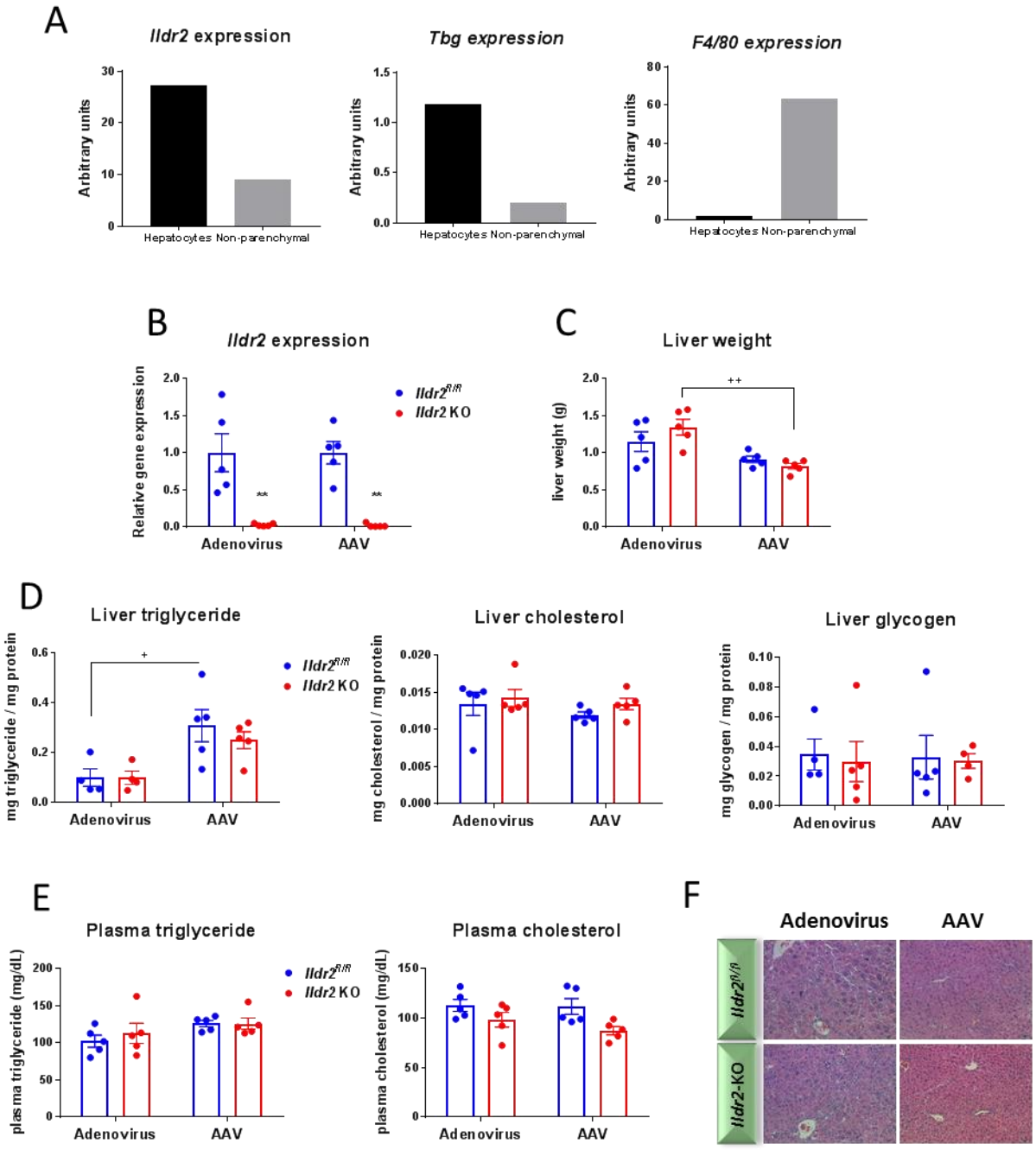

Figure 2.3: Adenoviral *Ildr2* KO mice do not develop hepatic steatosis.

(A) qPCR expression of *Ildr2*, *Tbg* and *F4/80* in hepatocyte or non-parenchymal cell fractions isolated from 12-week old wild-type (B6) mice. (B) qPCR expression of *Ildr2* in livers of 11-week old mice, 10 days after i.v. injection with adenoviral-Cre ($Ildr2^{Adv}$ KO), adenoviral-GFP ($Ildr2^{fl/fl}$ controls), AAV-TBG-Cre ($Ildr2^{AAV}$ KO) or AAV-TBG-GFP ($Ildr2^{fl/fl}$ controls). (C) Liver weights at sac. (D) Liver triglyceride, total cholesterol and glycogen content. (E) Plasma triglyceride and total cholesterol concentration at sac following a 12hr fast (F) Hematoxylin and eosin staining of representative liver sections at 20X magnification. n=4-5 mice per group. * $p<0.05$, ** $p<0.01$, *** $p<0.001$ for *Ildr2* KO vs. $Ildr2^{fl/fl}$ control. + $p<0.05$, ++ $p<0.01$, +++ $p<0.001$ for adenovirus vs. AAV.

Figure 2.4: Adenoviral *Ildr2* shRNA in *Ildr2* KO mice

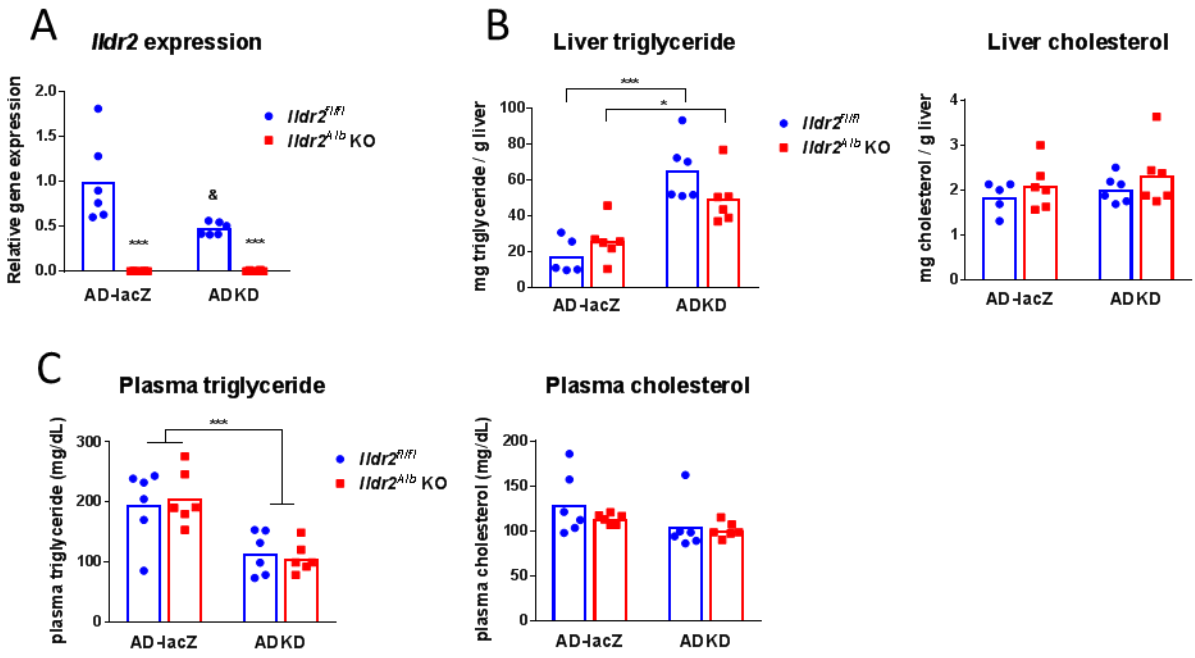

Figure 2.4: Adenoviral *Ildr2* shRNA in *Ildr2* KO mice.

(A) qPCR expression of *Ildr2* in livers of 10-week old mice *Ildr2*^{Alb} KO mice and littermate *Ildr2*$^{fl/fl}$ controls, 10 days after i.v. injection with ADKD or AD-lacZ. (B) Liver triglyceride and total cholesterol content. (C) Plasma triglyceride and total cholesterol concentration at sac following a 24hr fast. n=5-6 mice per group. * $p<0.05$, ** $p<0.01$, *** $p<0.001$ for *Ildr2*$^{fl/fl}$ vs. *Ildr2*^{Alb} KO; & $p<0.05$ for ADKD vs. AD-lacZ

Figure 2.5: RNAseq analysis

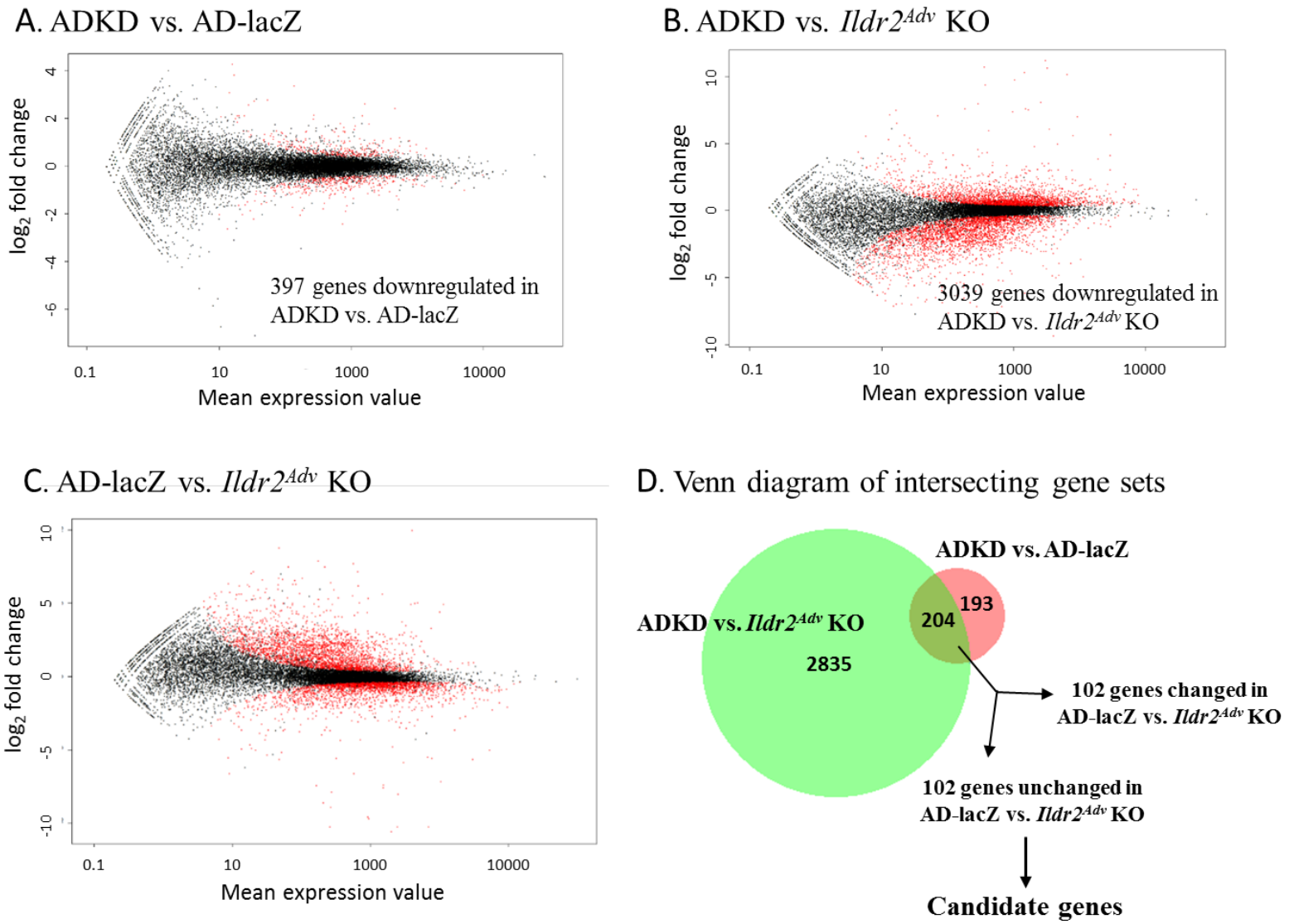

Figure 2.5: RNAseq analysis of AdV-KD vs. *Ildr2*^{Adv} KO livers reveals candidate genes for shRNA off-target effects.

"Minus over average" (MA) plots showing $\log_2$ fold change vs. normalized mean for each comparison. Red dots represent significantly upregulated or downregulated genes in (A) ADKD vs. AD-lacZ mice, (B) ADKD and *Ildr2*^{Adv} KO mice, (C) AD-lacZ vs. *Ildr2*^{Adv} KO mice. (D) Venn diagram illustrating how the 102 candidate genes were identified. The intersection of genes downregulated in ADKD mice vs. <u>*both*</u> AD-lacZ and *Ildr2*^{Adv} KO was 204. 102 of these genes were not significantly changed in AD-lacZ vs. *Ildr2*^{Adv} KO. These became the gene candidates (see **Table 2.2** for complete list).

Table 2.1: Mouse models - nomenclature and abbreviations

Mouse model	**Abbreviation in text**	**Cell type(s) targeted**	**Developmental Timing**	**Control used**	**Phenotype without *Ildr2* shRNA**	**Phenotype with *Ildr2* shRNA**
Adenoviral *Ildr2* shRNA	ADKD	All liver cells	Adult; acute	Adenoviral *lacZ* shRNA		Hepatic steatosis (extreme) and inflammation
Ildr2$^{fl/fl}$; albumin-cre	*Ildr2*^{Alb} KO	Hepatocytes	E14.5 (upon albumin expression)	*Ildr2*$^{fl/fl}$	No difference from control	Hepatic steatosis (mild) and inflammation
Ildr2$^{fl/fl}$; adeno-associated virus-thyroid-binding globulin (TBG)-cre	*Ildr2*^{AAV} KO	Hepatocytes	Adult; acute	*Ildr2*$^{fl/fl}$; AAV-TBG-GFP	No difference from control	
Ildr2$^{fl/fl}$; adenoviral-cre	*Ildr2*^{Adv} KO	All liver cells	Adult; acute	*Ildr2*$^{fl/fl}$; Adv-GFP	No difference from control	

Table 2.2: RNAseq candidate gene list

	Average counts			p_{adj} values		
Gene name	**AD-lacZ**	**ADKD**	***Ildr2*^{Adv} KO**	**ADKD vs. AD-lacZ**	**ADKD vs. *Ildr2*^{Adv} KO**	**AD-lacZ vs. *Ildr2*^{Adv} KO**
Rps19bp1	276	66	267	6.98E-28	6.49E-18	0.199
Slc39a1	1314	422	1524	2.18E-26	1.42E-31	1.000
Slc27a4	1167	473	1504	3.05E-23	1.04E-08	0.666
Aldh4a1	5277	2521	6117	3.63E-19	9.96E-05	1.000
Ndst1	3091	1464	3079	8.28E-19	1.37E-10	0.127
Ppp1ca	3562	1720	4107	4.12E-18	1.20E-15	0.956
Rab1b	3043	1523	3700	4.45E-16	3.10E-16	0.882
2900097C17Rik	1326	662	1417	2.73E-14	5.36E-10	0.478
Ptp4a1	529	246	558	4.76E-13	1.85E-06	0.463
6330578E17Rik	2685	1434	2716	5.05E-13	2.98E-07	0.174
Tbc1d13	852	426	1090	1.00E-12	5.29E-15	0.571
Ubfd1	972	494	1155	1.28E-12	3.30E-12	1.000
Gm98	1354	708	1630	1.54E-12	1.30E-12	0.948
Tmem123	1090	563	1404	2.37E-12	5.18E-15	0.520
Nt5dc2	336	151	374	1.68E-11	2.06E-09	0.819
Neo1	671	345	676	7.21E-11	1.09E-05	0.224
Sumf2	291	135	290	9.58E-10	8.90E-06	0.283
Acpl2	266	124	338	4.16E-09	9.22E-11	0.711
Pcgf2	181	79	210	2.44E-08	2.32E-04	1.000
Cpsf2	783	448	841	4.44E-08	9.82E-06	0.539
Wfdc2	201	59	190	5.30E-08	6.97E-09	0.260
Ccdc50	1569	946	2019	7.78E-08	1.72E-10	0.518
Tspan4	626	359	772	1.70E-07	1.80E-04	0.876
Reck	81	27	87	4.09E-07	6.94E-06	0.776
Pef1	1057	642	1345	4.99E-07	3.00E-09	0.599
Scpep1	1018	618	1254	5.33E-07	2.74E-08	0.814
Diablo	560	326	548	7.33E-07	2.44E-03	0.148
Icmt	1088	675	1172	1.65E-06	1.36E-04	0.535
Celf1	3216	2074	3415	1.96E-06	4.12E-04	0.405
Dgka	**160**	**75**	**187**	**2.38E-06**	**1.57E-06**	**1.000**
Ssu72	986	613	1306	2.66E-06	1.26E-09	0.360

Stat6	1590	1019	1825	4.42E-06	1.33E-05	0.946
Chtf8	1247	792	1459	4.68E-06	5.19E-06	1.000
Dpp8	1734	1118	1816	5.03E-06	1.21E-03	0.352
Ipo5	1941	1256	2423	5.06E-06	2.05E-04	0.748
Snx4	802	500	980	6.65E-06	6.53E-07	0.884
1810011O10Rik	785	491	927	7.77E-06	4.37E-06	1.000
Trappc9	395	232	451	8.09E-06	2.62E-05	0.930
Erp29	949	602	1228	8.70E-06	2.19E-08	0.489
Eif3h	2005	1332	2224	2.32E-05	3.12E-04	0.712
Pja2	1062	693	1459	3.17E-05	1.63E-09	0.191
Arl4d	531	312	756	4.58E-05	8.90E-05	0.370
Cdt1	233	121	366	5.32E-05	6.90E-05	0.207
Rab34	205	97	260	6.48E-05	3.52E-09	0.749
Pogk	155	82	225	7.69E-05	6.56E-09	0.216
Gtf3c1	1771	1062	1764	9.27E-05	1.34E-03	0.140
Pofut1	410	255	540	1.02E-04	2.24E-07	0.454
Atr	601	389	716	1.29E-04	8.64E-05	1.000
Tbc1d20	807	534	894	1.38E-04	1.04E-03	0.733
Rpa2	295	155	341	1.44E-04	6.00E-04	1.000
Nol3	24	4	36	1.49E-04	1.04E-07	0.533
Psmd14	1404	955	1472	1.54E-04	9.94E-03	0.359
Tax1bp3	72	30	82	1.58E-04	2.18E-04	0.969
Tab2	1916	1221	2563	1.77E-04	2.59E-10	0.272
Cenpm	148	62	167	1.77E-04	6.02E-07	0.915
Adss	1756	1163	2309	1.97E-04	5.07E-04	0.602
Zdhhc2	178	74	216	1.97E-04	2.57E-04	1.000
Ern1	836	554	886	2.51E-04	5.07E-03	0.454
Sox12	129	68	142	2.55E-04	3.50E-03	0.850
Slc4a4	3541	2086	3876	2.74E-04	5.33E-07	0.621
Setd8	1595	1039	1698	2.80E-04	1.04E-03	0.440
S100a16	385	245	425	2.90E-04	1.66E-03	0.753
Rassf5	334	210	429	3.19E-04	4.41E-06	0.623
Tmem189	331	208	364	3.42E-04	1.95E-03	0.751
Plod3	447	290	618	3.49E-04	6.00E-08	0.220
Scn8a	38	12	46	4.04E-04	1.18E-04	1.000
Pcnxl3	1147	795	1261	5.32E-04	4.14E-03	0.677
Akap11	1114	771	1316	5.49E-04	2.44E-04	1.000

2310022B05Rik	445	291	599	5.60E-04	5.46E-07	0.336
Vps39	584	391	754	5.91E-04	4.03E-06	0.543
Nacc1	1123	783	1361	7.35E-04	9.58E-05	0.911
Zswim7	182	107	196	7.37E-04	5.19E-03	0.680
Entpd5	11076	7174	13493	7.81E-04	9.33E-08	0.877
Ass1	4516	2710	8270	8.68E-04	2.85E-03	0.133
Pip4k2c	656	449	870	9.94E-04	1.80E-06	0.382
Dguok	231	144	250	1.15E-03	6.84E-03	0.693
Hfe	1107	783	1321	1.41E-03	4.08E-04	1.000
Atg16l2	212	133	238	2.03E-03	3.74E-03	0.892
P4hb	21192	15697	28758	2.26E-03	1.49E-05	0.181
Ctsz	4039	2972	4668	2.40E-03	2.43E-03	0.977
P4ha2	131	59	153	2.61E-03	2.92E-03	1.000
Slc34a2	47	13	38	2.86E-03	6.03E-03	0.350
Nle1	85	45	123	3.35E-03	5.77E-06	0.358
Grina	3684	2736	4162	3.76E-03	8.64E-03	0.835
Gnl3l	445	311	630	5.38E-03	8.05E-07	0.155
Unc13b	258	132	309	5.41E-03	3.97E-06	0.998
Tesk1	476	333	563	5.89E-03	1.98E-03	1.000
Mcm3	371	248	546	6.06E-03	4.12E-03	0.346
Maged1	2143	1603	2458	6.93E-03	8.08E-03	0.938
Frmd8	522	359	738	6.97E-03	1.74E-07	0.139
Eaf1	1713	1276	2136	7.07E-03	7.08E-04	0.725
Inppl1	1205	890	1596	7.12E-03	1.70E-05	0.351
4732418C07Rik	478	338	563	7.12E-03	3.10E-03	1.000
Slk	1319	980	1676	8.11E-03	1.49E-04	0.606
Comtd1	99	57	151	8.13E-03	1.72E-06	0.163
Dock8	823	553	1011	8.68E-03	1.93E-05	0.848
Pdia4	4016	2883	4695	8.70E-03	5.53E-04	1.000
Echdc3	948	700	1165	9.08E-03	7.53E-04	0.828
Galns	352	246	490	9.20E-03	6.04E-06	0.228
1110008P14Rik	390	275	474	9.37E-03	1.52E-03	0.928
Edem1	3313	2515	4237	9.87E-03	1.16E-04	0.533
AI597479	322	223	410	9.87E-03	3.30E-04	0.684

References

1. Angulo, P., *Nonalcoholic Fatty Liver Disease.* New England Journal of Medicine, 2002. **346**(16): p. 1221-1231.

2. Neuschwander-Tetri, B.A. and S.H. Caldwell, *Nonalcoholic steatohepatitis: Summary of an AASLD Single Topic Conference.* Hepatology, 2003. **37**(5): p. 1202-1219.

3. Younossi, Z.M., et al., *Global epidemiology of nonalcoholic fatty liver disease—Meta-analytic assessment of prevalence, incidence, and outcomes.* Hepatology, 2016. **64**(1): p. 73-84.

4. Farrell, G.C. and C.Z. Larter, *Nonalcoholic fatty liver disease: From steatosis to cirrhosis.* Hepatology, 2006. **43**(S1): p. S99-S112.

5. Dokmanovic-Chouinard, M., et al., *Positional cloning of "Lisch-Like", a candidate modifier of susceptibility to type 2 diabetes in mice.* PLoS Genet, 2008. **4**(7): p. e1000137.

6. Watanabe, K., et al., *ILDR2: an endoplasmic reticulum resident molecule mediating hepatic lipid homeostasis.* PLoS One, 2013. **8**(6): p. e67234.

7. Liu, Q. and D.A. Muruve, *Molecular basis of the inflammatory response to adenovirus vectors.* Gene Ther, 2003. **10**(11): p. 935-940.

8. Muruve, D.A., et al., *Adenoviral Gene Therapy Leads to Rapid Induction of Multiple Chemokines and Acute Neutrophil-Dependent Hepatic Injury in Vivo.* Human Gene Therapy, 1999. **10**(6): p. 965-976.

9. Worgall, S., et al., *Innate Immune Mechanisms Dominate Elimination of Adenoviral Vectors Following In Vivo Administration.* Human Gene Therapy, 1997. **8**(1): p. 37-44.

10. Ganz, M. and G. Szabo, *Immune and inflammatory pathways in NASH.* Hepatology International, 2013. **7**(2): p. 771-781.

11. Tilg, H. and A.R. Moschen, *Evolution of inflammation in nonalcoholic fatty liver disease: The multiple parallel hits hypothesis.* Hepatology, 2010. **52**(5): p. 1836-1846.

12. Wood, M., et al., *Biodistribution of an adenoviral vector carrying the luciferase reporter gene following intravesical or intravenous administration to a mouse.* Cancer Gene Therapy, 1999. **6**(4): p. 367-372.

13. Beatty, M.S. and D.T. Curiel, *Adenovirus Strategies for Tissue-Specific Targeting.* Advances in cancer research, 2012. **115**: p. 39-67.

14. Shayakhmetov, D.M., et al., *Analysis of Adenovirus Sequestration in the Liver, Transduction of Hepatic Cells, and Innate Toxicity after Injection of Fiber-Modified Vectors.* Journal of Virology, 2004. **78**(10): p. 5368-5381.

15. Jackson, A.L., et al., *Expression profiling reveals off-target gene regulation by RNAi.* Nat Biotech, 2003. **21**(6): p. 635-637.

16. Jackson, A.L., et al., *Widespread siRNA "off-target" transcript silencing mediated by seed region sequence complementarity.* RNA, 2006. **12**(7): p. 1179-1187.

17. Meehan, R.R., et al., *Pattern of serum protein gene expression in mouse visceral yolk sac and foetal liver.* The EMBO Journal, 1984. **3**(8): p. 1881-1885.

18. Weisend, C.M., et al., *Cre activity in fetal albCre mouse hepatocytes: Utility for developmental studies.* genesis, 2009. **47**(12): p. 789-792.

19. Rossi, A., et al., *Genetic compensation induced by deleterious mutations but not gene knockdowns.* Nature, 2015. **524**(7564): p. 230-233.

20. Hagelkruys, A., et al., *A single allele of Hdac2 but not Hdac1 is sufficient for normal mouse brain development in the absence of its paralog.* Development, 2014. **141**(3): p. 604-616.

21. Deconinck, A.E., et al., *Utrophin-Dystrophin-Deficient Mice as a Model for Duchenne Muscular Dystrophy.* Cell, 1997. **90**(4): p. 717-727.

22. Kolios, G., V. Valatas, and E. Kouroumalis, *Role of Kupffer cells in the pathogenesis of liver disease.* World Journal of Gastroenterology : WJG, 2006. **12**(46): p. 7413-7420.

23. Carpino, G., et al., *Role of Hepatic Progenitor Cells in Nonalcoholic Fatty Liver Disease Development: Cellular Cross-Talks and Molecular Networks.* International Journal of Molecular Sciences, 2013. **14**(10): p. 20112-20130.

24. Washington, K., et al., *Hepatic stellate cell activation in nonalcoholic steatohepatitis and fatty liver.* Human Pathology, 2000. **31**(7): p. 822-828.

25. Magee, N., A. Zou, and Y. Zhang, *Pathogenesis of Nonalcoholic Steatohepatitis: Interactions between Liver Parenchymal and Nonparenchymal Cells.* BioMed Research International, 2016. **2016**: p. 11.

26. Tacke, F. and H.W. Zimmermann, *Macrophage heterogeneity in liver injury and fibrosis.* Journal of Hepatology, 2014. **60**(5): p. 1090-1096.

27. Luedde, T. and R.F. Schwabe, *NF-kB in the liver - linking injury, fibrosis and hepatocellular carcinoma.* Nat Rev Gastroenterol Hepatol, 2011. **8**(2): p. 108-118.

28. Pradere, J.-P., et al., *Hepatic macrophages but not dendritic cells contribute to liver fibrosis by promoting the survival of activated hepatic stellate cells in mice.* Hepatology, 2013. **58**(4): p. 1461-1473.

29. Xu, F., et al., *Preparation of Kupffer cell enriched non-parenchymal liver cells with high yield and reduced damage of surface markers by a modified method for flow cytometry.* Cell Biology International, 2013. **37**(4): p. 284-291.

30. Xu, X., et al., *Obesity Activates a Program of Lysosomal-Dependent Lipid Metabolism in Adipose Tissue Macrophages Independently of Classic Activation.* Cell Metabolism, 2013. **18**(6): p. 816-830.

31. Alemany, R., K. Suzuki, and D.T. Curiel, *Blood clearance rates of adenovirus type 5 in mice.* Journal of General Virology, 2000. **81**(11): p. 2605-2609.

32. Tao, N., et al., *Sequestration of Adenoviral Vector by Kupffer Cells Leads to a Nonlinear Dose Response of Transduction in Liver.* Molecular Therapy, 2001. **3**(1): p. 28-35.

33. Birmingham, A., et al., *3' UTR seed matches, but not overall identity, are associated with RNAi off-targets.* Nat Meth, 2006. **3**(3): p. 199-204.

34. Anders, S. and W. Huber, *Differential expression analysis for sequence count data.* Genome Biology, 2010. **11**(10): p. R106.

35. Speliotes, E.K., et al., *Genome-Wide Association Analysis Identifies Variants Associated with Nonalcoholic Fatty Liver Disease That Have Distinct Effects on Metabolic Traits.* PLOS Genetics, 2011. **7**(3): p. e1001324.

36. Dimmock, D.P., et al., *Clinical and molecular features of mitochondrial DNA depletion due to mutations in deoxyguanosine kinase.* Human Mutation, 2008. **29**(2): p. 330-331.

37. Gao, H.-Z., et al., *Identification of 16 novel mutations in the argininosuccinate synthetase gene and genotype–phenotype correlation in 38 classical citrullinemia patients.* Human Mutation, 2003. **22**(1): p. 24-34.

38. Speliotes, E.K., et al., *Association analyses of 249,796 individuals reveal 18 new loci associated with body mass index.* Nat Genet, 2010. **42**(11): p. 937-948.

39. Xie, S., N. Naslavsky, and S. Caplan, *Diacylglycerol kinases in membrane trafficking.* Cellular Logistics, 2015. **5**(2): p. e1078431.

40. Milne, S.B., et al., *Dramatic Differences in the Roles in Lipid Metabolism of Two Isoforms of Diacylglycerol Kinase.* Biochemistry, 2008. **47**(36): p. 9372-9379.

41. Gorden, D.L., et al., *Increased Diacylglycerols Characterize Hepatic Lipid Changes in Progression of Human Nonalcoholic Fatty Liver Disease; Comparison to a Murine Model.* PLOS ONE, 2011. **6**(8): p. e22775.

42. De Souza, A.T., et al., *Transcriptional and phenotypic comparisons of Ppara knockout and siRNA knockdown mice.* Nucleic Acids Res, 2006. **34**.

43. Iacobas, D.A., et al., *Similar Transcriptomic Alterations in Cx43 Knockdown and Knockout Astrocytes.* Cell Communication & Adhesion, 2008. **15**(1-2): p. 195-206.

44. Kok, Fatma O., et al., *Reverse Genetic Screening Reveals Poor Correlation between Morpholino-Induced and Mutant Phenotypes in Zebrafish.* Developmental Cell, 2015. **32**(1): p. 97-108.

45. Daude, N., et al., *Knockout of the prion protein (PrP)-like Sprn gene does not produce embryonic lethality in combination with PrPC-deficiency.* Proceedings of the National Academy of Sciences, 2012. **109**(23): p. 9035-9040.

46. Smart, N. and P.R. Riley, *Thymosin β4 in Vascular Development Response to Research Commentary.* Circulation Research, 2013. **112**(3): p. e29-e30.

47. Gao, Y., et al., *Auxin binding protein 1 (ABP1) is not required for either auxin signaling or Arabidopsis development.* Proceedings of the National Academy of Sciences, 2015. **112**(7): p. 2275-2280.

48. Mannerås-Holm, L., et al., *mRNA expression of diacylglycerol kinase isoforms in insulin-sensitive tissues: effects of obesity and insulin resistance.* Physiological Reports, 2015. **3**(4).

49. Ugai, H., et al., *Stability of a Recombinant Adenoviral Vector: Optimization of Conditions for Storage, Transport and Delivery.* Japanese Journal of Cancer Research, 2002. **93**(5): p. 598-603.

50. Krajden, M., et al., *Effect of Multiple Freeze-Thaw Cycles on Hepatitis B Virus DNA and Hepatitis C Virus RNA Quantification as Measured with Branched-DNA Technology.* Journal of Clinical Microbiology, 1999. **37**(6): p. 1683-1686.

51. Furuse, M., et al., *Molecular organization of tricellular tight junctions.* Tissue Barriers, 2014. **2**(3): p. e28960.

52. Higashi, T., et al., *Analysis of the 'angulin' proteins LSR, ILDR1 and ILDR2 – tricellulin recruitment, epithelial barrier function and implication in deafness pathogenesis.* Journal of Cell Science, 2013. **126**(4): p. 966-977.

53. Halldorsdottir, S., et al., *Reproducibility and accuracy of body composition assessments in mice by dual energy x-ray absorptiometry and time domain nuclear magnetic resonance.* International journal of body composition research, 2009. **7**(4): p. 147-154.

54. Folch, J., M. Lees, and G.H.S. Stanley, *A simple method for the isolation and purification of total lipides from animal tissues.* J Biol Chem, 1956. **226**: p. 497.

55. Wang, Z., M. Gerstein, and M. Snyder, *RNA-Seq: a revolutionary tool for transcriptomics.* Nat Rev Genet, 2009. **10**(1): p. 57-63.

56. Trapnell, C., L. Pachter, and S.L. Salzberg, *TopHat: discovering splice junctions with RNA-Seq.* Bioinformatics, 2009. **25**(9): p. 1105-1111.

Chapter 3: The role of ILDR2 in pancreas islet function

Chapter 3: The role of ILDR2 in pancreas islet function

Introduction

Diabetes mellitus is highly prevalent affecting one in eleven adults worldwide (International Diabetes Federation Diabetes Atlas - 7th Edition, http://www.diabetesatlas.org/). Diabetes mellitus type 2 (T2D) accounts for ~95% of all instances of diabetes in adults, hence a major focus of metabolic research over several decades has been to understand the environmental and genetic contributors to this disease. Multiple genetic loci have been associated with T2D in humans [1-3] but the genetic components contributing to disease risk remain poorly understood.

Our laboratory utilized mouse strain differences along with the close association of T2D with obesity to uncover novel genes modulating T2D susceptibility [4]. Intercrossing T2D-susceptible (DBA) and T2D-resistant (BL6J) *Lep*$^{ob/ob}$ mice, we mapped several disease-relevant loci, then introgressed implicated DBA genetic intervals into C57BL/6J animals segregating for *Lep*^{ob}to further interrogate each genetic locus. We identified a 1.8Mb interval on chromosome 1 for which the DBA allele was associated with diabetes-related phenotypes, and established the causative gene as immunoglobulin-like domain-containing receptor 2 (*Ildr2*, previously *Lisch-like*), or *C1orf32* in humans. Initially, we demonstrated that *Ildr2* hypomorphic mice (derived from B6.DBA congenic lines) segregating for *Lep*^{ob} were hyperglycemic and hypoinsulinemic, with decreased glucose tolerance, reduced beta cell replication, and decreased beta cell area. Zebrafish treated with *Ildr2* morpholinos have defects in pancreas and liver development [4]. As discussed in **Chapter 2**, additional efforts in our lab to understand the role of ILDR2 have focused on its function in the liver.

In the studies described in this chapter, we utilized the Cre-loxP system to design beta cell-specific (RIP2-cre) and pancreas-specific (*Pdx*-cre) *Ildr2* knockout (KO) mice. The RIP2-cre and *Pdx*-cre constructs have been widely used to elucidate the roles of several genes in pancreas development, function, and the pathophysiology of diabetes and various pancreatic cancers [5-12]. RIP2-cre mice in particular have been extensively characterized in various experimental contexts, resulting in a number of caveats regarding their use. RIP2-cre is expressed mainly in beta cells, but also in a subset of hypothalamic neurons [13]. Thus, some RIP2-cre mediated KOs have exhibited feeding and body weight phenotypes due to hypothalamic effects of the gene KO [14-16]. RIP2-cre mice have also been shown to develop glucose intolerance, reduced insulin secretion, and age-dependent changes in beta cell mass in the absence of any floxed gene [6, 7, 17]. These confounding effects necessitate the careful phenotyping of KO models utilizing the RIP2-cre construct, and, preferably, the use of "Cre-only" controls which do not segregate for any floxed alleles.

Here we continue our investigation into the role of ILDR2 in T2D by characterizing RIP2-cre and *Pdx*-cre *Ildr2* KO mouse models. Assessing hyperglycemia, insulin secretion, and islet gene expression, we compare the phenotypes of these two KO models and discuss how they elucidate the role of ILDR2 in the beta cell and pancreas.

Results

Generation of pancreas-specific and beta cell-specific *Ildr2* KO mice

The development of *Ildr2* floxed mice ($Ildr2^{fl/fl}$) is described in **Chapter 2**. *Ildr2* floxed mice were crossed with mice expressing Cre recombinase under the control of the rat insulin II promoter (RIP2-cre, reported by Magnuson *et al*. [5]) or the *Pdx1* promoter (*Pdx*-cre, reported by Tuveson

et al. [8]). Mice were intercrossed until all offspring expressed two copies of the floxed *Ildr2* allele and one or zero copies of respective Cre gene. Mice expressing RIP2-cre were β cell-specific knockouts (KO) and those expressing *Pdx*-cre were pancreas-specific KOs. These KOs will be referred to as RIP2-KO and *Pdx*-KO for the remainder of the text. Littermates without Cre (*Ildr2*$^{fl/fl}$) were used as controls.

As detailed above, KO mice developed using the RIP2-cre mouse have to be carefully phenotyped with the understanding that changes in glucose homeostasis and islet biology may be influenced by the Cre construct rather than a direct consequence of gene ablation. In our studies with RIP2-cre *Ildr2* KO mice, we compare them with *Pdx*-cre *Ildr2* KO mice to assess the specific effect of *Ildr2* ablation. The different phenotypes of RIP2-KO and Pdx-KO mice are summarized in **Table 3.1**.

Pdx-KO and RIP2-KO mice are glucose-intolerant

We assessed these KO mice for phenotypes seen in the B6.DBA Chr 1q23 congenic mice [4]. Male, chow-fed RIP-KO and *Pdx*-KO mice displayed normal body weights (8-22 weeks of age) (**Fig. 3.1A,C**) and fasting blood glucose levels compared to *Ildr2*$^{fl/fl}$ littermate controls (**Fig. 3.1E,F**). Fat mass in RIP2-KO mice was slightly increased vs. controls from 17 weeks to 22 weeks old, but *Pdx*-KO mice showed no difference in fat mass at 20 weeks (**Fig. 3.1B,D**).

Intraperitoneal glucose tolerance testing (ipGTT) was performed at 8 weeks old. RIP2-KO and *Pdx*-KO mice displayed decreased glucose tolerance compared to littermate *Ildr2*$^{fl/fl}$ controls as indicated by increased area under the curve (AUC) for glucose (**Fig. 3.1G,H**). An additional ipGTT with increased glucose bolus (2mg/g vs. 1mg/g previously) was administered to RIP2-KO mice at 12 weeks old. As before, RIP2-KO mice displayed decreased glucose tolerance and

increased glucose AUC (**Fig. 3.1I**). Plasma insulin was decreased in RIP2-KO mice vs. *Ildr2*$^{fl/fl}$ controls, resulting in decreased insulin: glucose ratios (**Fig. 3.1J,K**). These results indicate that RIP2-KO and *Pdx*-KO mice are glucose intolerant, which may be due to reduced insulin secretion.

HFD feeding does not trigger diabetic phenotypes in *Pdx*-KO and RIP2-KO mice

Because the *Ildr2* gene was first identified in obese (leptin-deficient) mice and confirmed in high-fat diet fed wild-type C57BL/6J mice, we hypothesized that additional metabolic stress may be necessary to produce an easily observable phenotype. To test this possibility, RIP2-KO and *Pdx*-KO mice and *Ildr2*$^{fl/fl}$ littermate controls were fed a high-fat diet (HFD; 60% kcal from fat) from 6-30 weeks of age. While HFD-fed *Pdx*-KO mice gained weight similarly to *Ildr2*$^{fl/fl}$ HFD-fed mice and showed no difference in fasting (4hr) blood glucose concentration (**Fig. 3.2B,D**), RIP2-KO mice gained less weight when fed the HFD and had slightly, but consistently, lower fasting blood glucose concentrations than *Ildr2*$^{fl/fl}$ controls (**Fig. 3.2A,C**). RIP2-KO mice also exhibited reduced plasma insulin concentrations after 13 weeks of HFD feeding (**Fig. 3.2E**). However, HFD-fed RIP2-KO mice had significantly lower body weight than controls, a difference which, itself, could reduce circulating insulin concentration.

We measured glucose tolerance in HFD mice at 16 weeks old. As with the non-obese chow animals, both RIP2-KO and *Pdx*-KO mice exhibited impaired glucose tolerance, with significantly increased blood glucose concentrations at 15 and 60 minutes post glucose bolus (**Fig. 3.2G,H**). However, glucose AUC was not significantly increased. An ipGTT performed 8 weeks later, at 24 weeks of age, showed no difference between KO and control mice (**Fig. 3.2I,J**).

RIP2-KO mice show decreased insulin secretion by oral glucose tolerance test (OGTT), but increased glucose-stimulated insulin secretion (GSIS) in isolated islets

To investigate whether glucose intolerance in RIP2-KO mice was due to decreased insulin secretion, we performed an oral glucose tolerance test (OGTT). Delivering glucose directly to the gut, we exploited the incretin effect to stimulate an increased insulin response. 10-week old, low-fat chow fed, male mice were gavaged with 2 mg/g body weight glucose and blood was collected at 0, 15 and 60 minutes post bolus. Confirming our results from ipGTTs, RIP2-KO displayed glucose intolerance with increased glucose AUC (**Fig. 3.3A**). They also exhibited decreased plasma insulin concentrations compared to *Ildr2*$^{fl/fl}$ controls at 15 minutes post glucose bolus (**Fig. 3.3B**).

We also performed static glucose-stimulated insulin secretion (GSIS) assays on islets isolated from 8-week old, chow-fed RIP2-KO and *Ildr2*$^{fl/fl}$ mice. Islets were incubated in basal medium containing 2.8mM glucose, followed by stimulation with 16.8mM glucose. Adjusted for insulin content, RIP2-KO islets showed increased insulin secretion compared to *Ildr2*$^{fl/fl}$ controls (**Fig. 3.3C**).

Islets from *Pdx*-KO mice show impaired calcium signaling and decreased glucose- and potassium-stimulated insulin secretion

Islets isolated from 8-10 week old *Pdx*-KO mice and *Ildr2*$^{fl/fl}$ littermate controls were subjected to microfluidic perifusion at the University of Illinois JDRF Microfluidic-Based Functional Analysis Facility. Islets were stimulated with 14mM glucose and 30mM KCl and calcium signaling, mitochondrial potential, and insulin secretion analyses were performed.

Calcium signaling was impaired in *Pdx*-KO islets vs. *Ildr2*$^{fl/fl}$ islets (**Fig. 3.4A**), but mitochondrial potential was normal (**Fig. 3.4B**). *Pdx*-KO islets also showed decreased insulin secretion and reduced insulin AUC by both glucose and potassium stimulation compared to *Ildr2*$^{fl/fl}$ islets (**Fig. 3.4C,D)**. These results suggest a mechanism for the impaired glucose tolerance observed in *Pdx*-KO mice and indicate that *Ildr2* may play a role in maintaining calcium signaling in islets, possibly by regulating intracellular calcium concentrations at the ER membrane [18-20].

Decreased insulin secretion was observed in RIP2-KO mice *in vivo* but not *in vitro*, which could indicate defects in islet vascularization [21]. However, since dysregulation of insulin secretion is one of the confounding effects of RIP2-cre expression [6], we are inclined to accept the results in *Pdx*-KO mice as more reliable.

Islets of RIP2-KO mice, but not *Pdx*-KO mice, exhibit beta cell hyperplasia

To understand how changes in islet development and structure might affect the observed phenotypes of glucose intolerance and insulin secretion, pancreata from 23-29 week old, chow-fed, male RIP2-KO and *Pdx*-KO and *Ildr2*$^{fl/fl}$ control mice were fixed, sectioned and immunostained for insulin and glucagon (**Fig. 3.5A,G**). RIP2-KO mice had a 2-fold increase in beta cell area compared to controls (**Fig. 3.5B**), due to increases in both number of islets (**Fig. 3.5C**) and beta cell number (**Fig. 3.5D,E**), although alpha cells were not increased in RIP2-KO mice (**Fig. 3.5F**). In contrast, there was no change in islet size or beta/alpha cell ratio in *Pdx*-KO mice vs. *Ildr2*$^{fl/fl}$ controls (**Fig. 3.5H-J**).

***Ildr2* expression is completely ablated in *Pdx*-KO islets, but retained in the islets of RIP2-KO mice**

To confirm that *Ildr2* is knocked out in the RIP2-KO and *Pdx*-KO mice, we isolated islets from 10-24 week male RIP2-KO and *Pdx*-KO mice and controls, and measured *Ildr2* gene expression by qRT-PCR. Surprisingly, *Ildr2* expression in islets of RIP2-KO mice was comparable to $Ildr2^{fl/fl}$ controls (**Fig. 3.6A**). In *Pdx*-KO mice however, islet *Ildr2* expression was completely ablated (**Fig. 3.6D**). Cre was expressed in both RIP2-KO and *Pdx*-KO islets (**Fig. 3.6C,F**). Primers targeted to amplify only the floxed exon 1 segment also gave the same result: *Ildr2* was knocked out in *Pdx*-KO islets but not RIP2-KO islets (**Fig. 3.6B,E**). These results suggested that *Ildr2* expression in non-beta islet cell populations might be masking KO in the beta cells of RIP2-KO mice.

Because of previous reports of both RIP2-cre [13] and *Pdx*-cre constructs [22] expression in the hypothalamus, we also measured *Ildr2* and *Cre* expression in the hypothalami of our RIP2-KO and *Pdx*-KO mice and littermate $Ildr2^{fl/fl}$ controls. *Ildr2* expression was unchanged in the hypothalamus of both RIP2-KO and *Pdx*-KO mice (**Fig. 3.6G,I**), although Cre expression was detected in both (**Fig. 3.6H,J**).

To investigate *Ildr2* expression in non-beta islet cell populations, we interrogated mouse [23] and human (Bryan González, personal communication) islet single cell sequencing data for *Ildr2* expression. Mouse alpha and beta cell transcriptome sequencing analysis indicate that *Ildr2* is expressed at relatively low levels in both beta and alpha cells [23]. For comparison, *Arx*, an alpha cell-specific transcription factor, had higher expression in beta cells than *Ildr2*. Conversely, in alpha cells, expression of the beta cell-specific gene *Mafa* was an order of magnitude higher than *Ildr2* (ref. [23], additional data file 12). While it is possible that *Ildr2* could expressed in islet

delta, gamma, or epsilon cells, human islet single cell sequencing data showed that *Ildr2* was expressed at equivalently low levels in all five endocrine cell populations.

These data suggest that *Ildr2* may be expressed in some non-endocrine cell population in pancreatic islets. We hypothesize that islet macrophages could be the source of *Ildr2* expression. Islet macrophages play an important role in beta cell replication and proliferation, both in islet development [24] and after pancreatic injury [25]. In disease states, such as Type 1 or Type 2 diabetes, islet macrophages become activated to release inflammatory cytokines contributing to disease progression [26, 27]. *Ildr2* is expressed in tissue macrophages in liver (**Fig. 2.3**) and adipose tissue [28]. We propose that *Ildr2* may be expressed in islet macrophages at higher levels than in beta cells, and that this expression may be what was observed in RIP2-KO islets.

The RIP2-cre construct includes an *hGH* minigene which may affect beta cell function in RIP2-KO mice.

Several pancreas cell-specific Cre constructs (RIP-, MIP-, and Pdx-Cre's), include a 2.1kb human growth hormone (*hGH*) "minigene" to improve Cre expression [29]. At the time these Cre constructs were designed, it was believed that the *hGH* gene was not expressed and would not produce any active growth hormone. However, recent publications have shown that *hGH* is expressed in Cre-expressing mice and may cause diabetic phenotypes independent of any consequence for co-segregating floxed genes. The Cre construct used to create our RIP2-cre, *Ildr2* KO mice was developed and reported by Magnuson and others [5, 17]. This Cre construct includes the *hGH* minigene; and Cre mice – not segregating for any floxed allele – have been reported to be glucose-intolerant and hyperglycemic, with reduced insulin secretion and increased beta cell

mass [6, 13, 17]. The construct used to create the *Pdx*-cre *Ildr2* KO mice does not contain an *hGH* minigene [8, 29].

To determine whether *hGH* expression in our KO mice could account for the observed phenotypes, we measured *hGH* expression in islets of RIP2-KO and *Pdx*-KO mice, and *Ildr2*$^{fl/fl}$ controls. *hGH* was highly expressed in islets from RIP2-KO mice, but not in *Pdx*-KO islets (**Fig. 3.7A**). Brouwers et al. suggest that *hGH* acts as a lactogen in mouse beta cells [29, 30], stimulating prolactin receptor signaling which is responsible for increases in beta cell mass and insulin secretion that accompany pregnancy [31, 32]. Serotonin biosynthesis genes are also upregulated by lactogen signaling in pregnancy [33] consistent with the role of serotonin to increase beta cell proliferation [34]. *Tph1*, encoding tryptophan hydroxylase 1 which catalyzes the rate–limiting step of serotonin biosynthesis, was found by others to be upregulated in mice expressing *Cre-hGH* constructs [29]. We measured expression of *Tph1* in islets of RIP2-KO and *Pdx*-KO mice, and *Ildr2*$^{fl/fl}$ controls. *Tph1* expression was highly induced (~200-fold) in RIP2-KO mice but not in *Pdx*-KO or control mice (**Fig. 3.8B**). These results – in the context of the results in the *Pdx*-KO mice – suggest that the glucose intolerance and beta cell hyperplasia observed in RIP2-KO mice may be a consequence of Cre-mediated *hGH* expression, rather than of *Ildr2* KO in beta cells.

Discussion and Conclusions

We used beta cell-specific RIP2-cre *Ildr2* KO mice and pancreas-specific *Pdx*-cre *Ildr2* KO mice to confirm a role for ILDR2 in beta cell biology, a role previously suggested by positional cloning of a quantitative trait locus in leptin-deficient mice [4]. *Pdx*-KO mice display impaired glucose tolerance in vivo, and decreased calcium signaling in conjunction with reduced insulin secretion in islets *in vitro*. These phenotypes confirm a role for ILDR2 in islet function. RIP2-KO

mice also show impaired glucose tolerance with variable insulin secretion, and beta cell hyperplasia. However, the results in RIP2-KO mice are confounded by the expression of *hGH* and its downstream effects on beta cell development and function [29] the phenotypes of these animals are consistent with previously described consequences of the RIP2-cre construct and *hGH* expression on insulin/glucose homeostasis in transgenic mice. RIP2-cre mice not segregating for any floxed allele have been reported to display glucose intolerance [6, 13], decreased insulin secretion [6] and age-dependent changes in beta cell mass [7].

Comparison of RIP2-KO mice with *Pdx*-KO phenotypes indicates that some aspects of RIP2-KO phenotypes are probably due to *Ildr2* ablation, but in the absence of 'Cre-only' controls we cannot isolate specific effects of *Ildr2* KO vs. *hGH* expression. All of our control mice segregated for *Ildr2* floxed alleles with no Cre construct ($Ildr2^{fl/fl}$ mice). To elucidate which phenotypes in RIP2-cre *Ildr2* KO mice are specifically due to *Ildr2* KO, we would need to compare KO mice with controls expressing the Cre construct in the absence of the floxed alleles, as the presence of the *hGH* minigene may have masked more subtle effects of the beta cell-specific knockout of *Ildr2*. We are in the process of generating these mice for such studies.

Pdx-KO mice do not possess the *hGH* minigene (**Fig. 3.7**), and thus are free of these confounding issues. We conclude that phenotypes observed in *Pdx*-KO mice – glucose intolerance, decreased calcium signaling and decreased glucose- and potassium-stimulated insulin secretion – are the primary effects of *Ildr2* knockout in pancreatic islets.

The association of decreased insulin secretion with decreased calcium signaling in *Pdx*-KO islets suggests that ILDR2 may modulate calcium signaling in beta cells to regulate insulin secretion. These results may reflect a specific role for ILDR2 in regulating cellular calcium concentrations. As the major calcium storage organelle, the ER contains several transmembrane

proteins which function to regulate its calcium concentration, e.g. sarco/endoplasmic reticulum Ca^{2+} ATPase (SERCA) [35], and PKR-like ER kinase (PERK) [36] which also modulates ER stress. Since ILDR2 is located in the ER membrane, our data suggest that it may play a similar role in maintaining ER calcium concentration. As discussed in **Chapter 1**, in a protein screen (2D-PAGE) in W87* *Ildr2* "deficient" mice, several calcium regulatory proteins were decreased, suggesting a functional role for ILDR2.

Since *Pdx*-KO mice lack *Ildr2* in all islet, exocrine, and ductal cells in the pancreas, the phenotype observed in these mice may not be due solely to beta cell defects. Calcium signaling also regulates glucose-stimulated hormone secretion in alpha and delta cells [37], thus defects related to *Ildr2* ablation in these cell types may contribute to the overall phenotype of *Pdx*-KO mice.

Islet macrophages may also be affected. *Ildr2* expression in RIP2-KO islets highlighted the relatively low *Ildr2* expression in endocrine cells, and possible expression in another cell-type, i.e. macrophages. *Ildr2* is expressed in liver and adipose tissue macrophages suggesting that *Ildr2* may have a role in islet macrophages as well. Loss of *Ildr2* in macrophages could possibly stimulate pro-inflammatory signaling leading to decreased beta cell function [27]. Thus, one explanation for *Ildr2* expression in RIP2-KO islets could be that islet macrophages in RIP2-KO mice expressed *Ildr2*, while *Pdx*-KO islet macrophages were knocked out due to broader cell type expression by *Pdx1*. A caveat to this hypothesis, however, is that the *Pdx1* gene may not be expressed in islet macrophages to cause *Ildr2* ablation. An essential transcription factor for the development of pancreatic precursor cells, *Pdx1* has not been identified to play a role in the myeloid cell lineages from which macrophages develop. However, *Pdx1* is expressed in differentiated THP-1 cells, a human macrophage-like cell line [38]. Unfortunately, commercial ILDR2 antibodies fail to

recognize ILDR2 in pancreatic tissue, hindering our ability to specify cell-specific expression by immunohistochemistry. Thus to determine if *Ildr2* is knocked out in islet macrophages, it will be necessary to isolate different islet cell populations and profile them separately for *Ildr2* gene expression.

Pdx-KO mice have afforded initial insights regarding the role of *Ildr2* in pancreatic islet cells. Because the pancreas is a complex organ with diverse functions, additional cell-specific KO mouse models will be required to decipher specific effects of *Ildr2* KO. This work provides the first description of specific role for *Ildr2* in beta cell function since its designation as a modifier of diabetes susceptibility [4]. Despite concerns with the RIP2-cre mouse models, these initial observations suggest that further investigation into the function of ILDR2 in the pancreatic islet may provide important insights into the regulation of endocrine secretion.

Methods

Animal studies

Mice bearing 2 floxed alleles of *Ildr2* (*Ildr2*$^{fl/fl}$) were developed as described in Chapter 2. *Ildr2*$^{fl/fl}$ were bred with rat insulin promoter II cre (B6.Cg- Tg(Ins2-cre)25Mgn, Jackson Labs stock #003573) or *Pdx1* promoter-cre mice (B6.FVB- Tg(Pdx1-cre)6Tuv, Jackson Labs stock #014647) until all offspring segregated for 2 floxed alleles and one or no copies of Cre.

All animal experiments were approved by Columbia Institutional and Animal Care Use Committee (Protocol# AAAH0707 and AAAR0416). Mice were housed in a 12-hr light/12hr-dark vivarium, with ad libitum access to 5058 Purina PicoLab Mouse Diet 20 (9% fat) and water. High-fat diet (HFD) fed mice received chow with 60% kcal from fat (Research Diets #D12492i). Fat

and lean mass were measured with an EchoMRI Analyzer (Bruker Optics), calibrated using mouse carcasses [39].

Glucose tolerance tests

For intraperitoneal (ip) GTT, mice were i.p. injected with 1-2 mg glucose (50% dextrose, Hospira, Inc) per gram body weight following an overnight fast (16-18 hours). Blood glucose was measured at indicated time intervals after glucose bolus using a FreeStyle Lite (Abbott) or AlphaTRAK 2 (Zoetis) glucometer. For plasma glucose and insulin measurements, blood was collected by submandibular bleed.

For oral GTT, mice were gavaged with 2 mg glucose per gram body weight following an overnight fast (16-18 hours). Blood glucose was measured at indicated time intervals after glucose bolus using a glucometer. For plasma insulin measurements, blood was collected from the tail vein. Plasma glucose was measured enzymatically (Autokit Glucose, Wako Diagnostics) and plasma insulin was measured using mouse insulin ELISA kit (CrystalChem or Mercodia).

Mouse islet isolation and glucose-stimulated insulin secretion (GSIS) assay

Mouse islets were isolated as previously described [40] and incubated overnight in RMPI media (Thermo Fisher, 11879) with 10% FBS, 1% Pen Strep, 1% GlutaMAX, 5.6mM glucose at 37°C, 5% CO_2. For RNA extraction, islets were washed 2x in phosphate-buffered saline (PBS) and pelleted at 1000 rpm for 2 min. For GSIS, islets were washed and incubated in Krebs-Ringer-bicarbonate-HEPES buffer (KRBH, 140 mM NaCl, 3.6 mM KCl, 0.5 mMNaH_2PO_4, 0.5 mM $MgSO_4$, 1.5 mM $CaCl_2$, 2 mM$NaHCO_3$, 10 mM HEPES, 0.1% BSA) [41] with 2.8mM glucose for 1 hour 37°C, 5% CO_2. Media was discarded and islets were incubated in 2.8 mM glucose for 1 hour. This medium was collected (low glucose) and islets were incubated in 16.8 mM glucose for 1 hour. This medium was collected (high glucose) and islets were sonicated in

high salt buffer for insulin content measurement. Insulin concentration was measured using mouse insulin ELISA kit (Mercodia).

Islet perifusion analysis

After overnight culture post islet isolation, the islets were transferred into a petridish with 5 µM fura-2AM (Molecular Probes, Inc.) and 2.5 µM Rhodamine 123 (Sigma) for 30 min at 37 °C in Krebs-Ringer buffer (KRB) containing 2 mM glucose (KRB2). Islets were then introduced into temperature-controlled microfluidic device [42] through the inlet microchannel and mounted on inverted epifluorescence microscope (Leica DMI 4000B). The loaded islets were perifused by a continuous flow of KRB2 at 37°C (pH 7.4) for 10 minutes. Multiple islets were simultaneously observed for calcium influx, mitochondrial potentials, and insulin secretion kinetics with a 10X objective. The islets were stimulated with 14mM glucose for 25 min, washed with 2 mM glucose for 15 minutes, and stimulated again with 30mM KCl for 15 min, and followed by washing by 2 mM glucose for 10 minutes. Dual-wavelength fura-2AM is excited at 340 and 380 nm, and changes in $[Ca^{2+}]_i$ are expressed as F340/F380 (%). Rhodamine 123 is excited at 495 nm and expressed as percentage changes. Emission of fura-2AM and Rhodamine 123 are 510 and 530 nm, respectively. Excitation wavelengths were controlled by means of corresponding excitation filters (Chroma Technology) mounted in a Lambda DG-4 wavelength switcher. Emissions of fura-2AM and Rhodamine 123 fluorescence were filtered using a Fura2/FITC polychroic beamsplitter and double band emission filter (Chroma Technology. Part number: 73.100bs). A shutter controller was used to avoid continuous exposure of fluorescently stained cells to the excitation light. Time-lapse images were recorded with short exposure times between 0.1-0.3 s per image. A high-speed, high-resolution charge-coupled device (CCD, Retiga-SRV, Fast 1394, QImaging) was used for imaging captures and SimplePCI software (Hamamatsu Corp) for image acquisition and analysis.

Perifusates were collected by fraction collector (Gibson, FC203B Fraction collector) at 1mL/min. Dynamic insulin secretions were measured by mouse insulin ELISA kit (Alpco).

Pancreas histology and islet cell counting

Mouse pancreata were fixed in 10% formalin and paraffin-embedded. For morphometric analysis of β cell area and islet number, 3 animals of each genotype were analyzed. For each pancreas, 6 sections ~100 μm apart, were immunostained with insulin (Dako #A0564) and DAB peroxidase (Dako) were covered systematically by accumulating images from non-overlapping fields using a Nikon Eclipse E400 bright-field microscope (Nikon Instrument, Inc.). Images were captured using a Spot digital camera (Diagnostic Instruments), and analyzed using Image-Pro Plus software. (Media Cybernetics). Results are expressed as percentage of the total surveyed pancreatic area occupied by β cells (**Fig. 3.5B**). For immunofluorescent analysis of islet cell number, 3-4 animals of each genotype were analyzed. For each pancreas, 3 sections, 200-300 μm apart were immunostained with insulin (Dako #A0564) and glucagon (Cell Signaling Technologies #2760), AlexaFluor donkey and goat-conjugated secondary antibodies (Thermo Fisher), and Hoescht nuclear stain. Images were obtained at 20x on a Zeiss Confocal LSM 710 microscope and alpha, beta, and total islet cell number for 10 islets/section were counted using HALO software (Indica Labs) [43], with blinding for genotypes.

RNA extraction, reverse transcription and quantitative PCR

Islet RNA was extracted using the Total RNA Purification Micro Kit (Norgen Biotek). Reverse transcription was performed using the Transcriptor First Strand cDNA Synthesis kit (Roche). qPCR was performed using a Roche LightCycler® 480 instrument. qPCR primers are listed below. Tissue-specific standard curves for each gene (primer pair) were used to convert threshold crossing point (Cp) values to relative concentrations, which were then normalized to

36b4, *Actb*, and/or *Gapdh* expression. In cases were standard curves were not used, Cp values are shown, with lower Cp values indication greater mRNA expression.

List of qPCR primers

Mouse gene name	**Forward primer (5' to 3')**	**Reverse primer (5' to 3')**
36b4	ACCTCCTTCTTCCAGGCTTTGG	CGAAGGAGAAGGGGGAGATGTT
Actb	CGGGCTGTATTCCCCTCCAT	GGGCCTCGTCACCCACATAG
Gapdh	CTGGAGAAACCTGCCAAGTATGATG	GAGACAACCTGGTCCTCAGTGTAGC
Ildr2 – isoform 1	GATTATGCCAGAGTGGGTGTTTGTC	CCCTGCTTCATACAAGGCCTGAG
Ildr2 exon 1	AGCTGCTTAGCCTGTGGTGT	CAGGACTCGGAGCCTAACAA
Cre	GCGGTCTGGCAGTAAAAACTATC	GTGAAACAGCATTGCTGTCACTT
hGH	CCAGGAGTTTGAAGAAGCCT	GGAGGTCATAGACGTTGCTGT
Tph1	TTCCAGGAGAATCATGTGAGC	CATAACGTCTTCCTTCGCAGT

Figures and Tables

Figure 3.1: *Pdx*-KO and RIP2-KO mice are glucose-intolerant

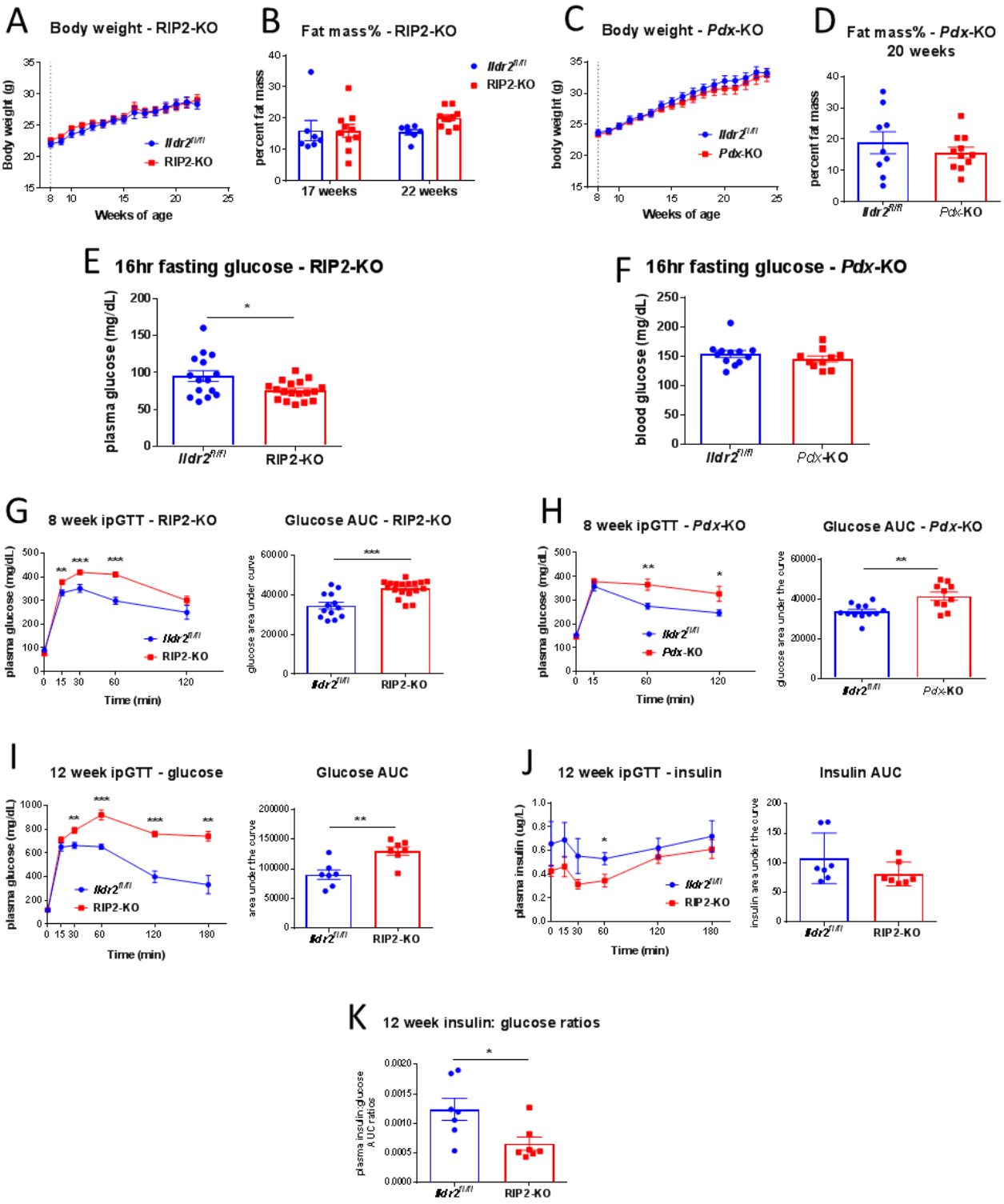

Figure 3.1: *Pdx*-KO and RIP2-KO mice are glucose-intolerant.

(A) Body weight curves of RIP2-KO and (C) *Pdx*-KO mice and *Ildr2*$^{fl/fl}$ controls from 8-22 weeks. (B) Percent fat mass of RIP2-KO mice at 17 and 22 weeks (D) Percent fat mass of *Pdx*-KO mice at 20 weeks. (E,F) Fasting glucose at 8 weeks in RIP2-KO and Pdx-KO mice. (G,H) Glucose curve and AUC of 8 week ipGTTs in (G) RIP2-KO or (H) Pdx-KO mice. **I-J**: ipGTT in 12 week RIP2-KO and *Ildr2*$^{fl/fl}$ mice. (I) Glucose curve and AUC (J) Insulin curve and AUC (K) Insulin:glucose ratios (from AUC). Data are represented as mean ± standard error (SEM) * $p<0.05$, ** $p<0.01$, *** $p<0.001$ (Two-tailed t-test). n = 13-18 mice/group for **A-H**. n = 7 mice/group for **I-J**.

Figure 3.2: HFD feeding in *Pdx*-KO and RIP2-KO mice

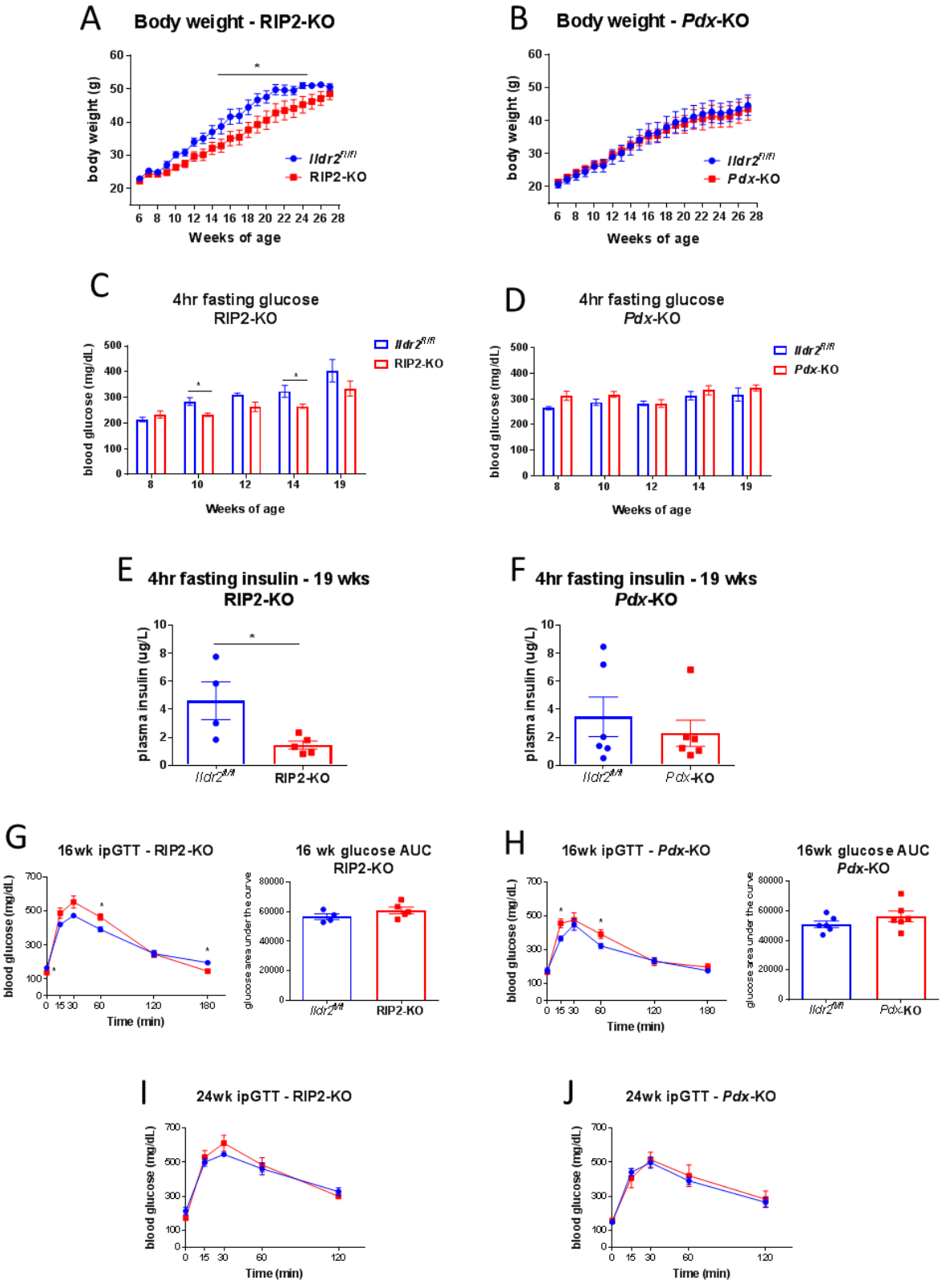

Figure 3.2: HFD feeding in *Pdx*-KO and RIP2-KO mice.

(A) Body weight curves of RIP2-KO mice and *Ildr2*$^{fl/fl}$ controls fed HFD from 6-28 weeks. (B) Body weight curves of *Pdx*-KO mice and *Ildr2*$^{fl/fl}$ controls fed HFD from 6-28 weeks (C,D) Blood glucose measurements after 4-hr fast. (E,F) Plasma insulin measurements after 4-hr fast mice at 19 weeks. (G,H) Glucose curves and AUC of ipGTTs performed at 16 weeks. (I,J) Glucose curves of ipGTTs at 24 weeks old. Data are represented as mean ± standard error (SEM) * $p<0.05$ (Two-tailed t-test). n = 4-6 mice/group.

Figure 3.3: Oral glucose tolerance test (OGTT) and islet glucose-stimulated insulin secretion (GSIS) in RIP2-KO mice

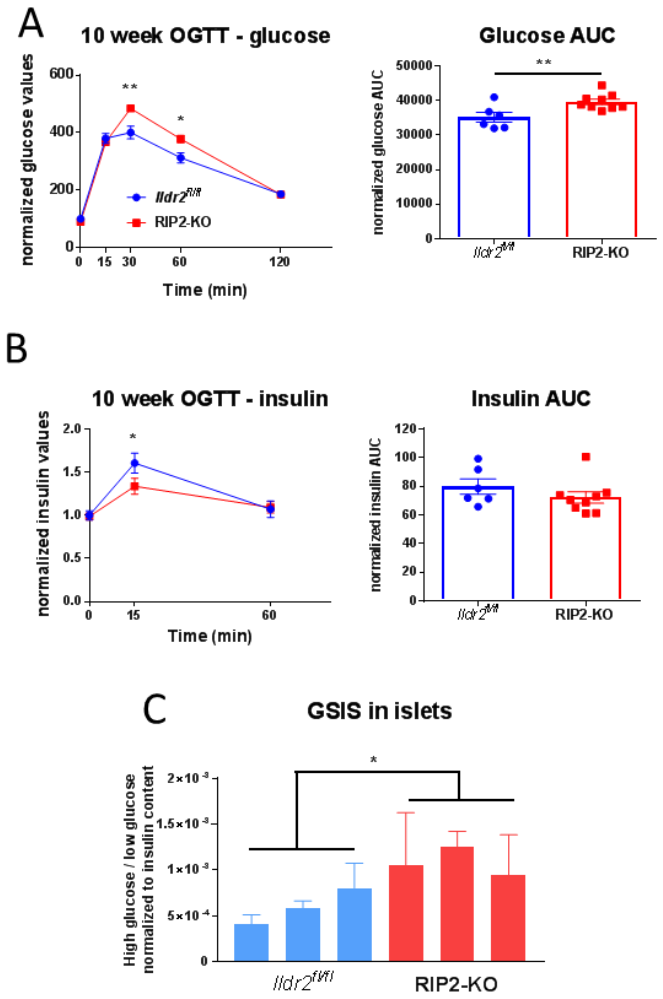

Figure 3.3: Oral glucose tolerance test (OGTT) and islet glucose-stimulated insulin secretion (GSIS) in RIP2-KO mice

(A) Glucose curve and AUC, (B) Insulin curve and AUC of OGTT in 10 week *Ildr2*$^{fl/fl}$ and RIP2-KO mice. n=6-9 mice/group. (C) GSIS in *Ildr2*$^{fl/fl}$ and RIP2-KO isolated islets. Graph is ratio of insulin secretion at high/low glucose, normalized by islet total insulin content. Bars represent aggregate of 3 experiments/mouse, ~5 islet/experiment. n=3 mice/group. Data are represented as mean ± standard error (SEM) * $p<0.05$, **$p<0.01$ (Two-tailed t-test).

Figure 3.4: Islet perifusion analyses in *Pdx*-KO mice

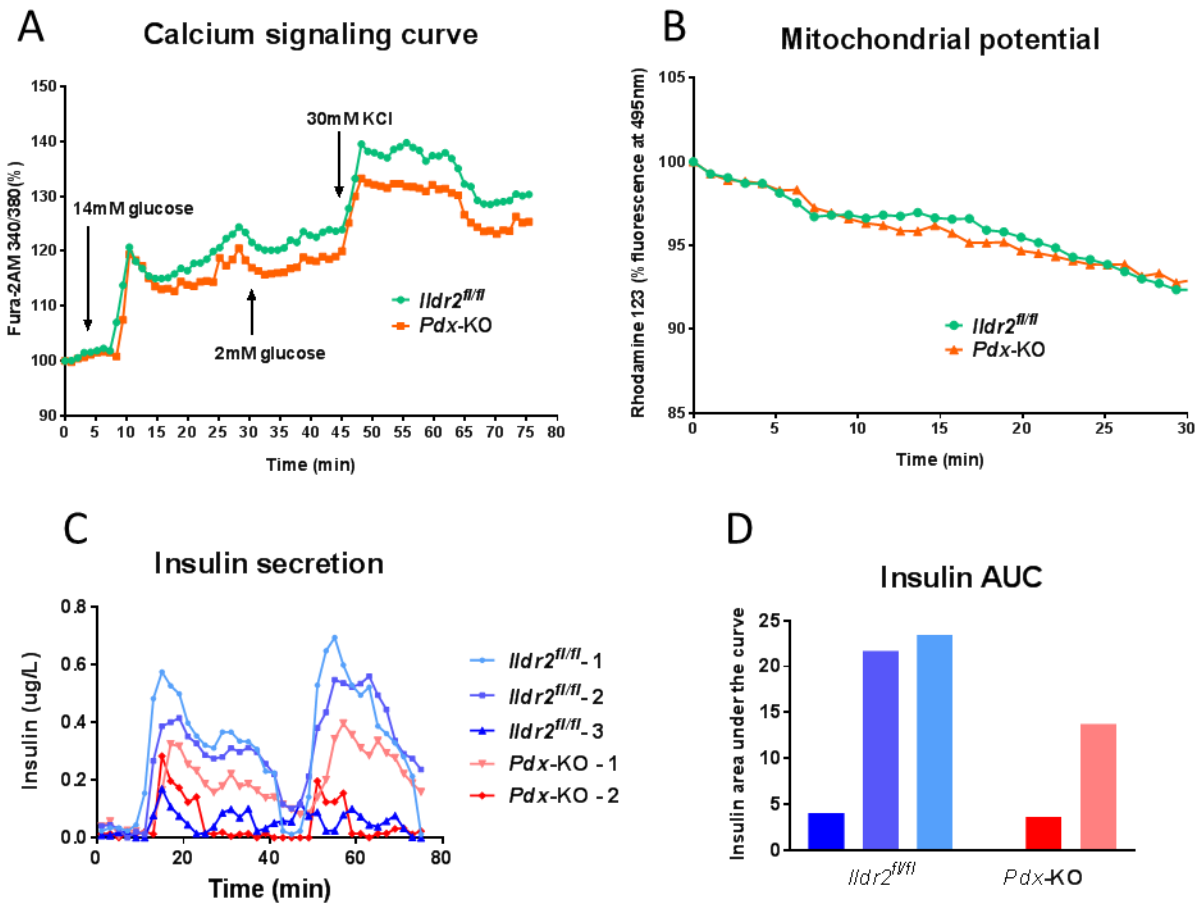

Figure 3.4: Islet perifusion analyses in *Pdx*-KO mice

Dynamic trace of calcium signaling (A) and mitochondrial potential (B) of primary islets from 6-8 week old *Ildr2*$^{fl/fl}$ and *Pdx*-KO mice in response to 14 mM glucose for 20 min and 30 mM KCI for 15 min. Average values from 3 mice, ~50 islets/mouse. (C) Dynamic insulin secretion measured in the same experiment as (A) and (B), less one *Pdx*-KO sample. (D) Area under the curve calculation for insulin traces in (C) with corresponding colors.

Figure 3.5: Islet cell quantification in RIP2-KO and *Pdx*-KO mice

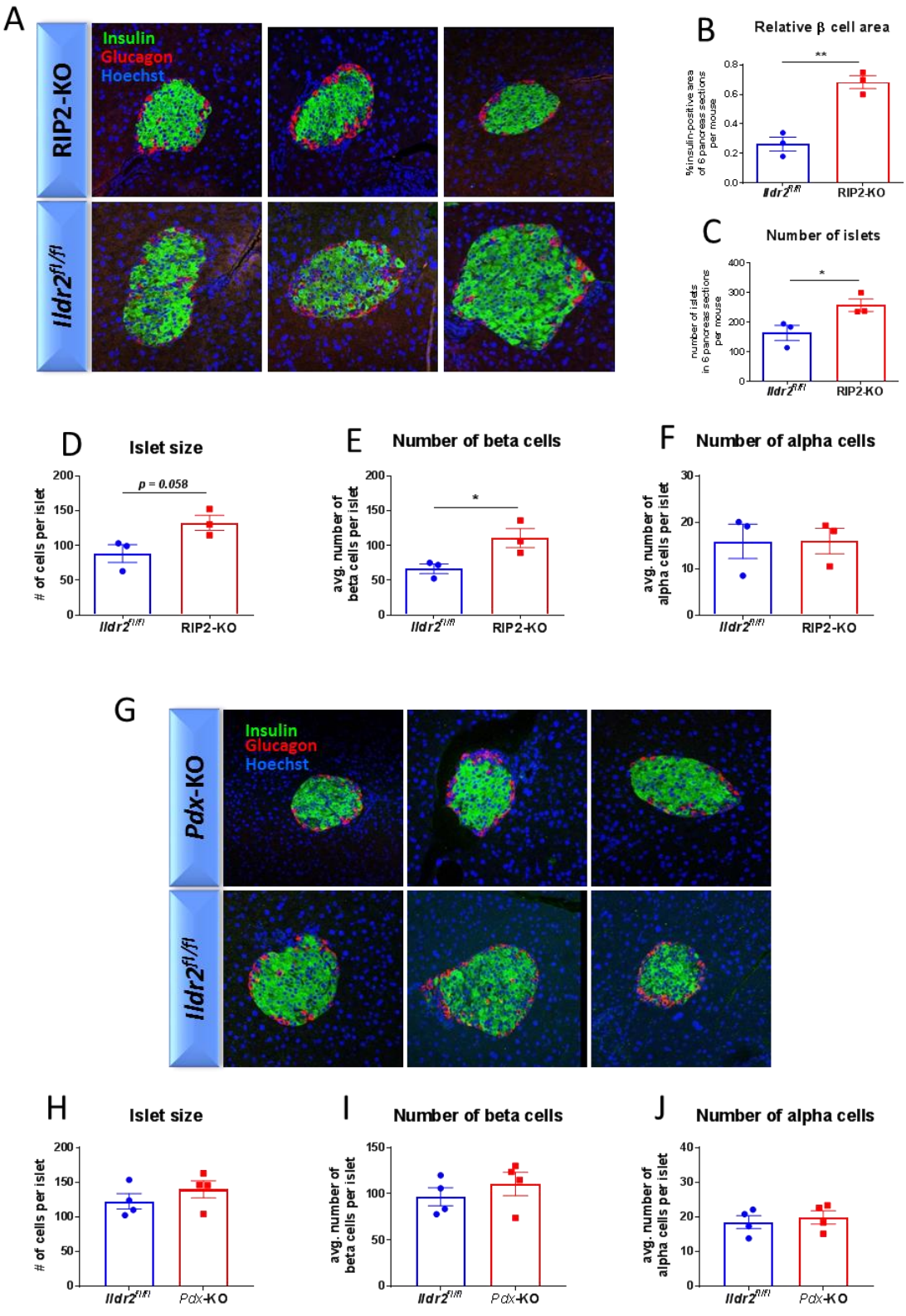

Figure 3.5: Islet cell quantification in RIP2-KO and *Pdx*-KO mice

A-C,G: Representative immunofluorescent images of pancreatic islets from (A) 23-29 week *Ildr2*$^{fl/fl}$ and RIP2-KO mice, (G) 24 week *Ildr2*$^{fl/fl}$ and *Pdx*-KO mice. (B) Percent insulin-positive area and (C) number of islets quantified by non-fluorescent immunohistochemistry in 23-29 week *Ildr2*$^{fl/fl}$ and RIP2-KO mice, 6 pancreatic sections per mouse. **D-F,H-J**: Quantification of immunofluorescent staining of 3 pancreas sections per mouse, 200-300 μm apart. ~10 islets/section were quantified. (D) Total cell number, (E) beta cell number, and (F) alpha cell number in 23-29 week *Ildr2*$^{fl/fl}$ and RIP2-KO mice. (H) Total cell number, (I) beta cell number, and (J) alpha cell number in 24 week *Ildr2*$^{fl/fl}$ and *Pdx*-KO mice. n=3 mice/genotype for all experiments. Data are represented as mean ± standard error (SEM) * $p<0.05$, ** $p<0.01$ (Two-tailed t-test)

Figure 3.6: *Ildr2* expression in islets and hypothalamic of RIP2- KO and *Pdx*-KO islets

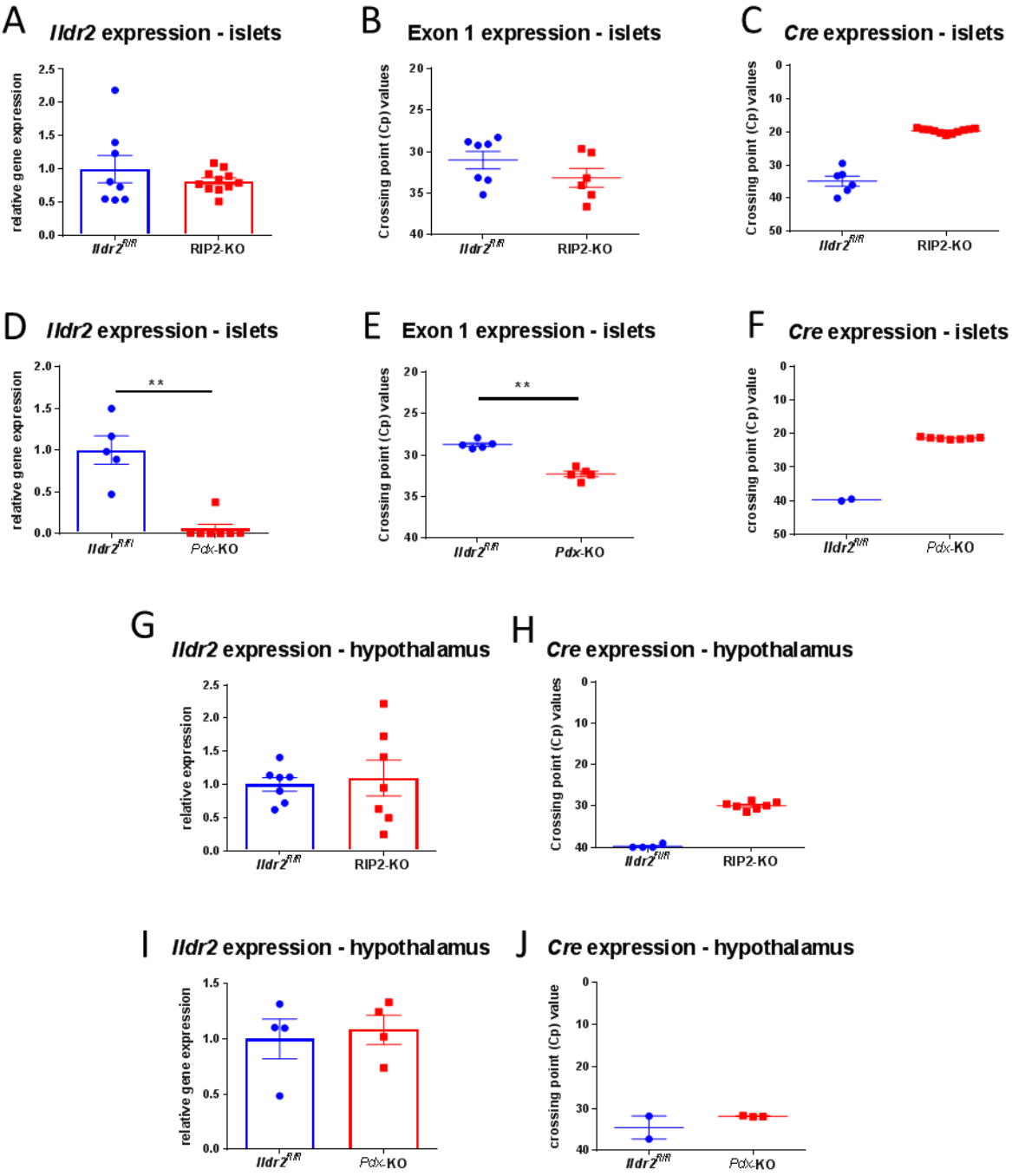

Figure 3.6: *Ildr2* expression in islets and hypothalamic of RIP2- KO and *Pdx*-KO islets

Islets: qPCR expression of (A) *Ildr2*-isoform 1, (B) exon 1 of *Ildr2*, and (C) Cre in 10-24 week *Ildr2*$^{fl/fl}$ control and RIP2-KO mice. (D) qPCR expression in 24 week control and *Pdx*-KO mice of *Ildr2*-isoform 1, (E) exon 1 of *Ildr2*, and (F) Cre. Hypothalamus qPCR expression: (G) *Ildr2*-isoform 1 and (H) Cre in *Ildr2*$^{fl/fl}$ control and RIP2-KO mice. (I) *Ildr2*-isoform 1 and (J) Cre expression in control and *Pdx*-KO mice. For exon 1 and Cre, expression is shown as Cp (threshold crossing point) values. Lower Cp values indicate higher expression and vice versa. n=4-10 mice per group. Data are represented as mean ± standard error (SEM) * p<0.05, ** p<0.01 (Two-tailed t-test)

Figure 3.7: *hGH* and *Tph1* expression in RIP2-KO, *Pdx*-KO, and WT islets

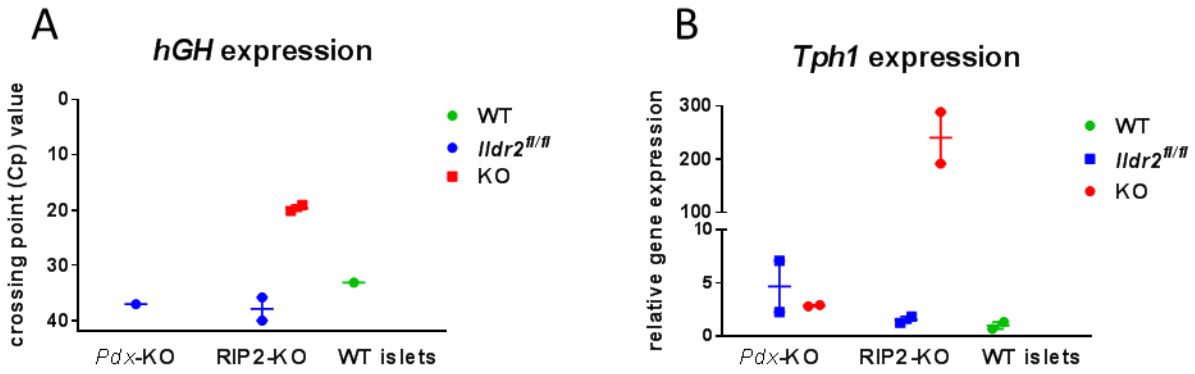

Figure 3.7: *hGH* and *Tph1* expression in RIP2-KO, Pdx-KO, and WT islets

Islet qPCR expression of (A) *hGH* and (B) *Tph1* in RIP2-KO, Pdx-KO, littermate controls, and WT (B6) mice. *hGH* expression is shown as Cp values; *Tph1* expression is normalized to *36b4*, *beta actin*, and *Gapdh* expression. Mice were 7-10 week old females. n=2 mice/genotype.

Table 3.1: Summary of phenotypes in RIP2-KO and *Pdx*-KO mice

Experimental assay	**RIP2-KO mice**	***Pdx*-KO mice**
Islet expression	Retain *Ildr2* expression; express *hGH*	Complete *Ildr2* KO; No *hGH* expression
HFD feeding	Decreased body weight, fasting glucose, and insulin	No difference in body weight, glucose or insulin
Intraperitoneal GTT	Impaired glucose tolerance	Impaired glucose tolerance
Oral GTT	Impaired glucose tolerance and decreased insulin secretion	--
GSIS	Increased insulin secretion	--
Islet perifusion	--	Reduced insulin secretion, decreased calcium signaling
Islet morphology	Increased islet size and beta cell number	No difference in islet size and beta cell number

References

1. Bonnefond, A., P. Froguel, and M. Vaxillaire, *The emerging genetics of type 2 diabetes.* Trends in Molecular Medicine, 2010. **16**(9): p. 407-416.

2. Zeggini, E., et al., *Meta-analysis of genome-wide association data and large-scale replication identifies additional susceptibility loci for type 2 diabetes.* Nat Genet, 2008. **40**(5): p. 638-645.

3. Voight, B.F., et al., *Twelve type 2 diabetes susceptibility loci identified through large-scale association analysis.* Nat Genet, 2010. **42**(7): p. 579-589.

4. Dokmanovic-Chouinard, M., et al., *Positional cloning of "Lisch-Like", a candidate modifier of susceptibility to type 2 diabetes in mice.* PLoS Genet, 2008. **4**(7): p. e1000137.

5. Postic, C., et al., *Dual Roles for Glucokinase in Glucose Homeostasis as Determined by Liver and Pancreatic β Cell-specific Gene Knock-outs Using Cre Recombinase.* Journal of Biological Chemistry, 1999. **274**(1): p. 305-315.

6. Lee, J.-Y., et al., *RIP-Cre Revisited, Evidence for Impairments of Pancreatic β-Cell Function.* Journal of Biological Chemistry, 2006. **281**(5): p. 2649-2653.

7. Pomplun, D., et al., *Alterations of Pancreatic Beta-cell Mass and Islet Number due to Ins2-controlled Expression of Cre Recombinase: RIP-Cre Revisited; Part 2.* Horm Metab Res, 2007. **39**(05): p. 336-340.

8. Hingorani, S.R., et al., *Preinvasive and invasive ductal pancreatic cancer and its early detection in the mouse.* Cancer Cell, 2003. **4**(6): p. 437-450.

9. Mastracci, T.L., et al., *Nkx2.2 and Arx genetically interact to regulate pancreatic endocrine cell development and endocrine hormone expression.* Developmental Biology, 2011. **359**(1): p. 1-11.

10. Zhang, J., et al., *Disruption of Growth Factor Receptor–Binding Protein 10 in the Pancreas Enhances β-Cell Proliferation and Protects Mice From Streptozotocin-Induced β-Cell Apoptosis.* Diabetes, 2012. **61**(12): p. 3189-3198.

11. Hanlon, L., et al., *Notch1 Functions as a Tumor Suppressor in a Model of K-ras–Induced Pancreatic Ductal Adenocarcinoma.* Cancer Research, 2010. **70**(11): p. 4280-4286.

12. Seeley, E.S., et al., *Pancreatic Cancer and Precursor Pancreatic Intraepithelial Neoplasia Lesions Are Devoid of Primary Cilia.* Cancer Research, 2009. **69**(2): p. 422-430.

13. Gannon, M., et al., *Analysis of the Cre-mediated recombination driven by rat insulin promoter in embryonic and adult mouse pancreas.* genesis, 2000. **26**(2): p. 139-142.

14. Lin, X., et al., *Dysregulation of insulin receptor substrate 2 in β cells and brain causes obesity and diabetes.* The Journal of Clinical Investigation, 2004. **114**(7): p. 908-916.

15. Cui, Y., et al., *Essential Role of STAT3 in Body Weight and Glucose Homeostasis.* Molecular and Cellular Biology, 2004. **24**(1): p. 258-269.

16. Nguyen, K.-T.T., et al., *Essential Role of Pten in Body Size Determination and Pancreatic β-Cell Homeostasis In Vivo.* Molecular and Cellular Biology, 2006. **26**(12): p. 4511-4518.

17. Fex, M., et al., *Rat insulin promoter 2-Cre recombinase mice bred onto a pure C57BL/6J background exhibit unaltered glucose tolerance.* Journal of Endocrinology, 2007. **194**(3): p. 551-555.

18. Koch, G.L.E., *The endoplasmic reticulum and calcium storage.* BioEssays, 1990. **12**(11): p. 527-531.

19. Berridge, M.J., *The endoplasmic reticulum: a multifunctional signaling organelle.* Cell Calcium, 2002. **32**(5): p. 235-249.

20. Worley, J.F., et al., *Endoplasmic reticulum calcium store regulates membrane potential in mouse islet beta-cells.* Journal of Biological Chemistry, 1994. **269**(20): p. 14359-14362.

21. Brissova, M., et al., *Pancreatic Islet Production of Vascular Endothelial Growth Factor-A Is Essential for Islet Vascularization, Revascularization, and Function.* Diabetes, 2006. **55**(11): p. 2974-2985.

22. Wicksteed, B., et al., *Conditional Gene Targeting in Mouse Pancreatic β-Cells.* Analysis of Ectopic Cre Transgene Expression in the Brain, 2010. **59**(12): p. 3090-3098.

23. Benner, C., et al., *The transcriptional landscape of mouse beta cells compared to human beta cells reveals notable species differences in long non-coding RNA and protein-coding gene expression.* BMC Genomics, 2014. **15**(1): p. 1-17.

24. Banaei-Bouchareb, L., et al., *A transient microenvironment loaded mainly with macrophages in the early developing human pancreas.* Journal of Endocrinology, 2006. **188**(3): p. 467-480.

25. Criscimanna, A., et al., *Activated Macrophages Create Lineage-Specific Microenvironments for Pancreatic Acinar- and β-Cell Regeneration in Mice.* Gastroenterology, 2014. **147**(5): p. 1106-1118.e11.

26. Ehses, J.A., et al., *Increased Number of Islet-Associated Macrophages in Type 2 Diabetes.* Diabetes, 2007. **56**(9): p. 2356-2370.

27. Westwell-Roper, C.Y., J.A. Ehses, and C.B. Verchere, *Resident Macrophages Mediate Islet Amyloid Polypeptide–Induced Islet IL-1β Production and β-Cell Dysfunction.* Diabetes, 2014. **63**(5): p. 1698-1711.

28. Xu, X., et al., *Obesity Activates a Program of Lysosomal-Dependent Lipid Metabolism in Adipose Tissue Macrophages Independently of Classic Activation.* Cell Metabolism, 2013. **18**(6): p. 816-830.

29. Brouwers, B., et al., *Impaired Islet Function in Commonly Used Transgenic Mouse Lines due to Human Growth Hormone Minigene Expression.* Cell Metabolism, 2014. **20**(6): p. 979-990.

30. Parsons, J.A., A. Bartke, and R.L. Sorenson, *Number and size of islets of Langerhans in pregnant, human growth hormone-expressing transgenic, and pituitary dwarf mice: effect of lactogenic hormones.* Endocrinology, 1995. **136**(5): p. 2013-2021.

31. Huang, C., F. Snider, and J.C. Cross, *Prolactin Receptor Is Required for Normal Glucose Homeostasis and Modulation of β-Cell Mass during Pregnancy.* Endocrinology, 2009. **150**(4): p. 1618-1626.

32. Green, I.C. and K.W. Taylor, *Effects of pregnancy in the rat on the size and insulin secretory response of the islets of Langerhans.* Journal of Endocrinology, 1972. **54**(2): p. 317-325.

33. Schraenen, A., et al., *Placental lactogens induce serotonin biosynthesis in a subset of mouse beta cells during pregnancy.* Diabetologia, 2010. **53**(12): p. 2589-2599.

34. Kim, H., et al., *Serotonin regulates pancreatic beta cell mass during pregnancy.* Nat Med, 2010. **16**(7): p. 804-808.

35. Ravier, M.A., et al., *Mechanisms of Control of the Free Ca^{2+} Concentration in the Endoplasmic Reticulum of Mouse Pancreatic β-Cells: Interplay With Cell Metabolism and $[Ca^{2+}]_c$ and Role of SERCA2b and SERCA3.* Diabetes 2011. **60**(10): p. 2533-2545.

36. Wang, R., et al., *Insulin Secretion and Ca^{2+} Dynamics in β-Cells Are Regulated by PERK (EIF2AK3) in Concert with Calcineurin.* The Journal of Biological Chemistry, 2013. **288**(47): p. 33824-33836.

37. Soria, B., et al., *Pancreatic islet cells: a model for calcium-dependent peptide release.* HFSP Journal, 2010. **4**(2): p. 52-60.

38. Chao, S.-H., et al., *PDX1, a Cellular Homeoprotein, Binds to and Regulates the Activity of Human Cytomegalovirus Immediate Early Promoter.* Journal of Biological Chemistry, 2004. **279**(16): p. 16111-16120.

39. Halldorsdottir, S., et al., *Reproducibility and accuracy of body composition assessments in mice by dual energy x-ray absorptiometry and time domain nuclear magnetic resonance.* International journal of body composition research, 2009. **7**(4): p. 147-154.

40. Zmuda, E.J., C.A. Powell, and T. Hai, *A Method for Murine Islet Isolation and Subcapsular Kidney Transplantation.* Journal of Visualized Experiments : JoVE, 2011(50): p. 2096.

41. Wang, H., et al., *The Transcription Factor SREBP-1c Is Instrumental in the Development of β-Cell Dysfunction.* Journal of Biological Chemistry, 2003. **278**(19): p. 16622-16629.

42. Adewola, A.F., et al., *Microfluidic perifusion and imaging device for multi-parametric islet function assessment.* Biomed Microdevices, 2010. **12**(3): p. 409-17.

43. Morabito, M.V., et al., *Weight Perturbation Alters Leptin Signal Transduction in a Region-Specific Manner throughout the Brain.* PLoS ONE, 2017. **12**(1): p. e0168226.

Chapter 4: Discussion

SUMMARY

This thesis describes efforts to characterize the function of *Ildr2*, a gene predicted by positional genetics to be a modifier of diabetes susceptibility [1], and implicated by knockdown studies in hepatic lipid metabolism and fatty liver disease [2]. Investigations of the molecular functions of ILDR2 have suggested that it is regulated by ER stress transducers, binds ApoE, and may negatively regulate components of the Notch signaling pathway [3]. However, the precise molecular bases for the physiological roles of ILDR2 have yet to be determined.

One of the obstacles to investigating the functions of ILDR2 has been the lack of precise *Ildr2* KO mouse models. Thus, our previous studies of ILDR2 were limited to hypomorphic congenic, mutagenized, or virus-infected mouse models, and molecular targeting *in vitro*. The recent development of a conditional *Ildr2* floxed mouse has facilitated further understanding of the role of ILDR2. The overall focus of my work has been to characterize tissue-specific *Ildr2* KO mice, defining the function of ILDR2 in different tissues. Using these mice, I have confirmed that ILDR2 plays a role in pancreas endocrine function, but disproved the hypothesis that ILDR2 is essential for hepatic lipid homeostasis.

PART I: Overview of ILDR2 in the liver

In **Chapter 2**, I describe the generation of congenital hepatocyte-specific, *Ildr2* KO mice. In these animals I found that, contrary to prior expectations based on studies of adenoviral shRNA-mediated *Ildr2* KD (ADKD) mice, they did not develop hepatic steatosis. Hypothesizing that this lack of phenotype could be due to developmental compensation for early loss of *Ildr2* expression, we developed acute, whole-liver (vs. hepatocyte-only) *Ildr2* KO mice. However, these animals also failed to develop hepatic steatosis. Neither prolonged *Ildr2* KO (6 weeks vs. 10 days) nor

metabolic stress conveyed by high-fat diet (HFD) triggered hepatic lipid dysregulation in hepatocyte-specific, *Ildr2* KO mice. We concluded that the adenoviral shRNA used to knockdown *Ildr2* in prior studies must have had off-target effects which could account for the hepatic steatosis apparent in ADKD mice. This inference was confirmed in *Ildr2* liver KO mice infected with the original *Ildr2*-shRNA adenovirus. *Ildr2* liver KO mice administered the adenoviral shRNA accumulated excess liver triglycerides, despite the absence of *Ildr2* expression before or after infection.

To identify the gene(s) inadvertently targeted by the *Ildr2*-shRNA, and potentially responsible for causing fatty liver disease in ADKD mice, we performed RNA sequencing on ADKD and *Ildr2* liver KO mouse livers. 102 candidate genes were selected using the following parameters (See **Table 2.2**):

(1) Significantly decreased expression in ADKD vs. AD-lacZ controls,

(2) Significantly decreased expression in ADKD vs. *Ildr2* liver KO samples, and

(3) No significant difference in expression between AD-lacZ controls and *Ildr2* liver KOs.

Because genes meeting these criteria could be decreased by secondary effects of shRNA rather than by direct targeting, BLAST searches were performed to identify genes bearing sequence similarity to *Ildr2* shRNA. *Dgka* was the only gene of 102 candidates found to match a portion of the shRNA sequence. *Dgka* encodes diacylglyceride kinase alpha (DGKα) which regulates cellular signaling by converting diacylglyceride to phosphatidic acid. *Dgka*$^{-/-}$ mice have been created to understand the role of DGKα in immune signaling and T-cell anergy [4]. Hepatic phenotypes of these mice have not been reported, and inhibitors of *Dgka* designed to stimulate immune responses to cancer are thought have no side effects [5]. However, embryonic fibroblasts cultured from *Dgka*$^{-/-}$ mice were reported to accumulate diacylglyceride species [6]. Thus, it remains to be seen if

these mice develop hepatic steatosis. Future work will include characterizing *Dgka*$^{-/-}$ mice for hepatic lipid accumulation.

ADKD mice can be thought of as a "double KD" model since the shRNA potentially targeted both *Ildr2* and *Dgka*. Although not sufficient to cause hepatic steatosis, reduction of ILDR2 may have contributed to the lipid phenotypes in ADKD mice. To test this hypothesis, we will develop *Dgka*/*Ildr2* double KO mice and observe their susceptibility to hepatic steatosis. Additionally, ILDR2 has been shown to bind ApoE, which is consistent with a potential role in lipid transport and metabolism. Thus our work does not necessarily eliminate, but rather minimizes the putative function of ILDR2 in maintaining hepatic lipid metabolism.

Significance of Ildr2 *overexpression*

Our original studies with ADKD mice also demonstrated that *Ildr2* overexpression greatly reduces lipid accumulation in the case of pre-existing steatosis (i.e. *Lep*$^{ob/ob}$ mice) [2]; this effect could have significant therapeutic applications. Confirming that *Ildr2* KD does not cause hepatic steatosis does not negate a functional impact of *Ildr2* overexpression on hepatic lipid content. It is quite plausible that the effects of *Ildr2* KD vs. *Ildr2* overexpression are related but not reciprocal. As reviewed in **Chapter 1**, additional experiments showed that *Ildr2* overexpression did not rescue hepatic steatosis in high-fat, high-fructose fed mice, which exhibited liver fibrosis in addition to lipid accumulation. Further study is required to confirm the effects of *Ildr2* overexpression in steatotic mice. Overexpression studies are necessarily problematic not only because they often utilize transiently-expressed molecular vehicles (in our case, adenovirus), but also because they can result in supra-physiological levels of expression which are not representative of normal protein function. While not ideal for deciphering gene or protein function, this limitation is less

critical when investigating the therapeutic utility of upregulating gene expression. However, to avoid the confounding effects of adenovirus treatment, gain-of-function conditional transgenic constructs will be the best option for further study.

PART II: Overview of ILDR2 in the pancreas

In **Chapter 3** we described the phenotype of pancreas-specific (*Pdx*-Cre) *Ildr2* KO mice and confirmed that they exhibited phenotypes consistent with those observed in the B6.DBA Chr.1q23 congenic *Ildr2* hypomorphic (congenic) mice. *Pdx*-KO mice displayed impaired glucose tolerance, and both reduced insulin secretion and decreased calcium signaling in isolated islets, suggesting that Ildr2 plays a role in glucose sensing and insulin secretion in beta cells. We also assessed diabetic phenotypes of beta cell-specific (RIP2-cre) *Ildr2* KO mice and observed impaired glucose tolerance, reduced insulin secretion *in vivo*, but increased insulin secretion *ex vivo*, and beta cell hyperplasia. However, the expression of human growth hormone (*hGH*) in RIP2-KO mice confounds these results. Because the RIP2-Cre construct, in isolation, has been shown to trigger these same phenotypes as a result of *hGH* expression, we cannot with certainty attribute them to loss of *Ildr2* in the beta cell. Since the controls used in our experiments were *Ildr2* floxed mice, rather than RIP2-Cre mice, we cannot certify the specificity of ILDR2 function in the RIP2-KO mice.

Additionally, islet expression analyses showed that *Ildr2* was knocked out in *Pdx*-KO islets, but not in RIP2-KO islets, indicating that *Ildr2* is expressed in islet cells other than beta cells. Thus, despite potential phenotypic confounding of the RIP2-KO mice, comparison of these two mouse models led us to consider *Ildr2* expression in alternative islet cell types. After examining *Ildr2* expression in human and mouse islet cell expression datasets [7], and in liver and

adipose tissue macrophages [8], we hypothesized that *Ildr2* may be expressed in islet macrophages at higher levels than in endocrine cells, and that the genes effects on islet function may be conveyed through this cell type.

Proposed function of ILDR2 in islet macrophages

Apart from their evident role in the development of autoimmune (Type 1) diabetes, islet macrophages have been primarily described as activators of beta cell proliferation and regeneration [9, 10]. Interestingly, congenic mice exhibited reduced beta cell mass due to decreased proliferation [1], thus if *Ildr2* is expressed in islet macrophages it might play a role in the proliferative function of these cells. *Pdx*-KO mice fed low-fat chow showed no difference in beta cell number compared to controls at 24 weeks, implying that they do not have a proliferative defect. A reduction in proliferation may be more apparent in HFD-fed *Pdx*-KO mice, as beta cell proliferation is stimulated in the context of insulin resistance [11]. Recall that *Ildr2* was cloned based on the diabetes phenotypes of $Lep^{ob/ob}$ mice. Additionally, we can examine beta cell proliferation in the peak perinatal window of islet development. These further investigations will determine if beta cell proliferation is affected in *Pdx*-KO mice.

ILDR2 and islet cell calcium signaling

The *in vivo* and *in vitro* phenotypes of *Pdx*-KO islets suggest that loss of *Ildr2* in cells of the islet (possibly the macrophage) leads to reduced calcium signaling and decreased insulin secretion by the beta cell, resulting in glucose intolerance. Insulin secretion is stimulated by a precise series of events starting with glucose sensing by the beta cell receptor, GLUT2, mitochondrial oxidation, and ATP-dependent closing of potassium ion channels. This depolarizes

the cell membrane causing calcium channels to open, upon which calcium ions diffuse into the cell and stimulate insulin granule secretion [12]. Mitochondrial potential was unchanged between *Pdx*-KO and control islets (**Fig. 3.4B**), implying that the defect caused by *Ildr2* KO is downstream of ATP production.

Since insulin secretion is dependent on voltage-gated calcium flux across the cell membrane, ion concentrations must be tightly regulated within the cell. The endoplasmic reticulum is the major calcium storage organelle with associated calcium regulatory proteins [13]. We hypothesize that ILDR2 in the ER membrane plays a role in maintaining cellular calcium concentrations, and that *Ildr2* KO in islets alters the calcium concentration gradient, impairing calcium channel signaling with detrimental effects for insulin secretion. Glucagon and somatostatin secretion also involve calcium signaling [14-16], thus loss of *Ildr2* in *Pdx*-KO mice may also affect alpha and delta cell function.

This proposed role for ILDR2 in calcium regulation is reminiscent of 2D polyacrylamide gel electrophoresis studies of hypothalamic and liver tissue of W87* mice (**Chapter 1**) in which amounts of several calcium-related signaling molecules (e.g. calbindin D, neurocalcin, visinin-like protein 3) were decreased. However, the persistence of *Ildr2* expression in W87* mice renders it doubtful that these changes were reflective of loss of ILDR2 function.

Future work on the role of ILDR2 in the pancreas

These studies of the function of ILDR2 in the pancreas are a work in progress. Our next step is to determine which cells in the pancreatic islet express *Ildr2*. We will start by isolating macrophage and beta cell populations by cell sorting to measure *Ildr2* expression in separate populations. We have had no success detecting ILDR2 by immunohistochemistry in pancreatic

islets, despite testing several antibodies. Thus, we will need to perform *in situ* hybridization to determine exactly which islet cells express *Ildr2*. Probing additional pancreatic islet single-cell sequencing results will also help define the expression pattern of *Ildr2*. While we and others have shown that *Ildr2* is expressed at low levels in islet endocrine cells [7], this may not denote functional irrelevance. Recently, subsets of lowly-expressed "disallowed" genes have been identified in alpha and beta cells which play a role in cell proliferation, but are transcriptionally repressed to limit growth of mature beta cells [17]. *Ildr2* could be similarly regulated, relating to its putative function in beta cell proliferation.

To understand how islet morphology may be affected in *Pdx*-KO mice, we will quantify islet cell number and macrophages by immunohistochemistry, and measure beta proliferation by Ki67 or Brdu immunostaining. We will also measure mRNA expression of known calcium regulatory proteins in *Pdx*-KO beta cells, perform patch-clamping studies on beta cell to better understand changes in ion channel function, and identify putative calcium binding domains in ILDR2 to further explore its role in islet cell calcium signaling mechanisms. To determine if calcium-stimulated secretion is affected by *Ildr2* KO in alpha and delta cells, we will measure glucagon and somatostatin secretion in *Pdx*-KO mice. Finally, RNAseq of whole islets, isolated beta cells, and/or islet macrophages could be used to identify genes differentially regulated in *Pdx*-KO mice and understand which mechanistic pathways are affected. Additionally, we have an ongoing collaboration with Dr. George Gittes at the University of Pittsburgh to infuse AAV-RIP-Cre [18] directly into the pancreata of *Ildr2* floxed mice, allowing for beta cell-specific, acute *Ildr2* KO in adult animals.

PART III: Additional proposed functions of ILDR2

ILDR2 in the brain

Ildr2 is more highly expressed in the brain than in any other tissue, suggesting a functional role in centrally-regulated metabolism. ILDR2 could be involved in the hypothalamic regulation of insulin secretion by various mechanisms such as, neuronal glucose sensing [19] or the melanocortin system [20]. Interestingly, the ectopic expression of RIP2-cre in the hypothalamus [21, 22] has helped establish critical roles for several hypothalamus-expressed genes hypothalamic regulation of metabolism and beta cell function, most notably *Irs2* [23-25], but also *Stat3* [26] and *Pten* [27]. Persistence of *Ildr2* expression in the hypothalami of RIP2-KO and *Pdx*-KO mice (**Fig.3.6G-J**) confirmed that floxed *Ildr2* alleles in the hypothalamus were not affected by RIP2-cre or *Pdx*-cre expressing hypothalamic neurons. However, since these Cre-expressing neurons are a poorly-defined subgroup distributed throughout the hypothalamus [22, 28, 29], this finding does not enable definitive conclusions regarding a role for ILDR2 in hypothalamic regulation of beta cell function.

The interaction between ILDR2 and ApoE could also be related to ILDR2's putative brain function. ApoE ε4, the major risk allele for Alzheimer's disease, is thought to be a hypomorphic allele; thus protective functions have been identified for ApoE in the brain. ILDR2 may participate with ApoE in its functional roles of neuronal lipid transport and clearance of amyloid beta proteins [30]. However, since the ApoE binding sites for ILDR2 and amyloid beta are overlapping, ILDR2 could also have the negative effect of sequestering ApoE, possibly leading to amyloid beta aggregation and plaque formation.

Proposed role of leptin in ILDR2 biology

Two of the most interesting phenotypes observed in *Ildr2* functional studies – hypoinsulinemic hyperglycemia due to reduced beta cell mass in congenic mice [1], and amelioration of hepatic steatosis by *Ildr2* overexpression [2] – were observed in *Lep*$^{ob/ob}$ mice. Neither of these phenotypes has been replicated in leptin-expressing mice, suggesting that ILDR2 effects may be context-dependent with regard to leptin sufficiency.

Potential mechanisms for such an interaction are informed by direct leptin action on the beta cell [31] whereby it inhibits insulin gene expression and secretion by various mechanisms, including activation of potassium channels in the beta cell [32-35]. However, insulin secretion is reduced in *Ildr2*-deficient mice which rather suggests that leptin and ILDR2 have opposing roles in modulating beta cell function. Alternatively, since the primary function of leptin is hypothalamic regulation of feeding behavior and body weight, ILDR2 could function in the brain downstream of leptin signaling.

Contribution of extra-pancreatic Ildr2 *deficiency to original diabetic phenotypes*

An additional point to consider in comparing congenic mice with *Pdx*-KO mice is that congenics were *Ildr2* deficient in every tissue; they were not organ or cell type-specific KOs. *Ildr2* is ubiquitously expressed and, in several tissues, at higher levels than in pancreatic islets. Thus, it very plausible that loss of *Ildr2* in related metabolic tissues; such as liver, adipose tissue, and hypothalamus; contributed to the primary manifestation of beta cell defects.

Ongoing studies

To explore the above-mentioned hypotheses about *Ildr2* cross-tissue regulation, as well as investigate the role of ILDR2 in the brain, we have generated whole-body *Ildr2* KO mice and confirmed complete *Ildr2* ablation in a range of organs (**Fig. 4.1A**). KO mice are viable and fertile, and have no obvious developmental or metabolic defects. However, upon HFD feeding, KO mice preferentially gain fat mass despite no significant difference in body weight from WT controls (**Fig. 4.1B,D,E**). This increase in fat mass is apparently not due to hyperphagia (**Fig. 4.1C**), suggesting that KO mice may have decreased energy expenditure.

Future work in these mice will focus on measurements of energy expenditure as well as assessing changes in hypothalamic leptin signaling. These preliminary results specify a role for ILDR2 in body mass determination and support the hypothesis that ILDR2 is involved in hypothalamic regulation of metabolism.

CONCLUSIONS

The contributions of this thesis work to metabolic research in general, and to the study of ILDR2 in particular, are three-fold. First, the discovery that *Ildr2* ablation is not responsible for a phenotype of massive hepatic steatosis led us to identify novel candidate regulators of hepatic lipid homeostasis, which will enable new mechanisms of lipid accumulation in fatty liver disease to be identified. Second, the diabetic phenotypes described in pancreas *Ildr2* KO mice provide the very first confirmation of the role of ILDR2 as a modifier of diabetes susceptibility. Further investigation into the mechanism of ILDR2 will lead to a better understanding of the role of ILDR2 in diabetes pathogenesis. Third, the development of conditional and whole-body *Ildr2* KO mice

will facilitate investigation into additional functions of ILDR2, e.g. as a component of tricellular tight junctions, or in metabolic partitioning of energy stores.

Figure 4.1: Whole-body Ildr2 KO mice have increased fat mass on HFD

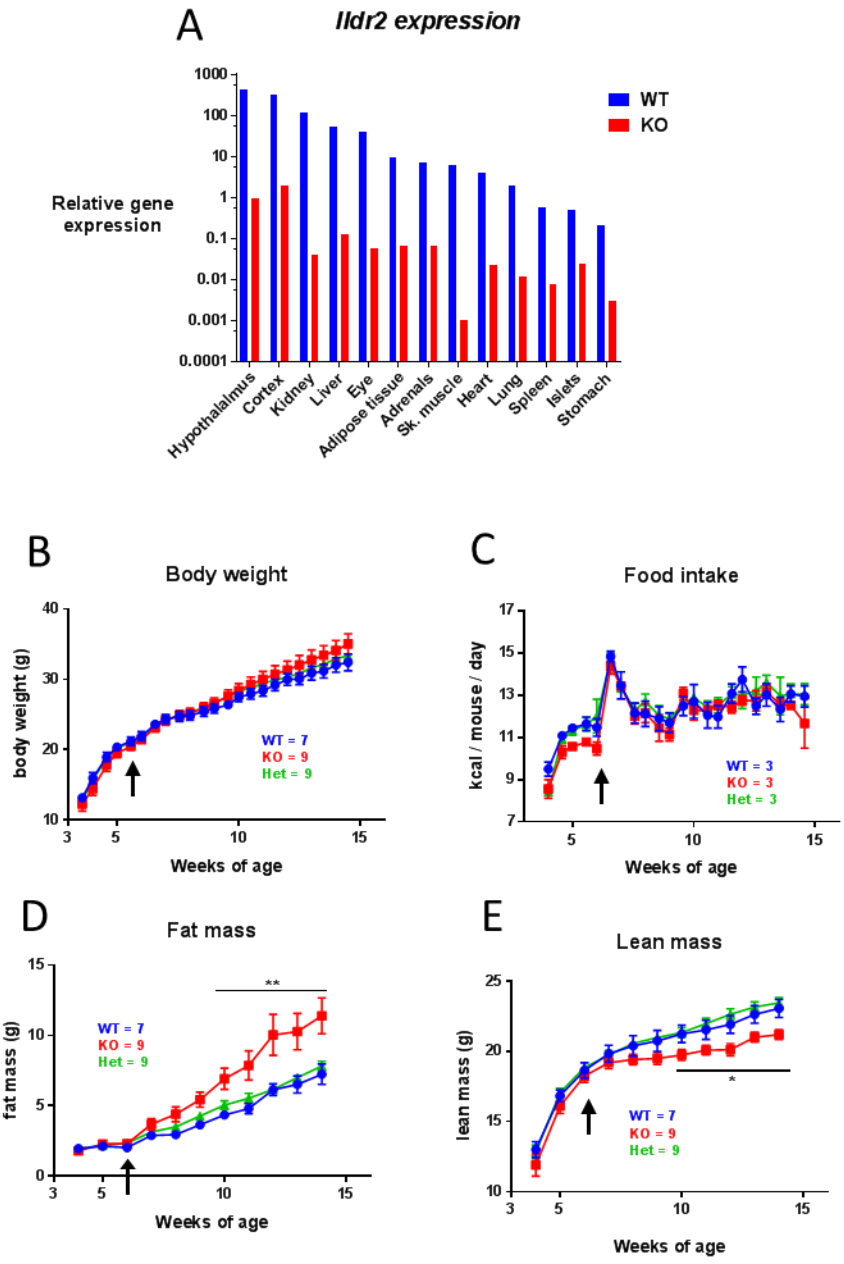

Figure 4.1: Whole-body *Ildr2* KO mice have increased fat mass on HFD

Ildr2 floxed mice were crossed with mice expressing Cre driven by the CMV promoter to produce whole-body *Ildr2* KO mice. (A) *Ildr2*-isoform 1 expression (log scale) in tissues from WT and KO mice in decreasing order of *Ildr2* expression, n=2. Gene expression was measured by qPCR and normalized to *beta actin* expression. >90% reduction in *Ildr2* expression was detected in each tissue. (B) Body weight of WT, KO and heterozygous (Het) male mice measured 2x/weekly from 3.5-14.5 weeks old. Mice were HFD-fed from 6 weeks old (indicated by arrows). (C) Food intake measured 2x/weekly from 4-14.5 weeks old. Mice were housed 2-3/cage, n=3 cages/genotype. (D) Fat mass measured weekly from 4-14 weeks old. (E) Lean mass measured weekly from 4-14 weeks old. Data are represented as mean ± standard error (SEM). ** $p<0.01$ for KO vs. WT (Two-way ANOVA). n = 7 WT, 9 KO, 9 Het mice.

References

1. Dokmanovic-Chouinard, M., et al., *Positional cloning of "Lisch-Like", a candidate modifier of susceptibility to type 2 diabetes in mice.* PLoS Genet, 2008. **4**(7): p. e1000137.

2. Watanabe, K., et al., *ILDR2: an endoplasmic reticulum resident molecule mediating hepatic lipid homeostasis.* PLoS One, 2013. **8**(6): p. e67234.

3. Watanabe, K., et al., *ZNF70, a novel ILDR2-interacting protein, contributes to the regulation of HES1 gene expression.* Biochemical and Biophysical Research Communications, 2016. **477**(4): p. 712-716.

4. Olenchock, B.A., et al., *Disruption of diacylglycerol metabolism impairs the induction of T cell anergy.* Nat Immunol, 2006. **7**(11): p. 1174-1181.

5. Liu, K., et al., *A novel diacylglycerol kinase α-selective inhibitor, CU-3, induces cancer cell apoptosis and enhances immune response.* Journal of Lipid Research, 2016. **57**(3): p. 368-379.

6. Milne, S.B., et al., *Dramatic Differences in the Roles in Lipid Metabolism of Two Isoforms of Diacylglycerol Kinase.* Biochemistry, 2008. **47**(36): p. 9372-9379.

7. Benner, C., et al., *The transcriptional landscape of mouse beta cells compared to human beta cells reveals notable species differences in long non-coding RNA and protein-coding gene expression.* BMC Genomics, 2014. **15**(1): p. 1-17.

8. Xu, X., et al., *Obesity Activates a Program of Lysosomal-Dependent Lipid Metabolism in Adipose Tissue Macrophages Independently of Classic Activation.* Cell Metabolism, 2013. **18**(6): p. 816-830.

9. Banaei-Bouchareb, L., et al., *A transient microenvironment loaded mainly with macrophages in the early developing human pancreas.* Journal of Endocrinology, 2006. **188**(3): p. 467-480.

10. Criscimanna, A., et al., *Activated Macrophages Create Lineage-Specific Microenvironments for Pancreatic Acinar- and β-Cell Regeneration in Mice.* Gastroenterology, 2014. **147**(5): p. 1106-1118.e11.

11. Mosser, R.E., et al., *High-fat diet-induced β-cell proliferation occurs prior to insulin resistance in C57Bl/6J male mice.* American Journal of Physiology - Endocrinology And Metabolism, 2015. **308**(7): p. E573-E582.

12. Soria, B., et al., *Pancreatic islet cells: a model for calcium-dependent peptide release.* HFSP Journal, 2010. **4**(2): p. 52-60.

13. Koch, G.L.E., *The endoplasmic reticulum and calcium storage.* BioEssays, 1990. **12**(11): p. 527-531.

14. Berts, A., et al., *Glucose stimulation of somatostatin-producing islet cells involves oscillatory Ca2+ signaling.* Endocrinology, 1996. **137**(2): p. 693-697.

15. Göpel, S.O., et al., *Patch-clamp characterisation of somatostatin-secreting δ-cells in intact mouse pancreatic islets.* The Journal of Physiology, 2000. **528**(3): p. 497-507.

16. Gromada, J., et al., *ATP-Sensitive K^+ Channel–Dependent Regulation of Glucagon Release and Electrical Activity by Glucose in Wild-Type and SUR1$^{-/-}$ Mouse α-Cells.* Diabetes, 2004. **53**(suppl 3): p. S181-S189.

17. Pullen, T.J., M.O. Huising, and G.A. Rutter, *Analysis of Purified Pancreatic Islet Beta and Alpha Cell Transcriptomes Reveals 11β-Hydroxysteroid Dehydrogenase (Hsd11b1) as a Novel Disallowed Gene.* Frontiers in Genetics, 2017. **8**(41).

18. Xiao, X., et al., *Pancreatic cell tracing, lineage tagging and targeted genetic manipulations in multiple cell types using pancreatic ductal infusion of adeno-associated viral vectors and/or cell-tagging dyes.* Nat. Protocols, 2014. **9**(12): p. 2719-2724.

19. Osundiji, M.A., et al., *Brain Glucose Sensors Play a Significant Role in the Regulation of Pancreatic Glucose-Stimulated Insulin Secretion.* Diabetes, 2012. **61**(2): p. 321-328.

20. Fan, W., et al., *The Central Melanocortin System Can Directly Regulate Serum Insulin Levels.* Endocrinology, 2000. **141**(9): p. 3072-3079.

21. Gannon, M., et al., *Analysis of the Cre-mediated recombination driven by rat insulin promoter in embryonic and adult mouse pancreas.* genesis, 2000. **26**(2): p. 139-142.

22. Wicksteed, B., et al., *Conditional Gene Targeting in Mouse Pancreatic β-Cells.* Analysis of Ectopic Cre Transgene Expression in the Brain, 2010. **59**(12): p. 3090-3098.

23. Choudhury, A.I., et al., *The role of insulin receptor substrate 2 in hypothalamic and β cell function.* The Journal of Clinical Investigation, 2005. **115**(4): p. 940-950.

24. Kubota, N., et al., *Insulin receptor substrate 2 plays a crucial role in β cells and the hypothalamus.* The Journal of Clinical Investigation, 2004. **114**(7): p. 917-927.

25. Lin, X., et al., *Dysregulation of insulin receptor substrate 2 in β cells and brain causes obesity and diabetes.* The Journal of Clinical Investigation, 2004. **114**(7): p. 908-916.

26. Cui, Y., et al., *Essential Role of STAT3 in Body Weight and Glucose Homeostasis.* Molecular and Cellular Biology, 2004. **24**(1): p. 258-269.

27. Nguyen, K.-T.T., et al., *Essential Role of Pten in Body Size Determination and Pancreatic β-Cell Homeostasis In Vivo.* Molecular and Cellular Biology, 2006. **26**(12): p. 4511-4518.

28. Kong, D., et al., *GABAergic RIP-Cre Neurons in the Arcuate Nucleus Selectively Regulate Energy Expenditure.* Cell, 2012. **151**(3): p. 645-657.

29. Schwartz, M.W., S.J. Guyenet, and V. Cirulli, *The Hypothalamus and β-Cell Connection in the Gene-Targeting Era.* Diabetes, 2010. **59**(12): p. 2991-2993.

30. Kim, J., J.M. Basak, and D.M. Holtzman, *The Role of Apolipoprotein E in Alzheimer's Disease.* Neuron, 2009. **63**(3): p. 287-303.

31. Covey, S.D., et al., *The pancreatic β cell is a key site for mediating the effects of leptin on glucose homeostasis.* Cell Metabolism, 2006. **4**(4): p. 291-302.

32. Kieffer, T.J., et al., *Leptin Suppression of Insulin Secretion by the Activation of ATP-Sensitive K^+ Channels in Pancreatic β-Cells.* Diabetes, 1997. **46**(6): p. 1087-1093.

33. Kulkarni, R.N., et al., *Leptin rapidly suppresses insulin release from insulinoma cells, rat and human islets and, in vivo, in mice.* The Journal of Clinical Investigation, 1997. **100**(11): p. 2729-2736.

34. Seufert, J., T.J. Kieffer, and J.F. Habener, *Leptin inhibits insulin gene transcription and reverses hyperinsulinemia in leptin-deficient ob/ob mice.* Proceedings of the National Academy of Sciences of the United States of America, 1999. **96**(2): p. 674-679.

35. Marroquí, L., et al., *Role of leptin in the pancreatic β-cell: effects and signaling pathways.* Journal of Molecular Endocrinology, 2012. **49**(1): p. R9-R17.